

ANALYSIS OF GAS PRODUCTION FROM HYDRAULICALLY FRACTURED
WELLS IN NATURALLY FRACTURED RESERVOIR USING SOURCE
FUNCTION METHOD

A Dissertation

by

YUN SUK HWANG

Submitted to the Office of Graduate and Professional Studies of
Texas A&M University
in partial fulfillment of the requirements for the degree of

DOCTOR OF PHILOSOPHY

Chair of Committee,	Ding Zhu
Committee Members,	David Schechter
	Eduardo Gildin
	Guy Battle
Head of Department,	A. Daniel Hill

December 2017

Major Subject: Petroleum Engineering

Copyright 2017 Yun Suk Hwang

ABSTRACT

According to the 2014 EIA statistics, natural gas production from shale and tight oil plays accounted for 48% of US natural gas production and this number is expected to grow to 69% in 2040. Natural fractures are commonly observed in these unconventional reservoirs. Multi-stage hydraulic fracturing in horizontal wells has been applied to develop these shale/tight sands. Natural fractures could be open during treatment or conductive even before treatment, providing a larger drainage by creating a complex network. It still remains a challenge to reasonably predict well performance in such a complex system, especially by honoring the distribution of natural fractures explicitly.

This study presents a methodology based on Green's source function and Fractal discrete fracture network (FDFN) model. Slab source is a plane source with finite thickness, which is a novel approach of classic source function by reducing the erroneous integration. The hydraulic and natural fractures together are represented by independent slab sources, and their influence on each other is considered, which is more realistic than summing the flow from each fracture as total flow. FDFN model was used to generate realistic natural fracture maps. Production from adsorbed gas, common in shale reservoirs, is also modeled using modified material balance equation.

I applied our model to estimate the multi-stage hydraulic fractured horizontal gas well performance in synthetically generated naturally fractured reservoirs. An extended number of natural fractures were handled by introducing several approaches to speed up the calculation. A parametric study was conducted to delineate important parameters

affecting well performance. Simulation results indicated that conductive natural fracture largely influence gas production in unconventional reservoirs. The characteristics of natural fractures, such as density, length and interaction with hydraulic fractures were found to be controlling parameters. It was also found that the inclusion of adsorbed gas could result in the total gas production increase up to 25%. Also, comparisons are provided with published or commercially available numerical and analytical approaches to verify the methodology of this study.

The novelty of the method is in the ability to respect the previously identified fracture distribution explicitly, either hydraulic or natural, even if the fractures are non-orthogonal to the horizontal wellbore. Since the approach is semi-analytical, it is easy to use and solves the problem in reasonable time using standard computers.

DEDICATION

To my family
for their love and support

ACKNOWLEDGEMENTS

Although this dissertation would not have been possible without the help of many people, my first gratitude would go to my adviser, Dr. Ding Zhu. I would like to express my sincere appreciation to Dr. Zhu for giving me the opportunity to pursue my Ph.D. at Texas A&M University. I am grateful to her commitment and encouragement throughout my study. Her guidance, patience, and generosity made me.

I also thank my committee members, Dr. Schechter, Dr. Gildin and Dr. Battle, for their guidance and support throughout the course of this research.

Thanks also go to my friends and colleagues and the department faculty and staff for making my time at Texas A&M University a great experience.

Finally, thanks to God, for the guidance and strength given to me.

CONTRIBUTORS AND FUNDING SOURCES

Contributors

This work was supported by a dissertation committee consisting of Professor Dr.Ding Zhu and Dr.Eduardo Gildin and Dr.David Schechter of the Department of Petroleum Engineering and Professor Dr.Guy Battle of the Department of Mathematics.

The source code for Chapter II, a Fractal Discrete Fracture Network model, was provided by Professor Dr.David Schechter.

All other work conducted for the dissertation was completed by the student independently.

Funding Sources

Graduate study was supported by a fellowship from Texas A&M University and Crisman Institute.

NOMENCLATURE

a	Reservoir length, ft
B_g	Gas formation volume factor, rcf/scf
b	Reservoir width, ft
c_t	Compressibility, psi^{-1}
D_c	Fractal dimension of fracture center distribution
D_l	Fractal dimension of fracture length distribution
D_q	Multi-fractal dimension
d	Distance between two points
G	Original gas in place, scf
G_p	Cumulative gas produced, scf
h	Reservoir thickness, ft
k	Reservoir permeability, md
L	Domain size
M	Location of the observed pressure drop
M_w	Location of the source
N	Number of fractures
p	Pressure, psi
p_L	Langmuir pressure, psi

\bar{p}	Average pressure, psi
Δp	Pressure drop, psi
q	Withdrawal rate per unit length, area or volume of source
q_d	Degree of dimension
S	Source function
S_g	Gas saturation, fraction
sr	Scale ratio
t	Flowing time
V_{ads}	Gas volume which can be adsorbed by a rock of unit mass, scf/ton
V_B	Rock bulk volume, scf
V_L	Langmuir volume, scf
x	Distance from the source
x, y, z	Coordinates in x, y and z direction
z	Gas deviation factor
z^*	King's gas deviation factor for free and adsorbed gas

Greek

α	Fracture density
ϕ	Formation porosity, fraction
η	Hydraulic diffusivity constant, $\eta_j = \frac{k_j}{\phi\mu c}$, $j = x, y \text{ or } z$

μ	Fluid viscosity, cp
τ	Dummy variable of integration

Subscripts

0	Source location
1,2	Initial and end points
f	Slab source thickness
i	Initial
sc	Standard conditions
x, y, z	Direction of permeability axis

TABLE OF CONTENTS

	Page
ABSTRACT	ii
DEDICATION	iv
ACKNOWLEDGEMENTS	v
CONTRIBUTORS AND FUNDING SOURCES.....	vi
NOMENCLATURE.....	vii
TABLE OF CONTENTS	x
LIST OF FIGURES.....	xii
LIST OF TABLES	xv
CHAPTER I INTRODUCTION	1
1.1 Background	1
1.2 Literature Review	3
1.2.1 Source functions	3
1.2.2 Representation of natural fractures.....	5
1.3 Objective and Approach.....	7
CHAPTER II MODEL DEVELOPMENT	9
2.1 Source Function Method	9
2.2 Slab Source Solution	12
2.2.1 Slab source approach for single fracture	12
2.2.2 Source function approach for multiple fractures	19
2.3 Plane Source Solution	22
2.4 Naturally Fractured Reservoir.....	29
2.4.1 Naturally fractured reservoir	29
2.4.2 Fractal discrete fracture network (DFDN) system.....	31
2.5 Building and Solving Complex Fracture System.....	35
2.6 Non-orthogonally Intersecting Natural and Hydraulic Fracture System	37
2.7 Gas Adsorption Phenomena.....	39
2.7.1 Adsorbed Gas	39

2.7.2 Gas Adsorption/Desorption Model	40
2.7.3 Material Balance.....	42
2.8 Effort to Improve Computation Efficiency	45
2.8.1 Parallelization of The Code	46
2.8.2 Comparison of Computation Time.....	47
CHAPTER III VALIDATION.....	49
3.1 Simplified Fracture System.....	49
3.2 Complex Fracture System with FracGen/NFFlow	54
CHAPTER IV RESULTS AND PARAMETRIC STUDY	63
4.1 Introduction	63
4.2 Parametric Study of Number of Hydraulic Fractures.....	65
4.3 Parametric Study of Hydraulic Fracture Length	70
4.4 Parametric Study of Number of Fracture Segments.....	74
4.5 Parametric Study of the Source Type.....	75
4.6 Chapter Summary.....	76
CHAPTER V APPLICATION EXAMPLE.....	77
5.1 Sparse Natural Fractures	77
5.2 Dense Natural Fractures	81
5.3 Large Number of Hydraulic Fractures	84
5.4 Field-scale Case Study	87
CHAPTER VI CONCLUSIONS	92
REFERENCES	94
APPENDIX I.....	98

LIST OF FIGURES

	Page
Fig. 1—US Natural gas production.	3
Fig. 2—Representation of natural fractures.	6
Fig. 3—DFN representation in commercial numerical simulators.	7
Fig. 4—Schematic of source function method.	10
Fig. 5—A slab source in three-dimensional finite domain as a multiplication of three one-dimensional infinite slab sources.	13
Fig. 6—Schematic of a slab source in three-dimensional domain.	15
Fig. 7—Flow chart of source function method.	16
Fig. 8—Schematic of a single fracture in three-dimensional domain.	17
Fig. 9—Multiple hydraulic fractures in three-dimensional domain.	20
Fig. 10—Schematic of a fracture used in plane source approach.	23
Fig. 11—Schematic of a straight line connecting 2 end points.	24
Fig. 12—Natural fractures. Reprinted from Cardott, 2006.	29
Fig. 13—Schematic of fracture interaction: (a) crossing (b) diverting (c) jogging. Reprinted from Wang et al. 2013.	30
Fig. 14—Open and closed natural fractures on cores. Reprinted from Gale et al. 2010.	30
Fig. 15—Fracture center distribution generated by a multiplicative cascade process. Reprinted from Darcel et al. 2003.	32
Fig. 16—Natural fracture systems generated using FDFN.	34
Fig. 17—Conceptual identification of fracture connectivity.	36
Fig. 18—Schematic of handling non-orthogonally intersecting fractures.	38
Fig. 19—Gas storage mechanism. Reprinted from Song, 2010.	39
Fig. 20—Gas transportation mechanism. Reprinted from Song, 2010.	40

Fig. 21—(a) Langmuir Isotherm (b) Free, adsorbed and total gas content vs pressure. ...	42
Fig. 22— p/z^* and p/z vs G_p plot. Reprinted from King, 1990.	44
Fig. 23—Flow chart for adsorbed gas production calculation.	45
Fig. 24—Concept of parallelism (a) Before (a) After.	46
Fig. 25—Calculation time estimation plot.	48
Fig. 26—Grids used in CMG for simplified fracture system.	50
Fig. 27—Enlarged map in CMG which shows stepped grids.	51
Fig. 28—Gas production rate comparison with CMG and source function method.	53
Fig. 29—Cumulative gas production comparison with CMG and source function method.	54
Fig. 30—Complex fracture system with FRACGEN/NFFLOW.	56
Fig. 31—Screen capture of NFFLOW program.	58
Fig. 32—Fracture network input file in NFFLOW:Fracture part.	59
Fig. 33—Fracture network input file in NFFLOW:Well part.	59
Fig. 34—Reservoir control file in NFFLOW:Fluid Properties part.	60
Fig. 35—Reservoir control file in NFFLOW:Production control part.	61
Fig. 36—Gas production rate comparison with NFFLOW and source function method.	62
Fig. 37—Complex fracture network for base case with 10 hydraulic fractures and 1000 ft hydraulic fracture length.	64
Fig. 38—Complex fracture network for 20 hydraulic fractures.	66
Fig. 39—Gas production rate with different number of hydraulic fractures.	67
Fig. 40—Cumulative gas production with different number of hydraulic fractures.	67
Fig. 41—Cumulative gas production with different number of hydraulic fractures with and without natural fractures in the system ($k=0.001$ md).	69

Fig. 42—Cumulative gas production with different number of hydraulic fractures with and without natural fractures in the system ($k=0.0001$ md).	70
Fig. 43—Complex fracture network with hydraulic fracture length of 500 ft.	72
Fig. 44—Complex fracture network with hydraulic fracture length of 750 ft.	72
Fig. 45—Gas production rate for different hydraulic fracture lengths.....	73
Fig. 46—Cumulative gas production with different hydraulic fracture lengths.	73
Fig. 47—Cumulative gas production with different number of segments.	75
Fig. 48—Gas production rate comparison using slab source and plane source	76
Fig. 49—Complex fracture network used for sparse natural fracture network.....	78
Fig. 50—Free gas, desorbed gas and total gas production rate.....	80
Fig. 51—Cumulative free gas, desorbed gas and total gas production.	80
Fig. 52—Complex fracture network used for dense natural fracture network.....	81
Fig. 53—Gas production rate for sparse and dense natural fracture network.	83
Fig. 54—Cumulative gas production for sparse and dense natural fracture network.	83
Fig. 55—Complex fracture network used for large number of hydraulic fractures.....	85
Fig. 56—Cumulative gas production for large number of hydraulic fractures.	86
Fig. 57—Natural fracture map used and the multiple hydraulic fractures.....	89
Fig. 58—Average reservoir pressure.....	90
Fig. 59—Gas production rate.	90
Fig. 60—Recovery factor.....	91

LIST OF TABLES

	Page
Table 1—Basic instantaneous source functions S in infinite reservoirs. Adapted from Gringarten and Ramey, 1973.	11
Table 2—Basic instantaneous source functions for an infinite slab source in an infinite slab reservoir. Adapted from Gringarten and Ramey, 1973.	13
Table 3—Necessary input values for FDFN generation.	33
Table 4—Computation time comparison.	47
Table 5—Computer hardware specifications.	48
Table 6—Input parameters for simplified fracture system.	52
Table 7—Input parameters for complex fracture system.	56
Table 8—Input parameters for base case.	64
Table 9—Input parameters for sparse natural fracture network.	78
Table 10—Input parameters for dense natural fractures network.	82
Table 11—Input parameters for large number of hydraulic fractures.	85
Table 12—Input parameters for field case study and their sources.	88

CHAPTER I

INTRODUCTION

1.1 Background

According to the 2014 EIA statistics, natural gas production from shale and tight oil plays accounted for 48% of US natural gas production and this number is expected to grow to 69% in 2040 (**Fig. 1**). These unconventional resources are hydrocarbon reservoirs that usually have low permeability and porosity, and often enhanced recovery techniques must be performed to get the hydrocarbon out of them. Multi-stage hydraulic fracturing in horizontal wells has been applied to develop these shale/tight sands, mainly since the huge success of Barnett Shale and rising of oil price in 2005.

In tight gas or shale reservoirs, natural fractures are widely observed.

Naturally fractured reservoir is a reservoir, where naturally occurring fractures have a significant effect on flow rates and recovery. These natural fractures could be open and reactivated during hydraulic fracturing or sealed by cement. When hydraulic fractures encounter natural fractures, if the natural fractures are conductive, they will contribute to production.

The existence of conductive natural fractures provide a larger drainage by creating a complex network. The statistical nature of natural fracture networks changes the flow characteristics from that of a single linear fracture. So simply using single linear fracture model for individual fractures, and then summing the flow from each fracture as the total flow rate for the network could introduce a significant error.

Although most of the solutions to the flow problem in porous media have been investigated in a similar case as in the heat transfer and the solution is originated from the heat transfer, Gringarten and Ramey's (1973) work is the first application of the Green's function and the approach of source function to the problem of unsteady-state fluid flow in the reservoirs. The application of the source and Green's function later extended to the unsteady-state pressure distribution for more complex well completion schematics by others (Cinco-Ley et al. 1978; Cinco-Ley et al. 1981; Raghavan and Hadinoto 1978). In this study, we present a methodology to predict the performance of horizontal wells with multi-stage fractures in naturally fractured formations. To reflect heterogeneous nature of natural fractures, a stochastic method of generating discrete fracture networks is applied. The fractal discrete fracture network model (DFDN) incorporates the various scale-dependent data, such as outcrops, logs and cores and creates more realistic natural fracture networks. We combine DFDN model with a slab source model to solve the flow problem in complex fracture systems. The fractures, natural or hydraulically induced, are treated as a series of sources. The analytical solution of superposed slab sources provides the overall flow from the fracture system created by DFDN with hydraulic fractures integrated in the system.

Extended number of natural fractures were handled by introducing several approaches to speed up the calculation.

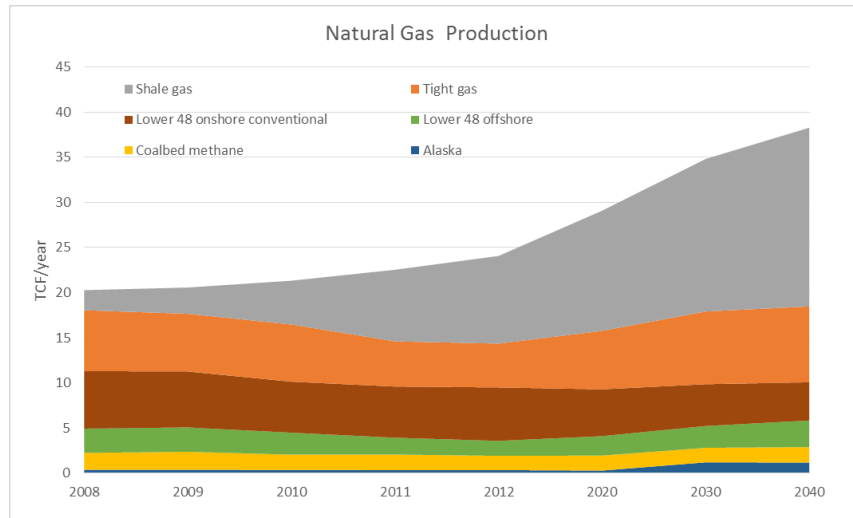


Fig. 1—US Natural gas production.

1.2 Literature Review

1.2.1 Source functions

Gringarten and Ramey (1973) were the first ones to apply the Green's and source function to the reservoir flow problems. They introduced the original work of Carslaw and Jaeger (1959)'s famous book, *Conduction of heat in solids*, to petroleum industry and provided tables of instantaneous source functions under various boundary conditions which can be used to generate solutions for a wide variety of problems.

Over the past several decades, Gringarten's source function has been extensively used in solving flow problems in porous media, especially in pressure transient analysis area. Gringarten et al. (1974) applied the Green's function to the unsteady state pressure distribution created by a vertical fractured well with infinite conductivity fracture. By dividing the fracture into N segments, a series of equations had been solved to calculate

the pressure distribution and contribution of each segment to the total flow by assuming each segment as a uniform flux source.

By integrating the point source to line source, Babu and Odeh (1989) developed a line source solution to predict horizontal well performance in a closed reservoir. The model is under pseudosteady-state condition. One of the limitations of this method is the well must be parallel to the reservoir boundary.

The application of point source solution was presented by Ozkan et al. (1995). He developed point source solution in Laplace domain in order to remove the limitations of the Gringarten and Ramey's model in considering the wellbore storage and skin effects.

Lin (2010) used source approach to predict the performance of horizontal wells with multiple hydraulic fractures. The main difference between all the others' work and her work is that she used "slab source" approach, which will be explained in detail later.

Guo et al. (1994) also used source function to analyze the pressure transient solutions for a horizontal well which intersects multiple fractures. He used plane source and integration to represent randomly distributed fractures but the interactions between the fractures were not considered.

More recently, Zeng and Zhao (2009) applied source function to compute pressure response in a reservoir with discrete fractures. Their approach is to divide the reservoir as two sub systems of fracture and matrix, and to solve the partial differential equation in Laplace space by applying various boundary conditions. Their work is limited to vertical well and parallel fractures.

1.2.2 Representation of natural fractures

There are largely 3 methods to represent natural fractures in studying the flow problems in the reservoir (**Fig. 2**).

The first one is the Discrete Fracture Network (DFN) method. It tries to honor the actual location, geometry of natural fractures. Therefore it is closer to the reality and fracture connectivity is well handled. It treats the fractures explicitly with high-permeability grid cells. So to represent non-orthogonal fracture networks, unstructured grids are needed and sometimes this could lead to heavy computation.

Second is the Dual Porosity approach. It is a concept developed by Warren and Root (1963) to simplify and idealize the fracture patterns as match-stick or sugar-cube, and to honor the existence of two distinguished continuum, matrix and fracture. In dual porosity approach, after simplifying natural fracture patterns, the effects of them are considered as shape factor for the whole reservoir. Therefore the calculation speed could be faster than discrete fracture network method.

Third approach is combined methods of discrete fracture network and dual porosity concept, which takes advantage of both methods to speed up the calculation. It captures the effect of fractures by upscaling a discrete fracture network model into a dual-porosity reservoir model, and by enhancing the permeability of stimulated reservoir.

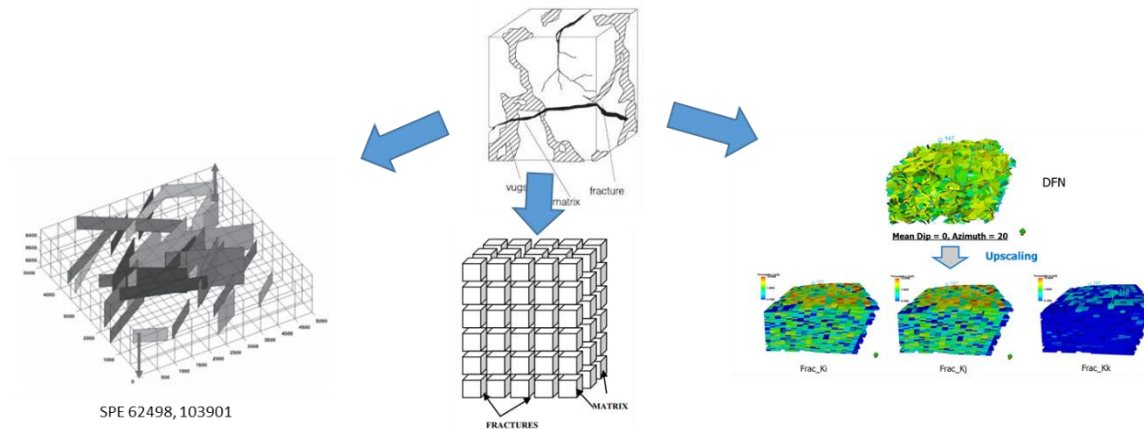


Fig. 2—Representation of natural fractures.

Although this approach provides a quick estimate of well productivity, they compromise the direct link between fracture configuration and well production (due to upscaling), which limits insight into the performance of the fracture network. Although it is not easy to honor discrete fracture network, the researchers have tried several approaches to handle it in commercial numerical simulators like Eclipse and CMG.

In Cartesian grid system, very fine local grids and enhanced permeability input are needed to represent fractures, either hydraulic fractures or natural fractures. This job needs to be done manually one by one for each fracture. It takes time but can be handled when all the fractures are parallel to x or y direction because we can just repeat the same procedure for all the fractures. But when we have non-orthogonal fractures in the system, describing fracture network has to be done basically grid by grid considering the geometry of fractures. Since the length, direction of each fracture is different, refinement is challenging for each fracture. We need to be very careful in modifying the grids, making sure that we're following the right fracture geometry. It is extremely time consuming.

The advanced gridding for fractured reservoirs uses unstructured grid, such as the one presented in Schlumberger's Mangrove, a fairly new software which is used for fracture treatment design and performance estimation (**Fig. 3**). Therefore, it is believed that there is no easy way to directly incorporate discrete fracture network model into widely used commercial numerical simulators and it leads to the motivation of this project, using semi-analytical approach to describe natural fracture network in the flow problem.

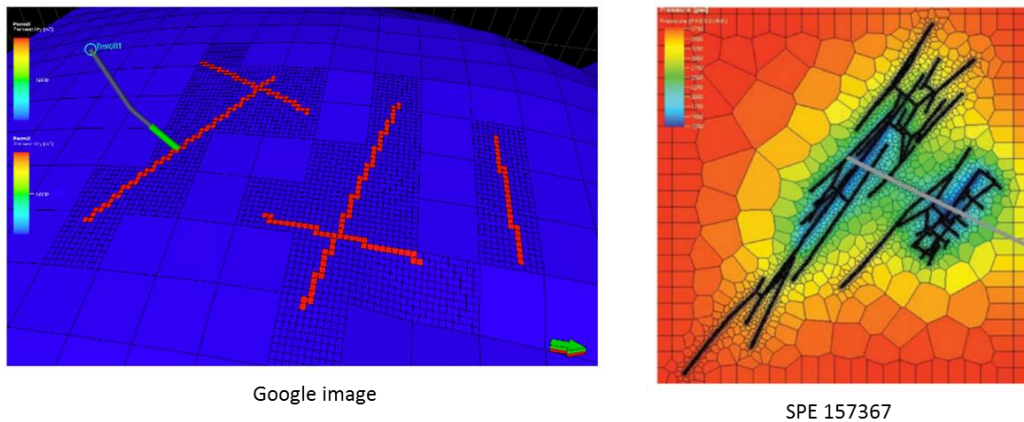


Fig. 3—DFN representation in commercial numerical simulators.

1.3 Objective and Approach

The objectives of the study are

1. Develop a methodology to predict the performance of horizontal wells with multiple transverse fractures in a naturally fractured reservoir by
 - Using source function and superposition method.
 - Applying a suitable natural fractures generation model.
 - Improving the calculation efficiency.

2. Establish a relationship between well performance and the characteristics of natural fractures.
3. Apply the new method as an optimization tool to obtain the best completion scheme for a given natural fracture cases.

CHAPTER II

MODEL DEVELOPMENT

The source function approach has long been used to solve various problems in petroleum industry. This chapter discusses the basic concept of source function. Among several forms of sources, a semi-analytical slab source developed to solve the fractured well problems in finite reservoir is first introduced. A plane source to handle the fractures which are non-orthogonally located with the boundaries of the reservoir is also presented. We then introduce the generation of natural fracture system, which will be used as a prior template for hydraulic fracture treatment. Combining hydraulic and natural fractures and building a complex fracture system follows. The approach to account for the adsorbed gas in the shale reservoir is presented. We will also discuss the computation efficiency issue.

2.1 Source Function Method

The flow problem of a single-phase incompressible fluid in a porous media is described by diffusivity equation. The diffusivity equation for a homogeneous medium is simply written as

$$\frac{\partial^2 p}{\partial x^2} = \frac{\phi \mu c_t}{k} \frac{\partial p}{\partial t} \quad (2.1)$$

There are many techniques to solve this diffusivity equation, such as Laplace transform and Fourier transform, and source function method is one of them. The solution from source function method for transient flow in a porous medium is the pressure that

would be created at certain point of a reservoir, by an instantaneously applied source at some other point of the reservoir. Sources/sinks are simply production/injection wells in petroleum engineering. As shown in **Fig. 4**, the pressure difference at point M (observer) in the reservoir at certain time t is due to a source of q at the well, which is a point M_w , at time τ . And the relationship between the pressure difference and the source of q is represented by source function S .

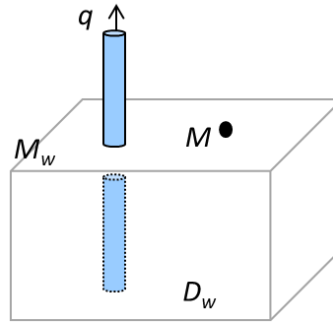


Fig. 4—Schematic of source function method.

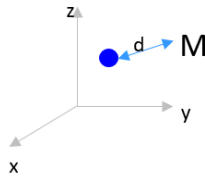
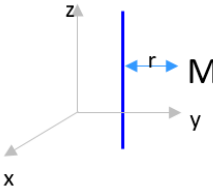
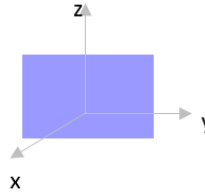
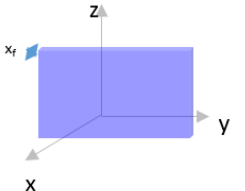
$$\Delta p(M, t) = p_i - p(M, t) = \frac{q}{\phi \mu c_i} \int_0^t q(M_w, \tau) S(M, t - \tau) d\tau \quad (2.2)$$

The source function S in the above equation is the integral of green's function G .

$$S(M, t) = \int_{D_w} G(M, M_w, t) dM_w \quad (2.3)$$

The advantage of using source function method is that S is known for many types of sources, such as point, line and plane at the defined boundary conditions. Gringarten and Ramey (1973) first introduced this method into petroleum industry, honoring the original work of Carslaw and Jaeger (1959). **Table 1** summarizes known basic instantaneous source functions S in infinite reservoirs.

Table 1—Basic instantaneous source functions S in infinite reservoirs. Adapted from Gringarten and Ramey, 1973.

Type of source	Instantaneous source function
Point source	
	$S = \frac{1}{8(\pi\eta t)^{3/2}} \exp\left[-\frac{d^2}{4\eta t}\right]$
Infinite line source	
	$S = \frac{1}{4\pi\eta_r t} \exp\left[-\frac{r^2}{4\eta_r t}\right]$
Infinite plane source	
	$S = \frac{1}{2\sqrt{\pi\eta_x t}} \exp\left[-\frac{(x-x_o)^2}{4\eta_x t}\right]$
Infinite slab source	
	$S = \frac{1}{2} \left[\operatorname{erf} \frac{x_f + (x-x_o)}{2\sqrt{\eta_x t}} + \operatorname{erf} \frac{x_f - (x-x_o)}{2\sqrt{\eta_x t}} \right]$

For a three-dimensional problem, the solution can also be solved easily with this approach. The diffusivity equation in one-dimensional anisotropic medium is written as

$$k_x \frac{\partial^2 p}{\partial x^2} + k_y \frac{\partial^2 p}{\partial y^2} + k_z \frac{\partial^2 p}{\partial z^2} = \phi\mu c_t \frac{\partial p}{\partial t} \quad (2.4)$$

Newman (1936) has shown that the solution of a three-dimensional problem is equal to the product of the solutions of three one-dimensional problems. In other words, the instantaneous Green's function for a reservoir that can be visualized as the intersection of one-dimensional reservoirs is equal to the product of the instantaneous Green's functions for each one-dimensional reservoir.

$$S(x, y, z, t) = S_x(t) \cdot S_y(t) \cdot S_z(t) \quad (2.5)$$

Therefore, we need to consider only a limited number of basic one-dimensional sources, such as plane source, in dealing with three-dimensional reservoir problems, for which instantaneous source functions will be obtained by product.

2.2 Slab Source Solution

2.2.1 Slab source approach for single fracture

The slab in the slab source approach is a box-shaped object, known as rectangular parallelepiped or a rectangular cuboid. A slab source in three-dimensional finite domain is considered as the intersection of three one-dimensional perpendicular slab sources in x, y and z direction (**Fig. 5**). A slab source in one-dimensional space is an infinite plane which has finite thickness. Therefore, the final source function, S, can be obtained by multiplying three one-dimensional slab sources, S_x, S_y and S_z together following Newman's method (**Eq. 2.5**).

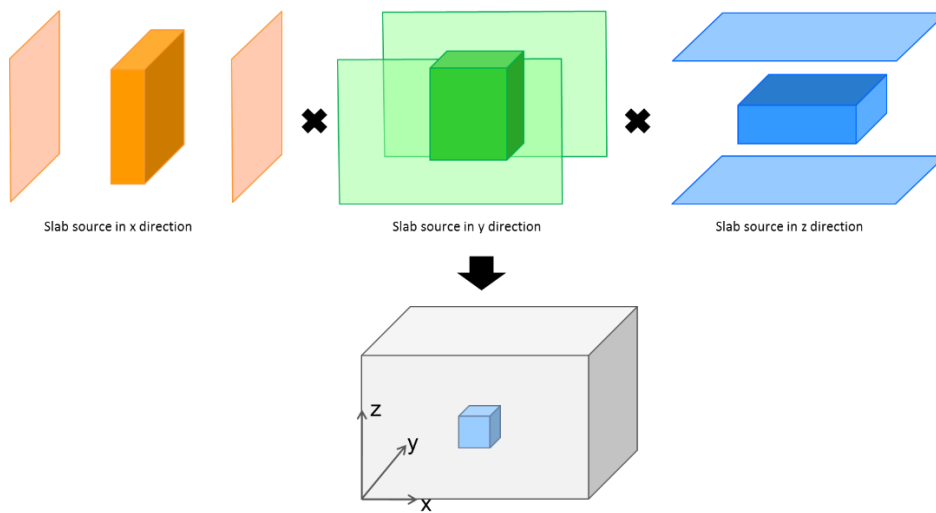


Fig. 5—A slab source in three-dimensional finite domain as a multiplication of three one-dimensional infinite slab sources.

The boundary condition of this approach can be constant pressure, no-flow or mixed boundary, which makes the solution practical to a wide range of flow problems in petroleum engineering. **Table 2** summarizes the basic instantaneous source functions for an infinite slab source in an infinite slab reservoir.

Table 2—Basic instantaneous source functions for an infinite slab source in an infinite slab reservoir. Adapted from Gringarten and Ramey, 1973.

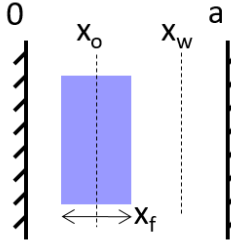
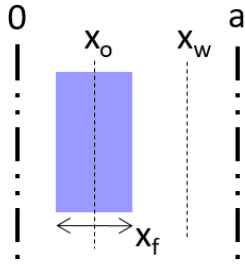
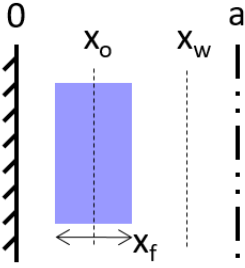
Boundary conditions	Instantaneous source function
No flow at $x=0$, $x=a$	$S_x = \frac{x_f}{a} \left[1 + \frac{4a}{\pi x_f} \sum_{n=1}^{\infty} \frac{1}{n} \sin \frac{n\pi x_f}{2a} \cos \frac{n\pi x_0}{a} \cos \frac{n\pi x}{a} \exp \left[-\frac{n^2 \pi^2 k_x \tau}{\alpha a^2} \right] \right]$
	

Table 2 Continued

Boundary conditions	Instantaneous source function
<p>Constant pressure at $x=0, x=a$</p> 	$S_x = \frac{4}{\pi} \sum_{n=1}^{\infty} \frac{1}{n} \sin \frac{n\pi x_f}{2a} \sin \frac{n\pi x_o}{a} \sin \frac{n\pi x}{a} \exp \left[-\frac{n^2 \pi^2 k_x \tau}{\alpha a^2} \right]$
<p>No flow at $x=0$, constant pressure at $x=a$</p> 	$S_x = \frac{8}{\pi} \sum_{n=1}^{\infty} \left(\frac{1}{2n+1} \sin \frac{(2n+1)\pi x_f}{4a} \cos \frac{(2n+1)\pi x_o}{a} \cdot \cos \frac{(2n+1)\pi x}{a} \cdot \exp \left[-\frac{(2n+1)^2 \pi^2 k_x \tau}{4\alpha a^2} \right] \right)$

If no flow boundary condition is assumed, the pressure distribution in a reservoir having dimensions of a , b , and h due to the small source in the middle of the domain as in **Fig. 6** is calculated by

$$\Delta p = p_i - p(x, y, z, t) = \frac{q}{\phi \mu c_i} \int_0^t (S_x \cdot S_y \cdot S_z) d\tau \quad (2.6)$$

Here, the source functions in x , y and z directions are

$$S_x = \frac{x_f}{a} \left[1 + \frac{4a}{\pi x_f} \sum_{n=1}^{\infty} \frac{1}{n} \sin \frac{n\pi x_f}{2a} \cos \frac{n\pi x_o}{a} \cos \frac{n\pi x}{a} \exp \left(-\frac{n^2 \pi^2 k_x \tau}{\alpha a^2} \right) \right] \quad (2.7)$$

$$S_y = \frac{y_f}{b} \left[1 + \frac{4b}{\pi y_f} \sum_{n=1}^{\infty} \frac{1}{n} \sin \frac{n\pi y_f}{2b} \cos \frac{n\pi y_0}{b} \cos \frac{n\pi y}{b} \exp\left(-\frac{n^2 \pi^2 k_y \tau}{\alpha b^2}\right) \right]$$

$$S_z = \frac{z_f}{h} \left[1 + \frac{4h}{\pi z_f} \sum_{n=1}^{\infty} \frac{1}{n} \sin \frac{n\pi z_f}{2h} \cos \frac{n\pi z_0}{h} \cos \frac{n\pi z}{h} \exp\left(-\frac{n^2 \pi^2 k_z \tau}{\alpha h^2}\right) \right]$$

In the above equations, x_0, y_0 and z_0 are the location of a source and x_f, y_f, z_f are the widths of the source, respectively.

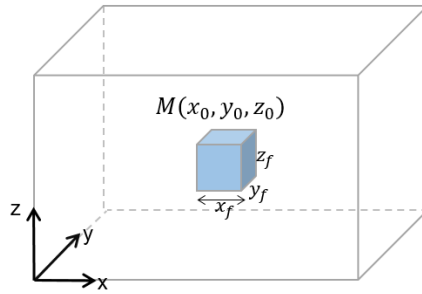


Fig. 6—Schematic of a slab source in three-dimensional domain.

The advantage about the slab source approach is that it is simple to use without the integration of **Eq. 2.4** and it enables the calculation of pressure at the point of source. The solution from this technique applies to both transient flow and stabilized flow. Also, the slab source approach can handle various geometries of interest. The geometries can be a vertical well, a horizontal well, a slanted well, a single hydraulic fracture or multiple hydraulic fractures. For example, if we want to calculate the pressure drop inside the reservoir due to production through single hydraulic fracture, which is a source, we simply need to follow the procedures as,

Step 1 - Obtain instantaneous one-dimensional slab source under defined boundary conditions in x, y and z directions.

Step 2 – Multiply one-dimensional solutions in x, y and z directions and derive a three-dimensional solution.

Step 3 - Integrate obtained three-dimensional solution over time since the source is continuous.

Step 4 - Integrate the solution over the geometry of our interest, a single hydraulic fracture in this case, to accommodate the actual volume of the source.

In **Fig. 7**, the procedure for applying slab source function method to solve real reservoir problems is summarized.

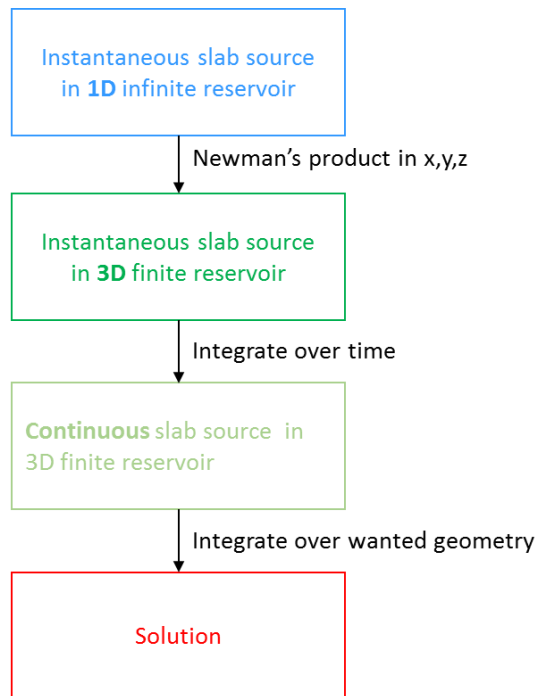


Fig. 7—Flow chart of source function method.

As an example, the pressure solution for a slab source representing a fracture as in **Fig. 8** can be written as,

$$\Delta p = p_i - p(x, y, z, t) = \frac{q}{\phi \mu c_t} \int_0^t \int_{z_1}^{z_2} \int_{y_1}^{y_2} \int_{x_1}^{x_2} (S_x \cdot S_y \cdot S_z) dx dy dz d\tau \quad (2.8)$$

As we discussed, the source function is integrated for the time to give continuous solution and for the space to give the geometry of the fracture. The final solution of **Eq. 2.8** in oil field unit is concluded as follows (**Eq. 2.9**).

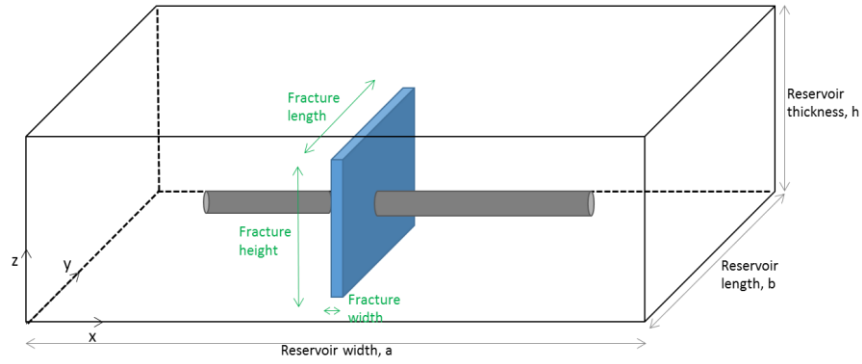


Fig. 8—Schematic of a single fracture in three-dimensional domain.

$$P_{\text{int}} - p(x, y, z, t) = \frac{B\mu q x_f y_f z_f}{\alpha a b h} [A_0 + A_1 + A_2 + A_3 + A_{12} + A_{13} + A_{23} + A_{123}] \quad (2.9)$$

The each elements on the right hand side of **Eq. 2.9** is the obtained after the integration in time and space.

$$A_0 = t(x_2 - x_1)(y_2 - y_1)(z_2 - z_1)$$

$$A_1 = \frac{4\alpha a^4}{\pi^4 x_f k_x} \sum_{n=1}^{\infty} \frac{1}{n^4} \sin \frac{n\pi x_f}{2a} \cos \frac{n\pi x_0}{a} \left(\sin \frac{n\pi x_2}{a} - \sin \frac{n\pi x_1}{a} \right) (y_2 - y_1)(z_2 - z_1)$$

$$A_2 = \frac{4\alpha b^4}{\pi^4 y_f k_y} \sum_{m=1}^{\infty} \frac{1}{m^4} \sin \frac{m\pi y_f}{2b} \cos \frac{m\pi y_0}{b} \left(\sin \frac{m\pi y_2}{b} - \sin \frac{m\pi y_1}{b} \right) (x_2 - x_1)(z_2 - z_1)$$

$$A_3 = \frac{4\alpha h^4}{\pi^4 z_f k_z} \sum_{l=1}^{\infty} \frac{1}{l^4} \sin \frac{l\pi z_f}{2h} \cos \frac{l\pi z_0}{h} \left(\sin \frac{l\pi z_2}{h} - \sin \frac{l\pi z_1}{h} \right) (x_2 - x_1)(y_2 - y_1)$$

$$A_{12} = \frac{16\alpha a^2 b^2}{\pi^6 x_f y_f} \sum_{n=1}^{\infty} \sum_{m=1}^{\infty} \left\{ \frac{(z_2 - z_1)}{n^2 m^2} \left(\frac{1}{\frac{n^2 k_x}{a^2} + \frac{m^2 k_y}{b^2}} \right) \sin \frac{n\pi x_f}{2a} \cos \frac{n\pi x_0}{a} \sin \frac{m\pi y_f}{2b} \cos \frac{m\pi y_0}{b} \cdot \right. \\ \left. \left(\sin \frac{n\pi x_2}{a} - \sin \frac{n\pi x_1}{a} \right) \left(\sin \frac{m\pi y_2}{b} - \sin \frac{m\pi y_1}{b} \right) \right\}$$

$$A_{13} = \frac{16\alpha a^2 h^2}{\pi^6 x_f z_f} \sum_{n=1}^{\infty} \sum_{l=1}^{\infty} \left\{ \frac{(y_2 - y_1)}{n^2 l^2} \left(\frac{1}{\frac{n^2 k_x}{a^2} + \frac{l^2 k_z}{h^2}} \right) \sin \frac{n\pi x_f}{2a} \cos \frac{n\pi x_0}{a} \sin \frac{l\pi z_f}{2h} \cos \frac{l\pi z_0}{h} \cdot \right. \\ \left. \left(\sin \frac{n\pi x_2}{a} - \sin \frac{n\pi x_1}{a} \right) \left(\sin \frac{l\pi z_2}{h} - \sin \frac{l\pi z_1}{h} \right) \right\}$$

$$A_{23} = \frac{16\alpha b^2 h^2}{\pi^6 y_f z_f} \sum_{m=1}^{\infty} \sum_{l=1}^{\infty} \left\{ \frac{(x_2 - x_1)}{m^2 l^2} \left(\frac{1}{\frac{m^2 k_y}{b^2} + \frac{l^2 k_z}{h^2}} \right) \sin \frac{m\pi y_f}{2b} \cos \frac{m\pi y_0}{b} \sin \frac{l\pi z_f}{2h} \cos \frac{l\pi z_0}{h} \cdot \right. \\ \left. \left(\sin \frac{m\pi y_2}{b} - \sin \frac{m\pi y_1}{b} \right) \left(\sin \frac{l\pi z_2}{h} - \sin \frac{l\pi z_1}{h} \right) \right\}$$

$$A_{123} = \frac{64\alpha a^2 b^2 h^2}{\pi^8 x_f y_f z_f} \sum_{n=1}^{\infty} \sum_{m=1}^{\infty} \sum_{l=1}^{\infty} \left\{ \frac{1}{n^2} \frac{1}{m^2} \frac{1}{l^2} \left(\frac{1}{\frac{n^2 k_x}{a^2} + \frac{m^2 k_y}{b^2} + \frac{l^2 k_z}{h^2}} \right) \cdot \right. \\ \left. \sin \frac{n\pi x_f}{2a} \cos \frac{n\pi x_0}{a} \sin \frac{m\pi y_f}{2b} \cos \frac{m\pi y_0}{b} \sin \frac{l\pi z_f}{2h} \cos \frac{l\pi z_0}{h} \cdot \right. \\ \left. \left(\sin \frac{n\pi x_2}{a} - \sin \frac{n\pi x_1}{a} \right) \left(\sin \frac{m\pi y_2}{b} - \sin \frac{m\pi y_1}{b} \right) \cdot \right. \\ \left. \left(\sin \frac{l\pi z_2}{h} - \sin \frac{l\pi z_1}{h} \right) \right\}$$

where, $\alpha = 158.73\phi\mu c_i$. The solutions for the other boundary conditions are summarized in Appendix I.

2.2.2 Source function approach for multiple fractures

The analytical solution for fractured wells have been first developed by Gringarten et al. (1974a, 1974b) for the uniform flux and infinite conductivity fractures. With the uniform flux solution, the flow per unit of fracture surface is assumed constant along the fracture length, while the infinite conductivity model is based on the assumption that the pressure is uniform in the fracture. The solutions are obtained by dividing the fracture length into M segments, and using the Green's function and Newman's product solution method. This segment approach can be extended to calculate the pressure response in a reservoir where multiple hydraulic fractures are located.

As a start for multiple fractures case, we have simplified two fractures case (**Fig. 9a**). We are assuming all the flows from the reservoir are occurring through the fractures. If we place fracture #1 in the system, this will cause pressure change and then, a flow of q_1 at its location. This q_1 causes subsequent pressure changes in the entire domain. If we put fracture #2 into the system, this will generate flow rate q_2 and affect the pressures at the locations of fracture #1 and fracture #2 as well.

Therefore, each fracture should be treated as an individual source. And the pressure changes at each fracture should be the sum of the pressure drops caused by all the fractures in the system. The problem can be solved under the constant flow rate or constant wellbore pressure constrains.

Let us make segments for the fractures to sub-sources (**Fig. 9b**), then the pressure change at segment i as a result of each segment producing at a constant rate of q_j is evaluated by multiplying q_j with $F(i, j)$.

$$p_{ini} - p(i, t) = \beta \sum_{j=1}^n q_j F(i, j) \quad (2.10)$$

where $F(i, j)$ represents the continuous source functions for the geometry of our interest and β is a coefficient.

$$F(i, j) = \int_{z_1}^{z_2} \int_{y_1}^{y_2} \int_{x_1}^{x_2} \int_0^t (s_x s_y s_z) d\tau dx dy dz \quad (2.11)$$

For this two fractures case, the pressure change at each segment i is summarized as follows:

$$\begin{aligned} p_i - p_1 &= \beta [q_1 F(1,1) + q_2 F(1,2)] \\ p_i - p_2 &= \beta [q_1 F(2,1) + q_2 F(2,2)] \end{aligned} \quad (2.12)$$

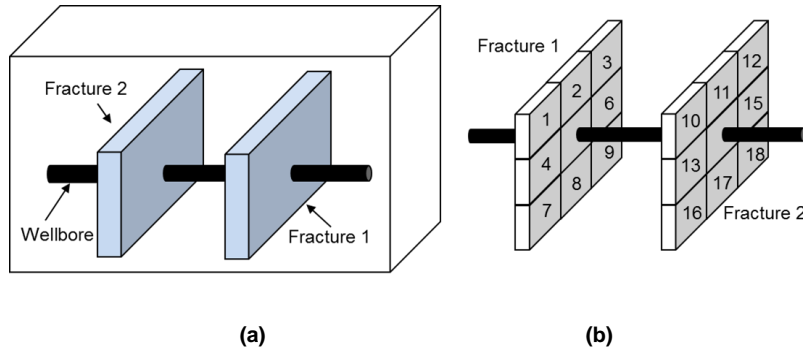


Fig. 9—Multiple hydraulic fractures in three-dimensional domain.

To account for the infinite conductivity condition for fracture, we need to divide the fracture into segments following the approach of Gringarten et al. (1974a, 1974b). For

example, as shown in **Fig. 9b**, we have two fractures in the reservoir, each has 9 (3 by 3) segments in it. The segments are in contact with each other inside the fracture and each segment will cause a flow rate from the reservoir. Because of the flow rate in the segment #1, the pressure for the other 17 segments will change. This pressure change as a result of flow rate q_1 is calculated using **Eq. 2.9**. Therefore, this results in 18 $F(1, j)$ terms, one term per each segment, such as $q_1 F(1,1), q_1 F(2,1), \dots, q_1 F(18,1)$. The pressure changes are calculated at the middle of each fracture segment.

Similarly, the flow rate of the second segment, q_2 , will change the pressure distribution in the other 17 segments, giving additional 18 $F(2, j)$ terms. By repeating this procedure for all 18 segments, we can obtain 18 by 18 $F(i, j)$ terms. By using superposition principle in space, a system of linear equations is obtained.

$$\begin{aligned}
q_1 F(1,1) + q_2 F(1,2) + q_3 F(1,3) + \dots + q_N F(1,N) &= \Delta p_1 \\
q_1 F(2,1) + q_2 F(2,2) + q_3 F(2,3) + \dots + q_N F(2,N) &= \Delta p_2 \\
q_1 F(3,1) + q_2 F(3,2) + q_3 F(3,3) + \dots + q_N F(3,N) &= \Delta p_3 \\
&\vdots \\
q_1 F(N,1) + q_2 F(N,2) + q_3 F(N,3) + \dots + q_N F(N,N) &= \Delta p_N
\end{aligned} \tag{2.13}$$

where, q_j is a constant flow rate into segment j and Δp_i is the pressure drop calculated at segment i as a result of the production into every segment. The total production from the

fracture is either the sum of production from each segment or the constant production rate constraint.

$$\sum_{j=1}^N q_j = q_{total} \quad (2.14)$$

The fractures could be in uniform flux, infinite conductivity or finite conductivity boundary condition (inner boundary condition). Constant flow rate or constant wellbore pressure can be applied as a well constraint (outer boundary condition) to solve the system of linear equations (**Eq. 2.13**). If infinite conductivity fracture is assumed, the wellbore pressure is constant along the fracture (**Eq. 2.15**), and therefore, flow rate for each segment q_j can be obtained by solving **Eq. 2.13**.

$$p_1 = p_2 = \dots = p_N = p_{wf} \quad (2.15)$$

If finite conductivity is assumed, pressure drop inside fractures can be calculated with defined conductivity (fracture permeability).

2.3 Plane Source Solution

Natural fractures can be added at any location, direction, pattern or arrangement in the reservoir. As an approach to handle these randomly distributed fractures with reduced calculation time, a plane source method was introduced. In this approach, fractures is regarded as a plane which does not have width. The plane has the initial and end points in x and y directions. And by connecting these points and having the fracture height the same as the reservoir, a plane which is perpendicular to the surface is created. **Fig. 10** shows a schematic of a fracture using the plane source concept.

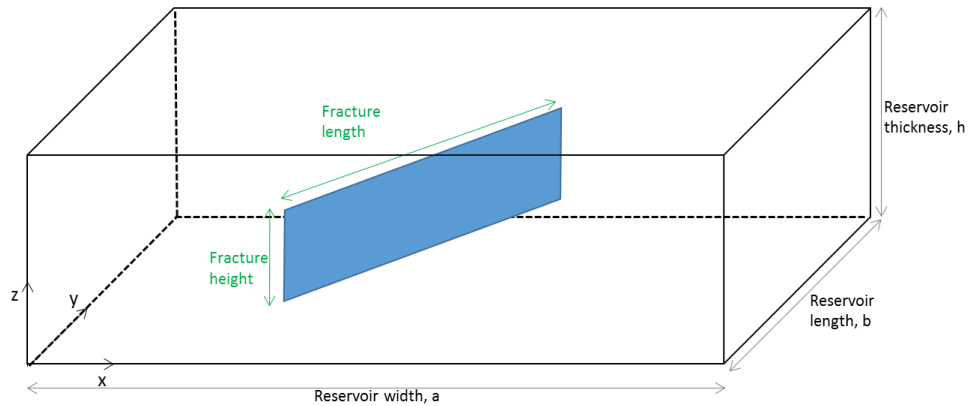


Fig. 10—Schematic of a fracture used in plane source approach.

As discussed previously, any type of new source function can be derived from basic source function shown in **Table 1** and **Table 2** by product or integration. The procedure for obtaining final form of plane sources is defined below.

First, we start by obtaining a point source in finite reservoir by multiplication of three plane sources in finite reservoir. Notice that in the original publication in **Table 1** and **Table 2**, there is no solution for finite reservoir. Secondly, a line source is obtained by integrating a point along line C which connects 2 end points, (x_1, y_1) and (x_2, y_2) . Finally, a plane source is derived by integrating the line source obtained in z direction. **Fig. 11** shows the schematic of creating plane source by connecting straight lines between points.

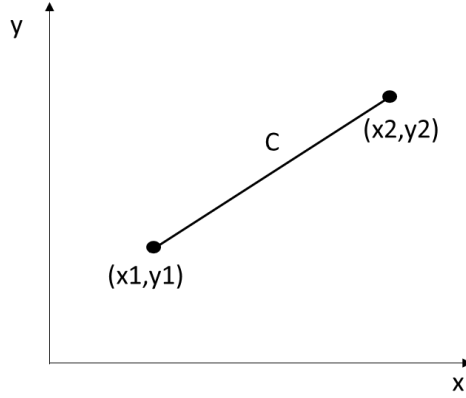


Fig. 11—Schematic of a straight line connecting 2 end points.

To show the equations for step 1, the point source in a reservoir size of a , b and h in x , y and z direction is given as

$$S = \frac{1}{abh} \left[\begin{array}{l} \left\{ 1 + 2 \sum_{n=1}^{\infty} \exp\left(-\frac{n^2 \pi^2 k_x}{\alpha a^2} \tau\right) \cos \frac{n \pi x_0}{a} \cos \frac{n \pi x}{a} \right\} \cdot \\ \left\{ 1 + 2 \sum_{m=1}^{\infty} \exp\left(-\frac{m^2 \pi^2 k_y}{\alpha b^2} \tau\right) \cos \frac{m \pi y_0}{b} \cos \frac{m \pi y}{b} \right\} \cdot \\ \left\{ 1 + 2 \sum_{l=1}^{\infty} \exp\left(-\frac{l^2 \pi^2 k_z}{\alpha h^2} \tau\right) \cos \frac{l \pi z_0}{h} \cos \frac{l \pi z}{h} \right\} \end{array} \right] \quad (2.16)$$

For step 2, parameterization of x and y is introduced for integration along a line C .

$$\begin{aligned} x_0 &= x_1 + (x_2 - x_1)T \\ y_0 &= y_1 + (y_2 - y_1)T \\ 0 &\leq T \leq 1 \end{aligned} \quad (2.17)$$

The arc length of the line C on the interval is calculated by

$$ds = \sqrt{\left(\frac{dx}{dT}\right)^2 + \left(\frac{dy}{dT}\right)^2} dT = \sqrt{(x_2 - x_1)^2 + (y_2 - y_1)^2} dT \quad (2.18)$$

The line integral is then

$$SS = \int_C S ds = \int_{y_1}^{y_2} \int_{x_1}^{x_2} S dx_0 dy_0 = \int_0^1 S \left(\sqrt{(x_2 - x_1)^2 + (y_2 - y_1)^2} dT \right) \quad (2.19)$$

By applying properties of trigonometric functions, **Eq. 2.19** is summarized to

$$SS = \frac{\sqrt{(x_2 - x_1)^2 + (y_2 - y_1)^2}}{abh} [1 + B_1 + B_2 + B_3 + B_{12} + B_{13} + B_{23} + B_{123}] \quad (2.20)$$

where,

$$B_1 = 2 \sum_{n=1}^{\infty} \left\{ \exp \left(-\frac{n^2 \pi^2 k_x}{\alpha a^2} \tau \right) \left(\frac{a}{n\pi(x_2 - x_1)} \right) \left(\sin \frac{n\pi x_2}{a} - \sin \frac{n\pi x_1}{a} \right) \cos \frac{n\pi x}{a} \right\}$$

$$B_2 = 2 \sum_{m=1}^{\infty} \left\{ \exp \left(-\frac{m^2 \pi^2 k_y}{\alpha b^2} \tau \right) \left(\frac{b}{m\pi(y_2 - y_1)} \right) \left(\sin \frac{m\pi y_2}{b} - \sin \frac{m\pi y_1}{b} \right) \cos \frac{m\pi y}{b} \right\}$$

$$B_3 = 2 \sum_{l=1}^{\infty} \left\{ \exp \left(-\frac{l^2 \pi^2 k_z}{\alpha h^2} \tau \right) \cos \frac{l\pi z_0}{h} \cos \frac{l\pi z}{h} \right\}$$

$$B_{12} = 4 \sum_{n=1}^{\infty} \sum_{m=1}^{\infty} \left\{ \frac{1}{2} \left[\frac{\exp \left(-\frac{n^2 \pi^2 k_x}{\alpha a^2} \tau - \frac{m^2 \pi^2 k_y}{\alpha b^2} \tau \right) \cos \frac{n\pi x}{a} \cos \frac{m\pi y}{b} \cdot \left[\frac{\sin \left(\frac{n\pi x_2}{a} - \frac{m\pi y_2}{b} \right) - \sin \left(\frac{n\pi x_1}{a} - \frac{m\pi y_1}{b} \right)]}{\left(\frac{n\pi(x_2 - x_1)}{a} - \frac{m\pi(y_2 - y_1)}{b} \right)} \right] \right. \right. \\ \left. \left. + \left[\frac{\sin \left(\frac{n\pi x_2}{a} + \frac{m\pi y_2}{b} \right) - \sin \left(\frac{n\pi x_1}{a} + \frac{m\pi y_1}{b} \right)]}{\left(\frac{n\pi(x_2 - x_1)}{a} + \frac{m\pi(y_2 - y_1)}{b} \right)} \right] \right\}$$

$$\begin{aligned}
B_{13} &= 4 \sum_{n=1}^{\infty} \sum_{l=1}^{\infty} \left\{ \exp \left(-\frac{n^2 \pi^2 k_x}{\alpha a^2} \tau - \frac{l^2 \pi^2 k_z}{\alpha h^2} \tau \right) \left(\frac{a}{n\pi(x_2 - x_1)} \right) \cdot \right. \\
&\quad \left. \left(\sin \frac{n\pi x_2}{a} - \sin \frac{n\pi x_1}{a} \right) \cos \frac{n\pi x}{a} \cos \frac{l\pi z_0}{h} \cos \frac{l\pi z}{h} \right\} \\
B_{23} &= 4 \sum_{m=1}^{\infty} \sum_{l=1}^{\infty} \left\{ \exp \left(-\frac{m^2 \pi^2 k_y}{\alpha b^2} \tau - \frac{l^2 \pi^2 k_z}{\alpha h^2} \tau \right) \left(\frac{b}{m\pi(y_2 - y_1)} \right) \cdot \right. \\
&\quad \left. \left(\sin \frac{m\pi y_2}{b} - \sin \frac{m\pi y_1}{b} \right) \cos \frac{m\pi y}{b} \cos \frac{l\pi z_0}{h} \cos \frac{l\pi z}{h} \right\} \\
B_{123} &= 8 \sum_{n=1}^{\infty} \sum_{m=1}^{\infty} \sum_{l=1}^{\infty} \left\{ \exp \left(-\frac{n^2 \pi^2 k_x}{\alpha a^2} \tau - \frac{m^2 \pi^2 k_y}{\alpha b^2} \tau - \frac{l^2 \pi^2 k_z}{\alpha h^2} \tau \right) \cdot \right. \\
&\quad \cos \frac{n\pi x}{a} \cos \frac{m\pi y}{b} \cos \frac{l\pi z_0}{h} \cos \frac{l\pi z}{h} \cdot \\
&\quad \left. \frac{\left[\sin \left(\frac{n\pi x_2}{a} - \frac{m\pi y_2}{b} \right) - \sin \left(\frac{n\pi x_1}{a} - \frac{m\pi y_1}{b} \right) \right]}{\left(\frac{n\pi(x_2 - x_1)}{a} - \frac{m\pi(y_2 - y_1)}{b} \right)} \right. \\
&\quad \left. + \frac{\left[\sin \left(\frac{n\pi x_2}{a} + \frac{m\pi y_2}{b} \right) - \sin \left(\frac{n\pi x_1}{a} + \frac{m\pi y_1}{b} \right) \right]}{\left(\frac{n\pi(x_2 - x_1)}{a} + \frac{m\pi(y_2 - y_1)}{b} \right)} \right\} \cdot
\end{aligned}$$

The plane source is finally obtained by integrating the line source in z direction from z_1 to z_2 .

$$SSS = \frac{\sqrt{(x_2 - x_1)^2 + (y_2 - y_1)^2}}{abh} \int_{z_1}^{z_2} SS dz_0 \quad (2.21)$$

After integrating with respect to time, **Eq. 2.21** is reduces to

$$SSS = \frac{\sqrt{(x_2 - x_1)^2 + (y_2 - y_1)^2}}{abh} [C_0 + C_1 + C_2 + C_3 + C_{12} + C_{13} + C_{23} + C_{123}] \quad (2.22)$$

where,

$$C_0 = (z_2 - z_1)t$$

$$C_1 = 2 \sum_{n=1}^{\infty} \left\{ \left(\frac{\alpha a^3}{n^3 \pi^3 k_x (x_2 - x_1)} \right) \left(1 - \exp \left(- \frac{n^2 \pi^2 k_x}{\alpha a^2} t \right) \right) \right. \\ \left. \left(\sin \frac{n\pi x_2}{a} - \sin \frac{n\pi x_1}{a} \right) \cos \frac{n\pi x}{a} (z_2 - z_1) \right\}$$

$$C_2 = 2 \sum_{m=1}^{\infty} \left\{ \left(\frac{\alpha b^3}{m^3 \pi^3 k_y (y_2 - y_1)} \right) \left(1 - \exp \left(- \frac{m^2 \pi^2 k_y}{\alpha b^2} t \right) \right) \right. \\ \left. \left(\sin \frac{m\pi y_2}{b} - \sin \frac{m\pi y_1}{b} \right) \cos \frac{m\pi y}{b} (z_2 - z_1) \right\}$$

$$C_3 = 2 \sum_{l=1}^{\infty} \left(\frac{\alpha h^3}{l^3 \pi^3 k_z} \right) \left(1 - \exp \left(- \frac{l^2 \pi^2 k_z}{\alpha h^2} t \right) \right) \left(\sin \frac{l\pi z_2}{h} - \sin \frac{l\pi z_1}{h} \right) \cos \frac{l\pi z}{h}$$

$$C_{12} = 2 \sum_{n=1}^{\infty} \sum_{m=1}^{\infty} \left\{ \left(\frac{\alpha a^2 b^2}{\pi^2 (b^2 n^2 k_x + a^2 m^2 k_y)} \right) \left(1 - \exp \left(- \left(\frac{n^2 k_x}{a^2} + \frac{m^2 k_y}{b^2} \right) \frac{\pi^2 t}{\alpha} \right) \right) \right. \\ \left. \cos \frac{n\pi x}{a} \cos \frac{m\pi y}{b} \cdot (z_2 - z_1) \cdot \right. \\ \left. \left[\frac{\left(\sin \left(\frac{n\pi x_2}{a} - \frac{m\pi y_2}{b} \right) - \sin \left(\frac{n\pi x_1}{a} - \frac{m\pi y_1}{b} \right) \right)}{(bn\pi(x_2 - x_1) - am\pi(y_2 - y_1))} \right] \right. \\ \left. + \left[\frac{\left(\sin \left(\frac{n\pi x_2}{a} + \frac{m\pi y_2}{b} \right) - \sin \left(\frac{n\pi x_1}{a} + \frac{m\pi y_1}{b} \right) \right)}{(bn\pi(x_2 - x_1) + am\pi(y_2 - y_1))} \right] \right\}$$

$$C_{13} = 4 \sum_{n=1}^{\infty} \sum_{l=1}^{\infty} \left\{ \left(\frac{\alpha a^3 h^3}{\pi^4 n l (h^2 n^2 k_x + a^2 l^2 k_z)} (x_2 - x_1) \right) \cdot \left(1 - \exp \left(- \left(\frac{n^2 k_x}{a^2} + \frac{l^2 k_z}{h^2} \right) \frac{\pi^2 t}{\alpha} \right) \right) \cdot \left(\sin \frac{n\pi x_2}{a} - \sin \frac{n\pi x_1}{a} \right) \left(\sin \frac{l\pi z_2}{h} - \sin \frac{l\pi z_1}{h} \right) \cos \frac{l\pi z}{h} \cos \frac{n\pi x}{a} \right\}$$

$$C_{23} = 4 \sum_{m=1}^{\infty} \sum_{l=1}^{\infty} \left\{ \left(\frac{\alpha b^3 h^3}{\pi^4 m l (h^2 m^2 k_y + b^2 l^2 k_z)} (y_2 - y_1) \right) \cdot \left(1 - \exp \left(- \left(\frac{m^2 k_y}{b^2} + \frac{l^2 k_z}{h^2} \right) \frac{\pi^2 t}{\alpha} \right) \right) \cdot \left(\sin \frac{m\pi y_2}{b} - \sin \frac{m\pi y_1}{b} \right) \left(\sin \frac{l\pi z_2}{h} - \sin \frac{l\pi z_1}{h} \right) \cos \frac{l\pi z}{h} \cos \frac{m\pi y}{b} \right\}$$

$$C_{123} = 4 \sum_{n=1}^{\infty} \sum_{m=1}^{\infty} \sum_{l=1}^{\infty} \left\{ \left(\frac{\alpha a^2 b^2 h^3}{\pi^3 l (b^2 h^2 n^2 k_x + a^2 h^2 m^2 k_y + a^2 b^2 l^2 k_z)} \right) \cdot \left(1 - \exp \left(- \left(\frac{n^2 k_x}{a^2} + \frac{m^2 k_y}{b^2} + \frac{l^2 k_z}{h^2} \right) \frac{\pi^2 t}{\alpha} \right) \right) \cdot \cos \frac{n\pi x}{a} \cos \frac{m\pi y}{b} \cos \frac{l\pi z}{h} \left(\sin \frac{l\pi z_2}{h} - \sin \frac{l\pi z_1}{h} \right) \cdot \left[\frac{\left(\sin \left(\frac{n\pi x_2}{a} - \frac{m\pi y_2}{b} \right) - \sin \left(\frac{n\pi x_1}{a} - \frac{m\pi y_1}{b} \right) \right)}{(bn\pi(x_2 - x_1) - am\pi(y_2 - y_1))} \right] \right. \\ \left. + \frac{\left(\sin \left(\frac{n\pi x_2}{a} + \frac{m\pi y_2}{b} \right) - \sin \left(\frac{n\pi x_1}{a} + \frac{m\pi y_1}{b} \right) \right)}{(bn\pi(x_2 - x_1) + am\pi(y_2 - y_1))} \right] \right\}$$

2.4 Naturally Fractured Reservoir

2.4.1 Naturally fractured reservoir

Naturally fractured reservoir is defined as any reservoir in which naturally occurring fractures either have or are predicted to have a significant effect on reservoir fluid flow by Nelson (2001). Fractures are massive planar discontinuity in formation rocks, which are occurred by deformation or diagenesis. Natural fractures are frequently observed in shale reservoirs. Actually, many experts believe that we should assume every reservoir is a fractured reservoir until the evidence against it is confirmed, which indicates that naturally fractured reservoirs are very common (**Fig. 12**).

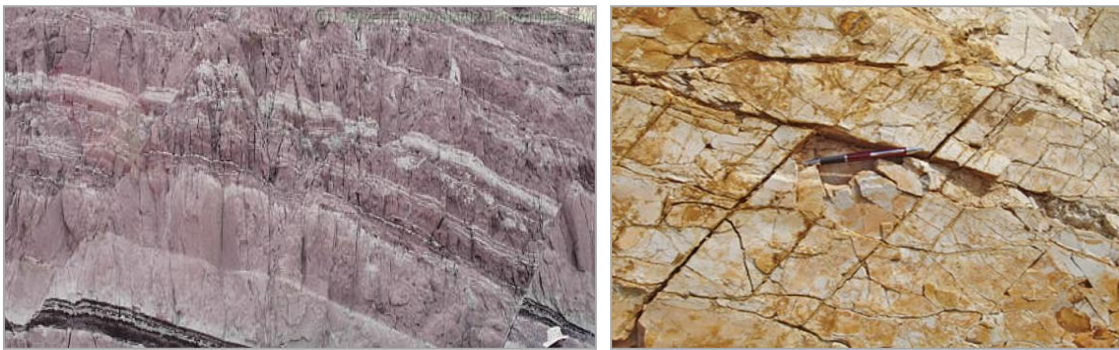


Fig. 12—Natural fractures. Reprinted from Cardott, 2006.

In shale reservoirs, gas production heavily relies on hydraulic fracturing stimulation. Natural fracture can play a significant role in it. There are several scenarios about natural fractures in shale reservoirs. The most common and advantageous case is open natural fractures. They act as conduit and enhance permeability. Natural fractures can be reactivated during hydraulic fracturing treatment, providing a larger rock volume in contact with the wellbore. But, open natural fractures may not always be beneficial. Based on the location and dimension, some fracture could cause massive leakoff during fracture

treatment and result in screen out. According to the study by Gale et al. (2010), fractured are often found sealed by cement. During a fracture treatment, the hydraulic fractures could be terminated due to natural fractures, or change its original path or simply pass through the encountered natural fractures (**Fig. 13**). Even the cores show highly sealed natural fractures, it is still possible that natural fractures are open. Cements in the fractures are not usually completely combined with grains in the wall, so the fractures act as planes of weakness that can reactivate. **Fig. 14** shows cores with open and closed natural fractures from Barnett shale, Texas (Gale et al. 2010).

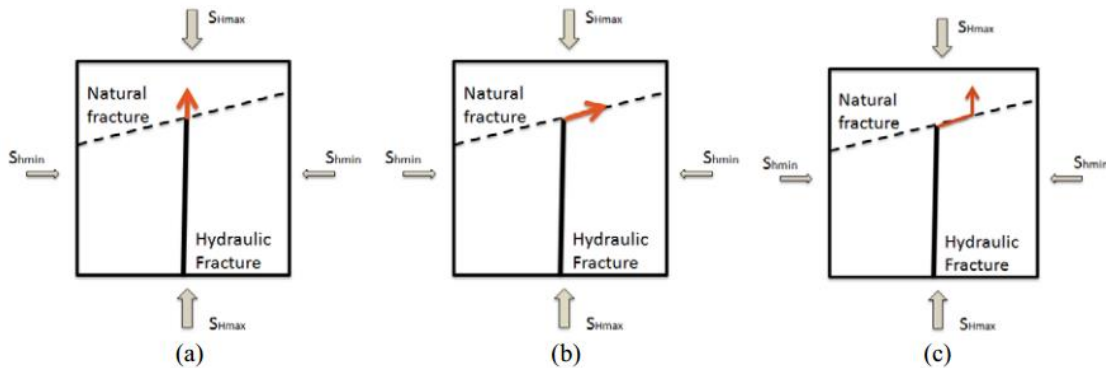


Fig. 13—Schematic of fracture interaction: (a) crossing (b) diverting (c) joggling. Reprinted from Wang et al. 2013.

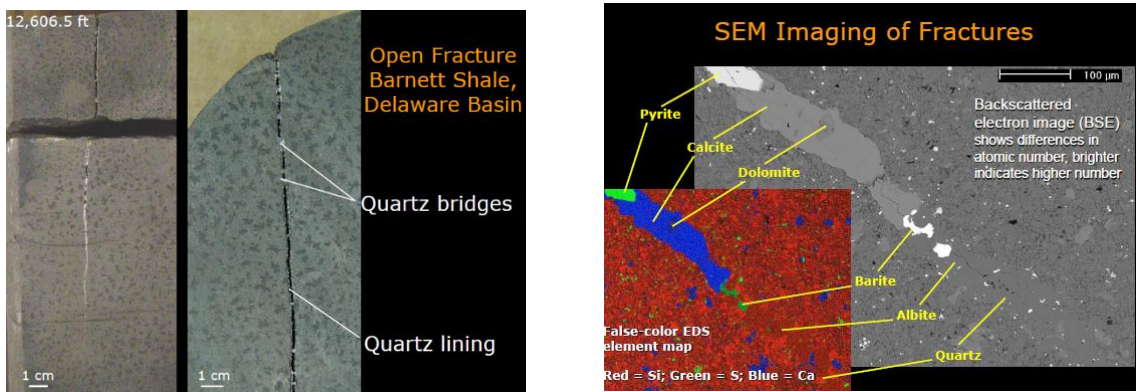


Fig. 14—Open and closed natural fractures on cores. Reprinted from Gale et al. 2010.

In this study, we assume the distribution of natural fractures are already existed and we only investigate the effects of natural fractures on hydraulically fractured well performances.

2.4.2 Fractal discrete fracture network (FDFN) system

In shale and tight sand reservoirs, extensive natural fracture systems are commonly observed. To estimate the well performance in such a reservoir, it is important to understand the characteristic structure of the natural fracture system and the impact of the natural fracture system to the flow after the well is hydraulically fractured. A stochastic method of generating fractal discrete fracture networks (FDFN) is applied in this work thanks to the help of Dr.Schechter. FDFN model was developed by Kim and Schechter (2009) originally to incorporate the various scale-dependent data, such as outcrop, log and core and predict the porosity of the fractures that have the ability to provide the essential storage capacity and permeability in a reservoir.

The theories behind the two-dimensional FDFN model vary for different parameters. Fracture length distribution is governed by first-order model, which relates the number of fractures of certain length to the domain size. Fracture density as a function of fractal parameters, expressed by (Davy et al. 1990):

$$N(L) = \frac{\alpha}{D_t} L^{D_c} l_{\min}^{-D_t} \quad (2.23)$$

where $N(L)$ is the number of fractures with the length longer than l_{\min} , minimum fracture length, L is the domain size, α is the fracture density, which is a constant value regardless

of the scale of measured or generated domains, D_c is a fractal dimension of fracture center distribution and D_l is a fractal dimension of the length distribution.

Fracture centers are generated by multiplicative cascade model. This iterative process divides a domain into smaller subdomains until the number of subdomains reaches the optimum number based on desired resolution of the domain and randomly assigns probability into each subdomain. The probabilities are calculated by (Darcel et al. 2003),

$$\sum_{i=1}^n \frac{P_i^{q_d}}{(1/sr)^{(q_d-1)D_q}} = 1 \quad (2.24)$$

where, P_i is a probability, sr is the scale ratio (ratio between the side lengths of a parent domain and subdomain), and D_q is a multi-fractal dimension. In Eq. 2.25, q_d is the degree of dimension, and it is set to 2 in this case. **Fig. 15** is an example of fracture center distribution using multiplicative cascade process. It is observed that the fracture centers are relatively uniformly distributed within the reservoir. And as we can see from the top left corner, some fractures are more clustered together than others, which resemble the nature of natural fractures.

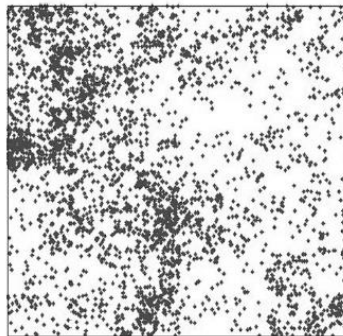


Fig. 15—Fracture center distribution generated by a multiplicative cascade process. Reprinted from Darcel et al. 2003.

Fracture orientation is obtained by Fisher distribution (Priest 1993). It relates the extent of deviation from the given mean value with the constant obtained by analyzing field data such as outcrop maps. The previously developed model can handle up to 3 distinct orientations. In FDFN model, unlike other fracture generation models, fracture is not considered as smooth parallel plates. It generates a profile of fracture aperture for each fracture using Brownian model (Voss 1988) instead of having a single value, creating more realistic natural fractures as a result. **Table 3** is a summary of some of necessary input values for generating one fracture network model.

Table 3—Necessary input values for FDFN generation.

Definition		Typical Values
Fracture Length, Numbers		
Side length of generation domain	L	
Minimum fracture length	L_{\min}	
<i>Fractal</i> dimension of fracture center distribution	D_c	1 ~ 3
<i>Fractal</i> dimension of fracture length distribution	D_l	1 ~ 3
Fracture density	α	1 ~ 10
Fracture Orientation		
Number of fracture sets	nSet	1 ~ 3
Orientation of fracture sets	FracAngle 1,2,3	0 ~ 180
Probability of fracture sets	OrienProb 1,2,3	Sum = 1
Fisher constant	K	

Fig. 16 shows the natural fracture systems examples generated by FDFN model. Several parameters can be used to characterize the natural fracture system such as L_{\min} and α . **Fig. 16** illustrates the effects of L_{\min} , the minimum fracture length, and α , the fracture density parameter, on the FDFN generated fracture systems. All three examples have the

same reservoir size ($L=3218$ ft). It shows that when l_{\min} is large but α is small (**Fig. 16a**), the natural fractures are long but sparse with mainly 2 dominating directions. They are only connected with crossing fractures. On **Fig. 16b**, it shows many short natural fractures (low l_{\min}) which are scattered over the entire reservoir. There are places where the fractures are gathered, but the main connectivity is not seen. On **Fig. 16c**, relatively long, dense natural fractures are observed with good connectivity. Obviously, the three natural fracture systems will affect the flow rate of fractured horizontal well differently. The performance of horizontal well with multiple transverse fractures can be estimated by combining this natural fracture network system with hydraulic fracture system.

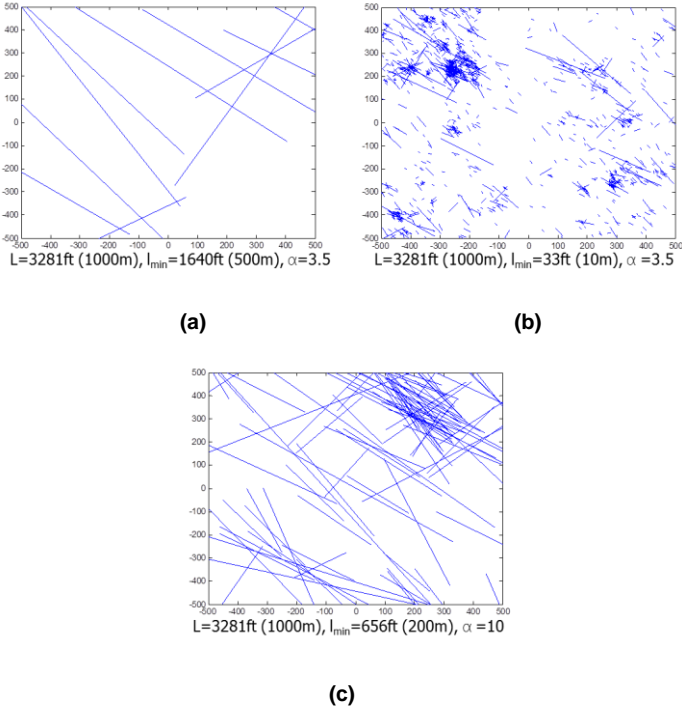


Fig. 16—Natural fracture systems generated using FDFN.

2.5 Building and Solving Complex Fracture System

By combination of the source method for fractured well flow problem and the FDFN for creating natural fracture network, we can predict well performance in complex fracture systems. To build a complex fracture system we first generate natural fracture network using FDFN method and then, we add horizontal wellbore and multiple transverse fractures to the natural fracture system.

After building the fracture system, with the assumption that all the reservoir flow occurs through fractures only and the reservoir does not directly contribute to the wellbore, the connectivity between the hydraulic fracture and the natural fractures, and the connectivity among the created natural fractures need to be identified. The main objective here is to eliminate all the isolated natural fractures which are not connected to any hydraulic fracture or to the natural fractures that are connected to the hydraulic fractures. To achieve this, we start from the hydraulic fractures and identify the natural fractures which intersect with any of hydraulic fracture. After that, the intersecting natural fractures become the 1st set of natural fracture system and the natural fractures which cross with this 1st set of natural fractures becomes the 2nd set of natural fractures. Next, natural fractures which meet with 2nd set of natural fractures become 3rd set of fractures and this identification process is repeated until the entire domain is covered. We are interested in only these intersecting sets, and the natural fractures which are not included in these sets are simply eliminated. **Fig. 17** briefly shows this concept. On **Fig. 17**, the grey lines represent horizontal wellbore and multiple transverse hydraulic fractures. **Fig. 17a** is the natural fracture system before the identification procedure and. **Fig. 17b** is the system after

the identification process. On **Fig. 17b**, blue lines are the natural fractures which are directly connected to the hydraulic fractures and they are the 1st set of natural fractures. Green lines are natural fractures which intersect with the 1st set of natural fractures and they become the 2nd set of natural fractures.

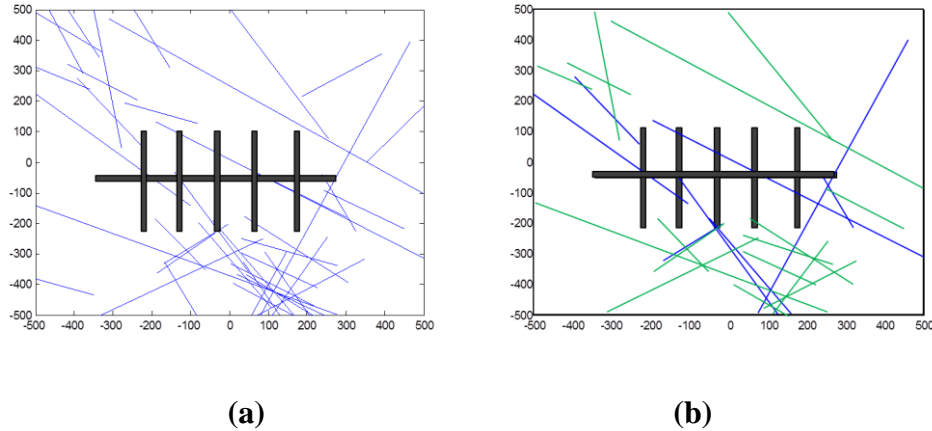


Fig. 17—Conceptual identification of fracture connectivity.

All the identified intersecting natural fractures and hydraulic fractures are considered as separate sources. And each fracture is divided into several segments as mentioned earlier for slab source approach. For example, if we have 20 intersecting natural fractures and 10 hydraulic fractures, and if we make 25 segments for each fracture, we have 750 (25 x 30) individual sources. This becomes a set of 750 linear equations (a matrix of 750 x 750) which needs to be solved to calculate the flow rate. After solving the set of linear equations, the flow rate of each segment is summed up back to the fracture where the segment belongs. Finally, the flow rate of intersecting natural fracture is distributed into hydraulic fractures which the natural fracture intersects with.

2.6 Non-orthogonally Intersecting Natural and Hydraulic Fracture System

The multiple transverse hydraulic fractures combined with natural fractures create complex fracture networks. In real life, these fractures are more likely intersected non-orthogonally. Because one of the assumptions for the slab source solution is that the sources are parallel to the boundary of the domain, we need to modify the system before solving the flow equations. A simplified fracture system is used here to illustrate the approach of using the slab source model to estimate flow rate in such a system.

Fig. 18 shows an example of complex fracture system. Four hydraulic fractures and four natural fractures are placed in the domain. Natural fracture #1 and #2 intersect two hydraulic fractures, and natural fracture #3 and #4 only intersect one hydraulic fracture. The natural fractures are local sources providing a flow rate at the locations where they intercept with hydraulic fractures. If a natural fracture intercepts more than one hydraulic fracture, the flow rate from the natural fracture is allocated to all the intersected hydraulic fractures at the location it crosses the hydraulic fractures. To relax the restriction of orthogonal source in a box-shaped reservoir in a Cartesian coordinate system, we set the hydraulic fractures orthogonal to the reservoir domain. We divide the natural fractures into two groups, either a series of vertical sources, or a series of horizontal sources, depending on the intersecting angle of the fracture. If the intersecting angle is higher than 45° , then the fracture becomes a series of vertical sources; correspondingly, if the intersecting angle is smaller than 45° , then the fracture becomes a series of horizontal sources. For example, natural fracture #1 intersects hydraulic fractures #1 and #2 with an angle higher than 45° , and then it becomes 5 vertical sources. After calculating the flow

rate, the total rate from natural fracture #1 is evenly distributed between hydraulic fractures #1 and #2. Similarly, natural fracture #2 is divided to 5 horizontal sources, and the rate is split between hydraulic fractures #3 and #4.

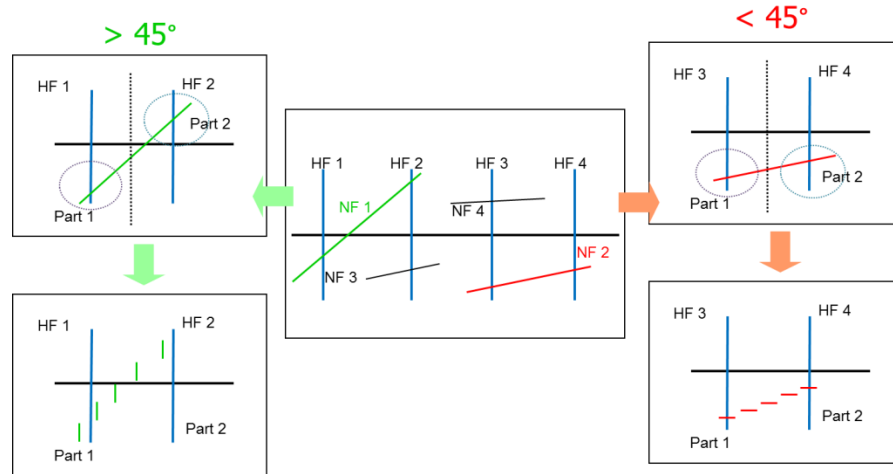


Fig. 18—Schematic of handling non-orthogonally intersecting fractures.

Hydraulic fractures are the main fractures and the natural fractures are branch fractures which only connect with the main fractures, not the wellbore. Therefore, the fluid inside the main fracture flows from the reservoir to the wellbore. The fluid inside the branch fractures flows from the reservoir to the main fractures, and then flows to the wellbore with the fluid from the main fracture. The total flow from the well will be the sum of all fracture sources in the domain.

With the procedure, the size of the system of equations can quickly become large, and extensive computation can be involved. Even though, the approach still has advantage of flexibility of handling numerous fractures especially when there are many small fractures in the system. If using reservoir numerical simulation approaches, the gridding

systems have to be verified to handle the fractures. Since there is no gridding in the source approach, the fracture size does not affect the computation time.

2.7 Gas Adsorption Phenomena

2.7.1 Adsorbed Gas

In shale, it is believed that gas is stored in two ways: as free gas and adsorbed gas. Free gas is stored within micro-pores and natural fractures, which is the conventional concept for the gas. Adsorbed gas is the gas which is adsorbed on the surface of matrix in shale by adsorption phenomena (**Fig. 19, Song 2010**). Adsorption is the adhesion of atoms, ions or molecules from a gas, liquid or dissolved solid to a surface due to the surface energy, similar to surface tension.

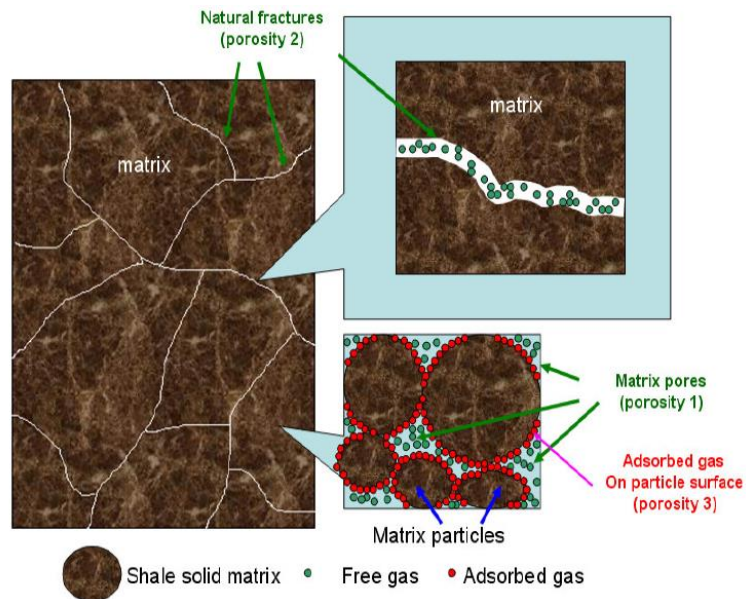


Fig. 19—Gas storage mechanism. Reprinted from Song, 2010.

For the flow of gas in shale reservoir, free gas flows through matrix pores into the fracture system by Darcy’s law. Adsorbed gas desorbs from the matrix surface when pore pressure decreases and diffuses to the pore spaces. It then becomes free gas and follows the same transportation mechanism through matrix and fractures (**Fig. 20**). This diffusion is most popularly explained by Fick’s law. But, applying Fick’s law to accommodate the flow of adsorbed gas is beyond the scope of this project, a novel approach using material balance is applied.

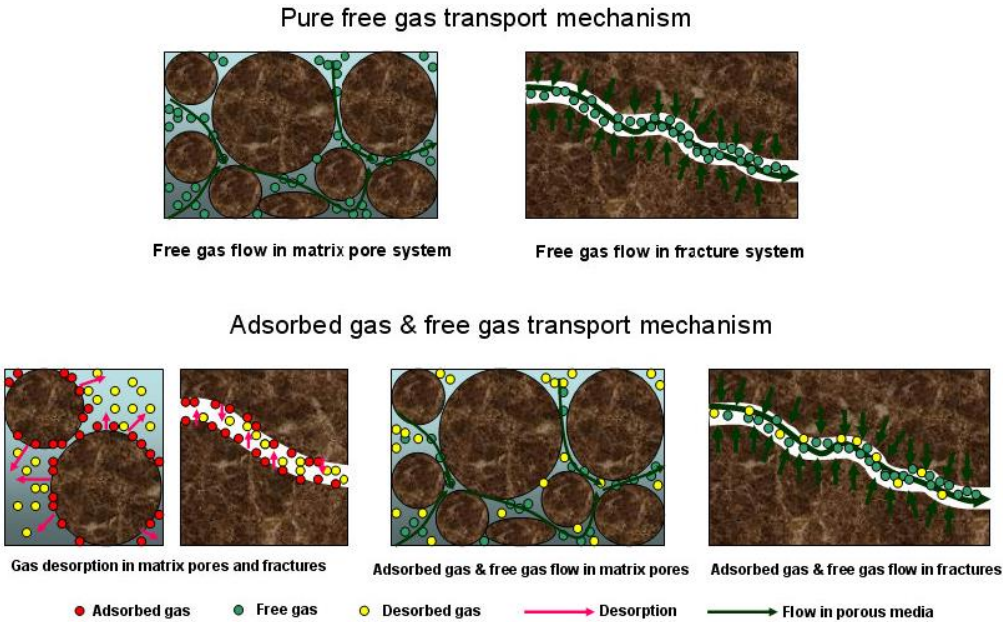


Fig. 20—Gas transportation mechanism. Reprinted from Song, 2010.

2.7.2 Gas Adsorption/Desorption Model

The Langmuir model is the most commonly used models for quantifying the description of gas adsorption/desorption. Adsorbed gas is represented by

$$V_{ads} = \frac{V_L p}{p_L + p} \quad (2.25)$$

where, V_{ads} [scf/ton] is the gas volume which can be adsorbed by a rock of unit mass, V_L [scf] is Langmuir volume; the maximum gas volume which can be adsorbed. p_L [psi] is Langmuir pressure, at which half of Langmuir volume gas can be adsorbed and p [psi] is random pressure. The Langmuir model assumes that temperature is constant. Therefore, the graph, which shows the relationship between adsorbed gas and pressure, is usually called Langmuir isotherm (**Fig. 21a**). As indicated in **Eq. 2. 26**, it is Langmuir pressure and Langmuir volume that controls the gas desorption behavior and these values can be obtained by core lab experiments.

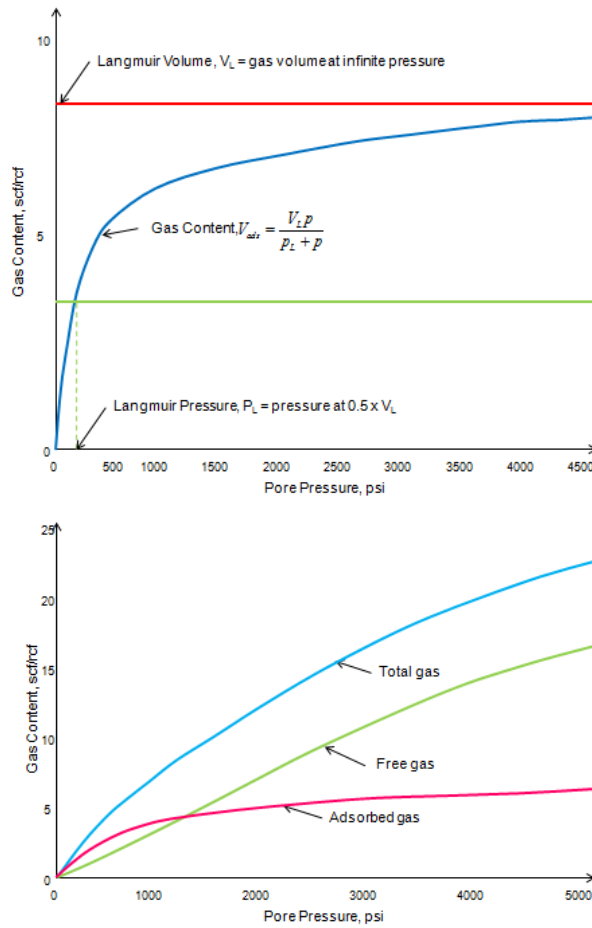


Fig. 21—(a) Langmuir Isotherm (b) Free, adsorbed and total gas content vs pressure.

2.7.3 Material Balance

In the previous study by Mengal and Wattenbarger (2011), it was concluded that the OGIP estimates can be increased up to 30% when adsorbed gas is included. At high pressure, the adsorbed gas are not produced much, but as pressure decreases, the desorption increases and it eventually produces more gas (**Fig. 21b**). As in Mengal and Wattenbarger’s research (2011), using of modified material balance was introduced. With the average pressure using modified material balance, the flow rate of adsorbed gas is

easily obtained (**Eq. 2.27**) and the difference of adsorbed gas for each time-step becomes desorbed gas production (**Eq. 2.28**).

$$GIP_{adsorbed} = V_B \left(V_L \frac{\bar{P}}{\bar{P} + P_L} \right) \quad (2.26)$$

$$q_{ads} = V_B V_L \left[\frac{\bar{P}_1}{\bar{P}_1 + P_L} - \frac{\bar{P}_2}{\bar{P}_2 + P_L} \right] \quad (2.27)$$

Modified material balance calculation starts from including adsorbed gas in the calculation of OGIP (**Eq. 2.29**).

$$G = V_B \left[\frac{\phi S_{gi}}{B_{gi}} + V_L \frac{P_i}{P_i + P_L} \right] \quad (2.28)$$

King (1990), presented a modified material balance technique to estimate the OGIP and to predict the future performance of the well for coal seams in Devonian shale including adsorbed gas. The technique works just like the conventional method, where p/z straight line plot is used to estimate OGIP (**Eq. 2.30**). But as in **Fig. 22**, instead of z, modified z* is used to include the adsorbed gas (**Eq. 2.31**).

$$\frac{\bar{P}}{\bar{z}^*} = \frac{P_i}{z_i^*} \left[1 - \frac{G_P}{G} \right] \quad (2.29)$$

$$z^* = \frac{z}{S_g + \frac{V_L T p_{sc} z}{\phi (P + P_L) T_{sc} z_{sc}}} \quad (2.30)$$

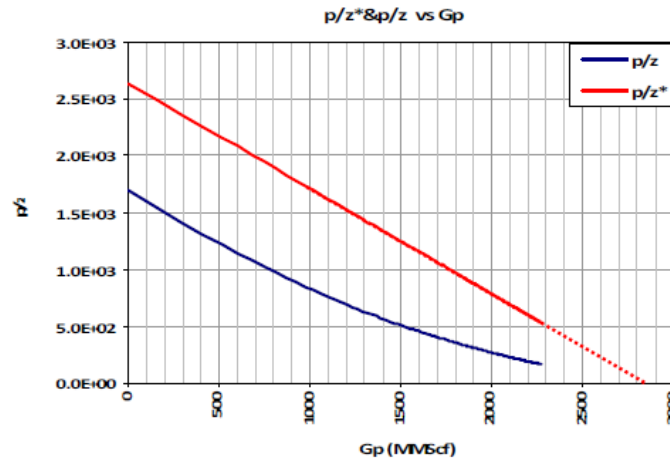
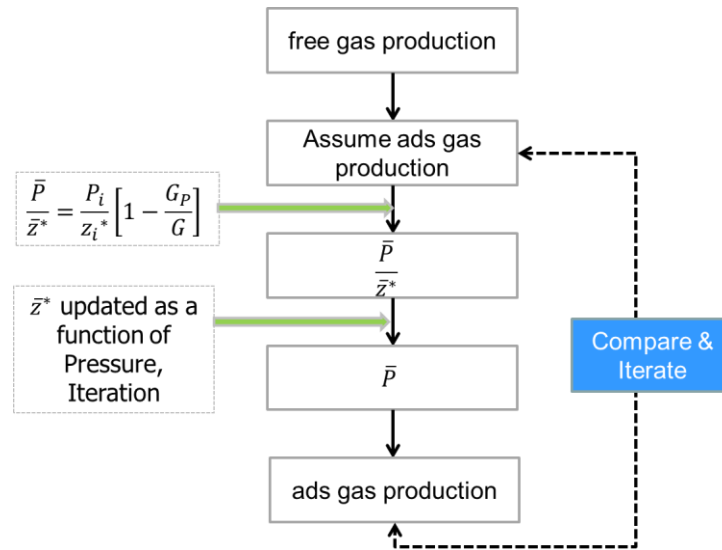


Fig. 22— p/z^* and p/z vs G_p plot. Reprinted from King, 1990.

Fig. 23 summarizes the procedure for adsorbed gas production. First, we consider all the production from source function method is free gas production. Then, we assume certain level of adsorbed gas production, for example, about 5% of free gas production. Now, we can calculate cumulative production, G_p , and can get the \bar{p}/\bar{z}^* . Since the compressibility factor \bar{z}^* itself is a function of pressure, we cannot get average pressure, \bar{p} directly. Instead, we again assume \bar{p} , and obtain \bar{z}^* and compare the values with previously obtained \bar{p}/\bar{z}^* . If they are in close proximity, we use the value of \bar{p} . If not, we update \bar{p} until we get close enough value. After \bar{p} is calculated, the adsorbed gas can be easily calculated. But this is not the final result, since we started from assuming adsorbed gas production. If calculated adsorbed gas production is close to the assumed value at the beginning, we calculated the correct amount of the adsorbed gas production. If not, we update the assumed adsorbed gas production and iterate this process again. It usually takes within 5 iteration until we get reasonable adsorbed gas production.



After one timestep, \bar{P} becomes new pressure
Fig. 23—Flow chart for adsorbed gas production calculation.

2.8 Effort to Improve Computation Efficiency

As the number of hydraulic fractures and natural fractures increases, the problem size of the systems of linear equations, which is determined by the number of total sources, becomes large and the computational time increases almost exponentially. As a starting point of effort to speed up the calculation, the executed time for each part of the code was carefully examined. Most of the computational time was spent on calculation of source function term, F and constructing the matrix (88~90% of the total execution time). The remaining time (9~10%) was on solving the source function matrix. It was predicted since the calculation of source function term, F, is actually the key component in this program.

Three kinds of approaches were taken to increase the computational efficiency. The first one is about constructing the source function matrix. Parallelization of parts of the code was conducted to exploit the multi-core hardware. The analytical solution of

source function method was rearranged and slightly modified in more efficient way so that redundant and unnecessary calculation can be removed. Second, even solving the source function matrix takes about 10% of total calculation time, it was tried to reduce that time as much as possible by adopting LAPACK, a highly optimized public library, in solving the source function matrix. The third approach is to run the program in time-reducing way such as utilizing “O3 optimization” and not carrying intermediate debugging values.

2.8.1 Parallelization of The Code

Most PCs and laptops are multi-core, multi-threads machines these days. The concept of parallelism is to utilize every possible hardware features favorably. As shown on **Fig. 24a**, for a 8-core machine, if only 1 core is working, the remaining 7 cores are idling unless the command to work is made to the 7 cores and we waste most of the computational power. But by parallelism, it is possible to make all the cores to work (**Fig. 24b**) by giving them assignments. In our program, Openmp was applied for the source function term calculation. For example, if we have 100 sources and use one core in the calculation, then one core has to calculate the source terms 10000 times repeatedly. If we can command 8 cores to work, then each and every core does 1250 calculations and the total executed time can be greatly reduced.

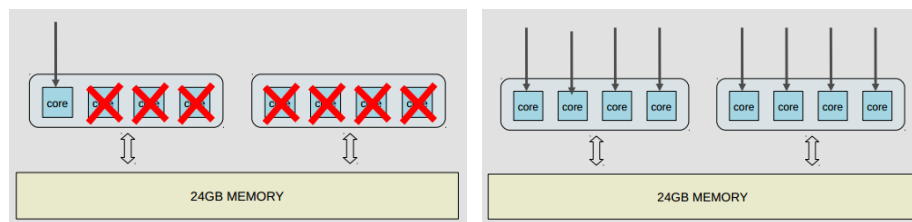


Fig. 24—Concept of parallelism (a) Before (a) After.

2.8.2 Comparison of Computation Time

Table 4 is the summary of time elapsed before and after the effort of time reduction. For 64 natural fractures and 20 hydraulic fractures, 224 sources were identified after examining intersection. 1 cycle of calculation involves 9 repeated production rate and pressure calculation at time 10, 50, 100, 250, 500, 1000, 2000, 5000 and 10000 days. The processor for the desktop used has a clock speed of 2.66 GHz (**Table 5**).

The calculation time before conducting any work to accelerate the calculation was almost 7 hours for this problem size, and it reduced to 10 minutes on the desktop computer with 8 threads, threads means number of workers. When it was tested on the supercomputer of Texas A&M University using 8 threads, the time further reduced to 6 minutes.

Table 4—Computation time comparison.

	Desktop				TAMU Supercomputer				
	Before	Windows Visual Studio IDE; Parallelization (Openmp)				Linux fortran compiler; Parallelization (Openmp)			
Elapsed Time	6 hr 52 min	nth=1	nth=2	nth=4	nth=8	nth=1	nth=2	nth=4	nth=8
				48 min	29 min	13 min	10 min	43 min	22 min

Table 5—Computer hardware specifications.

	Desktop	Supercomputer at TAMU (EOS)
Processor	Intel Xeon W3520	Intel Xeon 5560
# of Cores	4	4
# of Threads	8	8
Clock Speed	2.66 GHz	2.8 GHz
Memory	4 GB	24 GB
System Type	64 bit	64 bit

By examining the table, we can see the calculation time was almost inversely proportional to the number of threads, which kind of follows the theoretical speedup. Theoretical speedup means if n number of threads are used, the calculation time should be n times faster than using 1 thread. **Fig. 25** is the computation time estimation plot based on theoretical speedup. X axis is the number of sources and y axis is the time taken for the calculation. Blue line is obtained from the actual run, with 20, 50, 224 and 300 sources. And red dot line is an estimation by extrapolating the trend following the theoretical speedup. So it is estimated that the calculation time would be around 1 hour with 1000 sources using 8 cores.

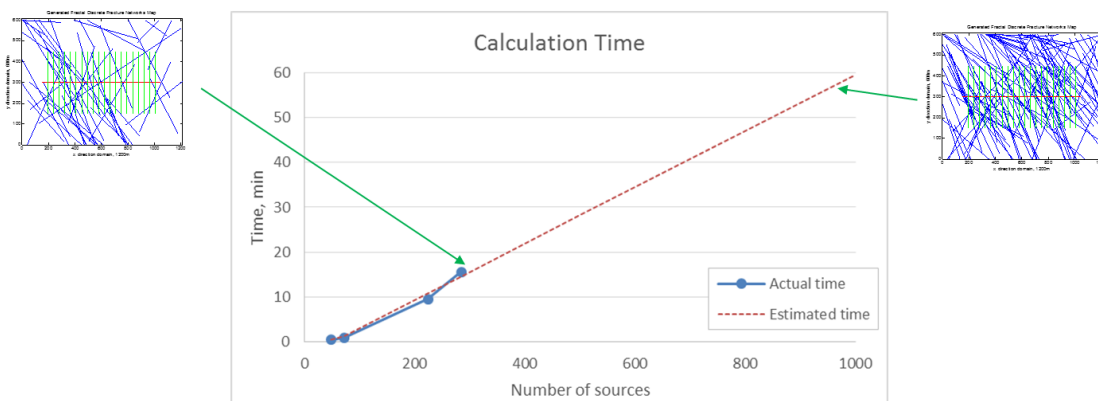


Fig. 25—Calculation time estimation plot.

CHAPTER III

VALIDATION

This chapter describes the verification of the model presented in Chapter 2. Commercial software and open source software are used for comparison. The purpose of this chapter is not to provide the best match of the solutions possible with the software but to demonstrate that the model developed in this study provides satisfactory accuracy.

3.1 Simplified Fracture System

A simplified fracture system was generated to compare the results of source function approach and commercial software, CMG[®], a reservoir simulator by Computer Modelling Group.

Gridding is used in reservoir simulation to turn the geological feature of the field into a discrete system on which the fluid flow equations can be solved. Cartesian grid system is most widely used in conventional three-dimensional reservoir simulation since it is easy to set up and to obtain the flow solutions. Certain grids were locally refined to represent the fractures which have smaller width. To represent non-orthogonal natural fractures, which do not run parallel to the x or y directions, Local Grid Refinement (LGR) needs to be conducted manually. This requires extensive time and attention, therefore, a simplified fracture system of 2 hydraulic fractures and 2 natural fractures were used.

Although LGR were used to represent the non-orthogonal natural fractures, the fractures are composed of continuous stepped grids, not exactly a continuous line of grids.

Fig. 26 shows the grid system used in CMG and **Fig. 27** is the enlarged map which well presents the stepped grids.

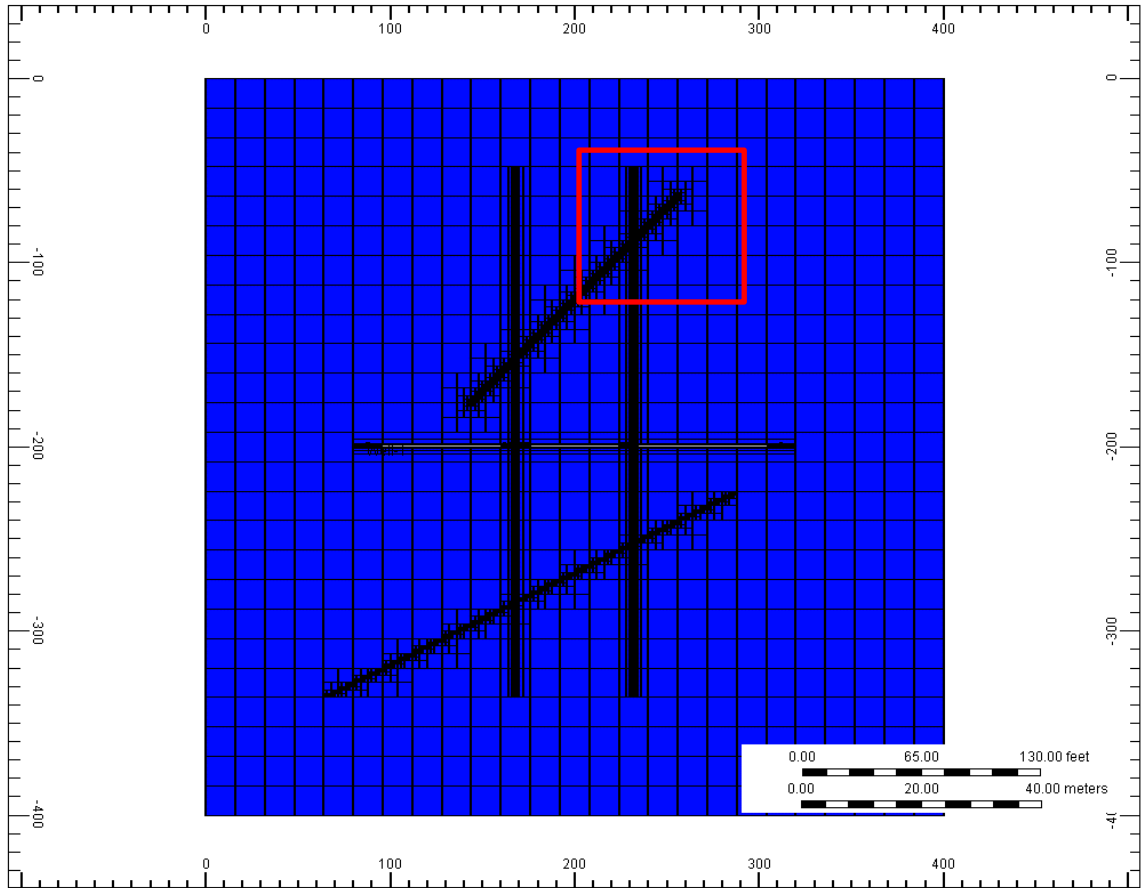


Fig. 26—Grids used in CMG for simplified fracture system.

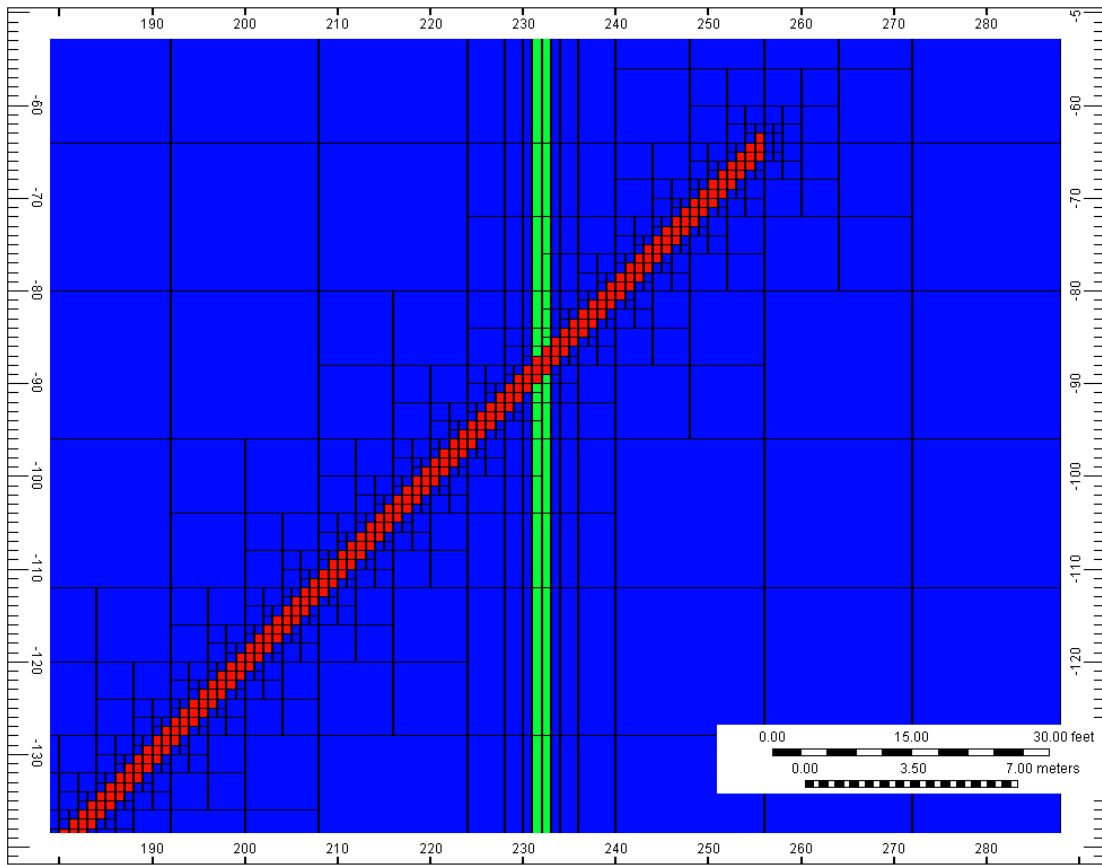


Fig. 27—Enlarged map in CMG which shows stepped grids.

The input parameters are listed in **Table 6**. Reservoir is assumed to be 400 ft by 400 ft wide. Reservoir height is assumed to be 10 ft high. Reservoir permeability is 0.001 md. Reservoir porosity is 9% and initial pressure is 3000 psi. Gas viscosity is 0.0156 cp and gas specific gravity is 0.746. Total compressibility is 0.0006. Horizontal well is 240 ft long and two hydraulic fractures are 288 ft long. Since the reservoir fluid properties are updated as a function of reservoir average pressure, the given data is the value at the reference initial reservoir pressure.

Table 6—Input parameters for simplified fracture system.

Reservoir Size, ft	400 x 400 x 10
Reservoir Permeability, md	0.001
Reservoir Porosity, fraction	0.09
Reservoir Initial Pressure, psi	3000
Bottom Hole Pressure, psi	1000
Gas Viscosity, cp	1.56e-2
Gas Specific Gravity, -	0.746
Total Compressibility	6.00e-4
Horizontal Well Length, ft	240
Number of Hydraulic Fractures	2
Hydraulic Fracture Length, ft	288

Comparing the source function approach with CMG, **Fig. 28** shows the results of the two solutions for the example of 2 hydraulic fractures and 2 natural fractures. Constraint of maximum production rate in addition to bottom hole pressure was introduced in CMG to follow industry practice and to examine the long term production trend. Both

CMG and the source function method presents very similar flow rate trend; a rapid decline during first 100 days but a constant, sustainable production for the rest of producing time. **Fig. 29** presents the cumulative production for both methods. The source function method gives slightly higher production rate at the beginning of the production, but it eventually yields the same cumulative production with CMG. Since the source function method is a semi-analytical approach, there is a limitation with it when compared with a three-dimensional numerical reservoir simulator. The source function method accommodates the varying reservoir fluid properties in its calculation of flow rate and reservoir pressure, but the approach and method could be different from the numerical simulators, which leads to this small discrepancy. The computation time from CMG is 81 seconds and from source function is 19 seconds.

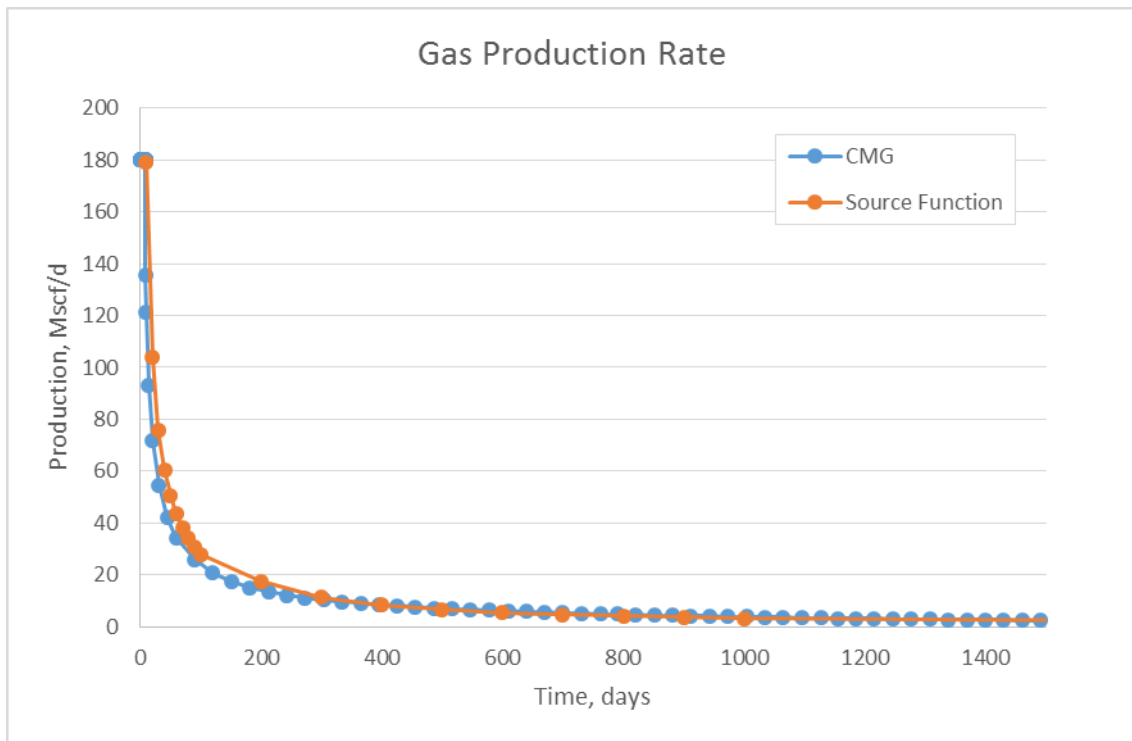


Fig. 28—Gas production rate comparison with CMG and source function method.

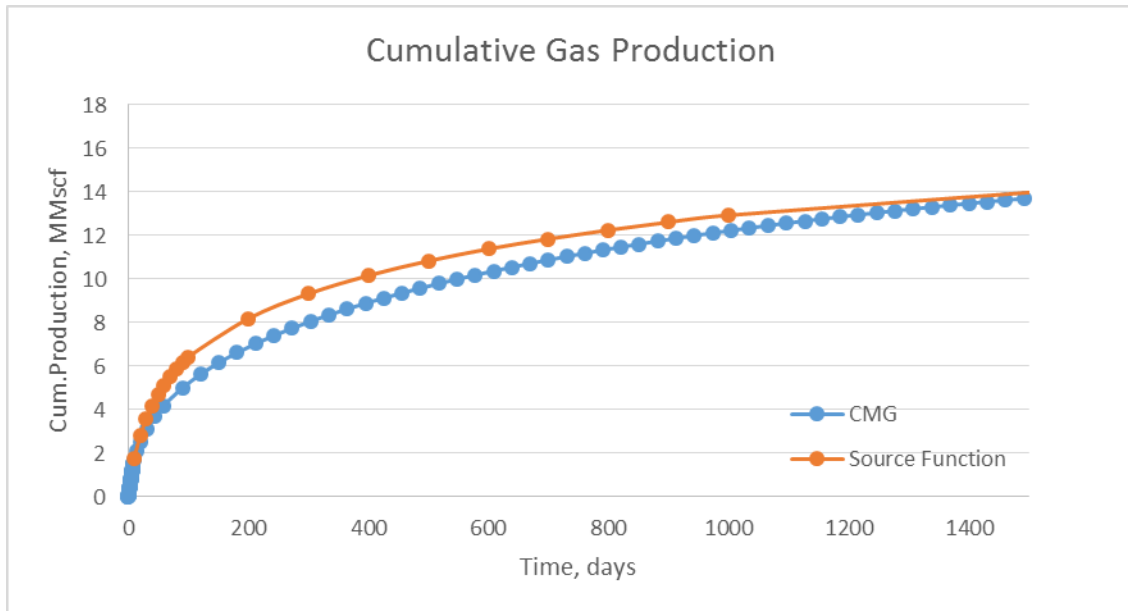


Fig. 29—Cumulative gas production comparison with CMG and source function method.

3.2 Complex Fracture System with FracGen/NFFlow

A complex fracture system, which has more realistic natural fracture geometries, was generated to compare the results of source function approach with an open source software. FRACGEN/NFFLOW, a fractured reservoir modeling software developed by National Energy Technology Laboratory (NETL) was used as an open source software.

FRACGEN/NFFLOW is designed to simulate gas flow in naturally-fractured reservoirs. FRACGEN generates a stochastic network of discrete fractures that represent the main conductor of flow using one of three models: randomly-located fractures, fracture swarms, patterns of fractures ranging from regular to uniform to random. All fractures extend vertically through the entire height of a layer, which is the same assumption with source function approach. NFFLOW handles reservoir simulation with the generated

fracture network by FRACGEN. Reservoir modeling with FRACGEN/NFFLOW is especially appropriate when

- The reservoir produces relatively dry gas, with little interference from water or oil
- The reservoir rock (matrix) has less than 1 md permeability
- Variations in fracture connectivity, density, aperture are the predominant factors affecting gas flow

The complex fracture network used is shown in **Fig. 30**. Although FRACGEN can generate stochastic network of discrete fractures, the fracture network developed by combined FDFN model was used for comparison with the source function method. Red lines represent hydraulic fractures and green lines represent natural fractures. There exist 20 hydraulic fractures and 55 natural fractures. The input parameters are summarized in **Table 7**. Reservoir is assumed to be 4000 ft by 2000 ft wide. Reservoir height is assumed to be 200 ft high. Reservoir porosity is 9% and initial pressure is 2335 psi. Gas viscosity is 0.0156 cp and gas specific gravity is 0.552. Total compressibility is 0.0006. Horizontal well is 3000 ft long. All the 20 hydraulic fractures are 1000 ft long. The widths of natural fractures are assumed to be 0.032 ft.

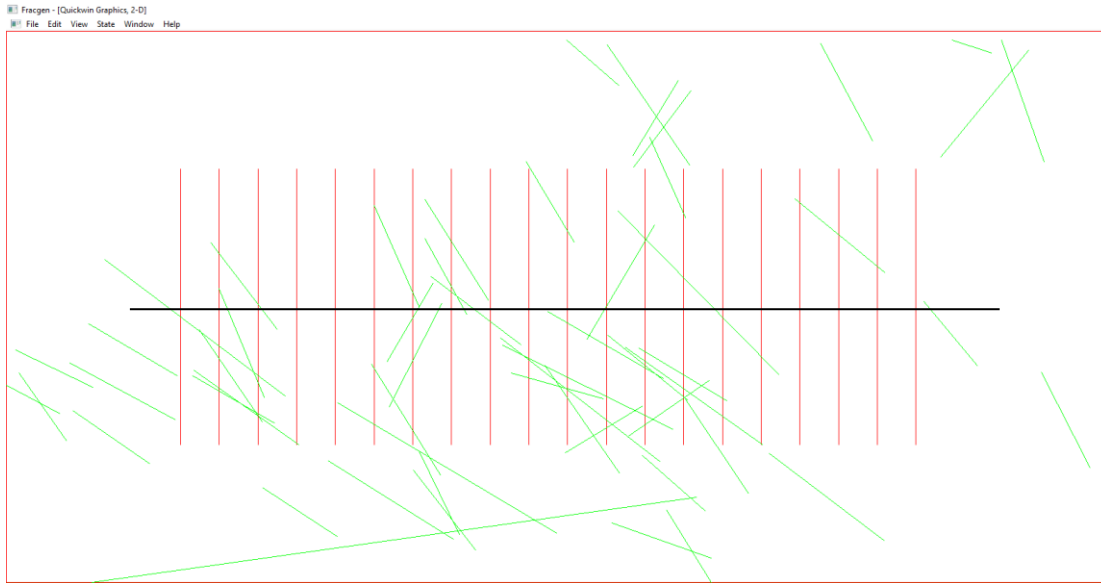


Fig. 30—Complex fracture system with FRACGEN/NFFLOW.

Table 7—Input parameters for complex fracture system.

Reservoir Size, ft	4000 x 2000 x 200
Reservoir Permeability, md	0.001
Reservoir Porosity, fraction	0.09
Reservoir Initial Pressure, psi	2335
Bottom Hole Pressure, psi	1000
Gas Viscosity, cp	1.56e-2
Gas Specific Gravity, -	0.552
Total Compressibility	6.00e-4
Horizontal Well Length, ft	3000
Number of Hydraulic Fractures	20
Hydraulic Fracture Length, ft	1000
Natural Fracture Aperture, ft	0.032

The NFFLOW, the reservoir simulator part of FRACGEN/NFFLOW program requires two types of input files for simulation run. First is the fracture network file (.flo file extension) and second is the reservoir control file (.res file extension) (**Fig. 31**). Fracture network file requires the information of each fracture and the wellbores. The ASCII format data sequence describing each fracture is: x-coordinate and y-coordinate of the left (or lower) endpoint, x-coordinate and y-coordinate of the right (or upper) endpoint, aperture, fracture layer number, and a fracture identification number (**Fig. 32**). Horizontal wells are represented in the simulator as constant pressure lines that extend from the vertical wellbore to the end point specified for the horizontal segment. The information required for the wellbore is the location of the vertical wellbore in x and y direction, well length, radius of the vertical wellbore, number of laterals, relative depth of the wells, x and y location of the end of the horizontal segment, radius of the horizontal segment and the layer number for the horizontal well. **Fig. 33** is an example about a wellbore information. The wellbore is assumed to be in the middle of the reservoir with start point

(500,1000) and end point (3500,1000) with wellbore radius of 0.25 ft for both vertical and horizontal sections, length of 3000 ft in 3100 ft depth of the reservoir.

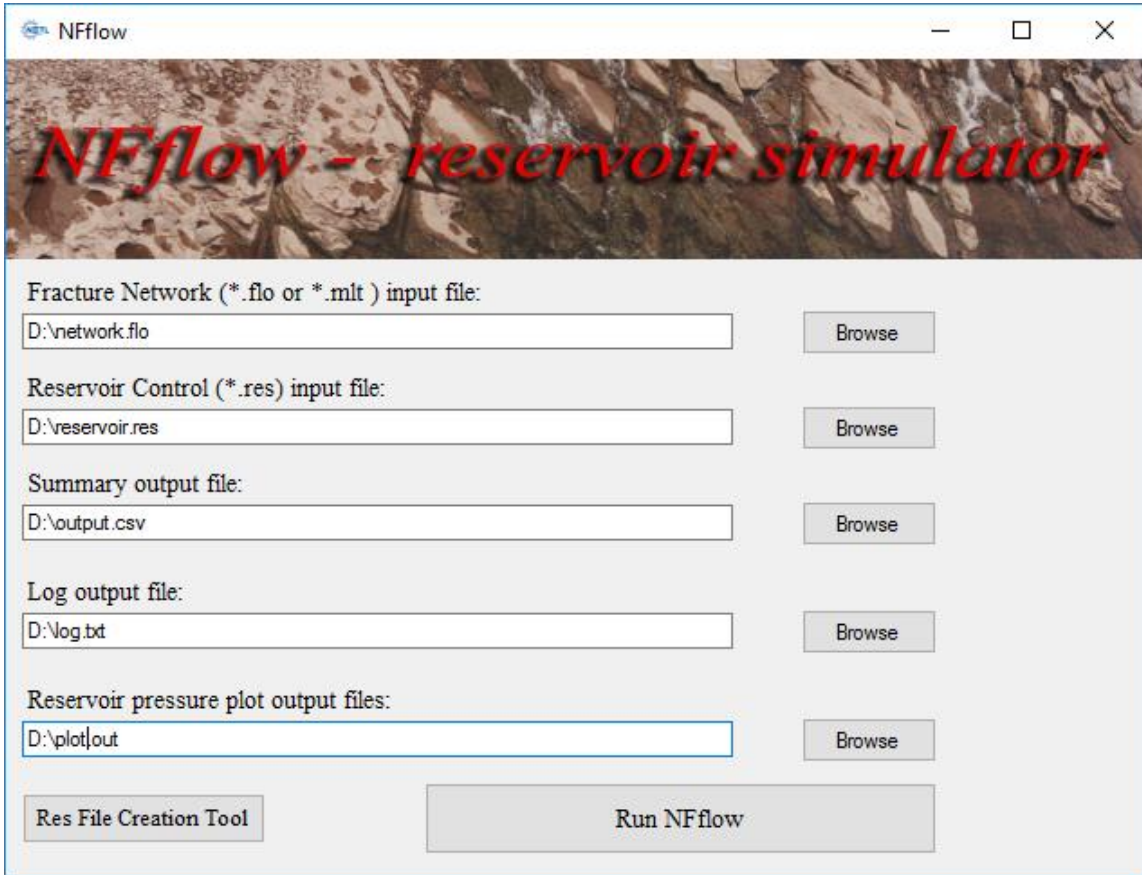


Fig. 31—Screen capture of NFFLOW program.

```

Well #1, Comparison between Source Model
4000.000 2000.000 200.000 0.000
  X-left  Y-left  X-right  Y-right  Aperture  Layer  Number
 632.720  500.000  632.730  1500.000  .100E-01  1      1
 773.340  500.000  773.350  1500.000  .100E-01  1      2
 913.960  500.000  913.970  1500.000  .100E-01  1      3
1054.580  500.000 1054.590  1500.000  .100E-01  1      4
1195.190  500.000 1195.200  1500.000  .100E-01  1      5
1335.810  500.000 1335.820  1500.000  .100E-01  1      6
1476.430  500.000 1476.440  1500.000  .100E-01  1      7
1617.050  500.000 1617.060  1500.000  .100E-01  1      8
1757.660  500.000 1757.670  1500.000  .100E-01  1      9
1898.280  500.000 1898.290  1500.000  .100E-01  1     10
2038.900  500.000 2038.910  1500.000  .100E-01  1     11
2179.510  500.000 2179.520  1500.000  .100E-01  1     12
2320.130  500.000 2320.140  1500.000  .100E-01  1     13
2460.750  500.000 2460.760  1500.000  .100E-01  1     14
2601.370  500.000 2601.380  1500.000  .100E-01  1     15
2741.980  500.000 2742.990  1500.000  .100E-01  1     16
2882.600  500.000 2882.610  1500.000  .100E-01  1     17
3023.220  500.000 3023.230  1500.000  .100E-01  1     18
3163.840  500.000 3163.850  1500.000  .100E-01  1     19
3304.450  500.000 3304.460  1500.000  .100E-01  1     20
1203.970  650.790 1999.770  179.620  .320E-01  1     21
2222.110 1347.660 2806.390  755.940  .320E-01  1     22
 358.640 1172.390 1011.680  675.250  .320E-01  1     23
1794.010  888.480 2374.040  438.850  .320E-01  1     24
1802.480  860.970 2419.970  555.200  .320E-01  1     25
2249.620  852.140 2747.380  498.920  .320E-01  1     26
2397.350  261.200 2560.320  0.000  .320E-01  1     27
1169.160  440.430 1623.140  155.750  .320E-01  1     28
2181.850 1952.180 2481.610 1513.670  .320E-01  1     29
2771.170  468.700 3187.170  153.040  .320E-01  1     30

```

Fig. 32—Fracture network input file in NFFLOW:Fracture part.

```

WELLS
500.000 1000.000 3000.000 0.250 1 3100.000
3500.000 1000.000 0.250 1

```

Fig. 33—Fracture network input file in NFFLOW:Well part.

The reservoir control file mainly contains the physical properties of the gas in the reservoir and the simulation control parameter. The initial pressure at a given depth,

varying gas deviation factor and dynamic viscosity of the gas as a function of gas are presented (**Fig. 34**). These values are imported from separately calculated reservoir fluid properties based on gas relative gravity, reservoir temperature and impurities. Simulation time and the control parameter, either fixed pressure or fixed flow rate, are also presented. **Fig. 35** shows an example of the fixed pressure of 1000 psi production control parameter.

PG_DATUM	DATUM		
2335.0	3100.0		
TSC	PSC	TRES	
60.0	14.7	147.13	
PG	ZG	UG	
300	0.979634852	0.012856	
600	0.961162539	0.012904	
700	0.955491561	0.013048936	
800	0.950087517	0.013405797	
900	0.944964373	0.01354416	
1200	0.931413222	0.01369143	
1500	0.920836628	0.013847318	
1800	0.913476597	0.014364451	
2100	0.909457229	0.014951612	
2400	0.908764315	0.015602944	
2700	0.911268542	0.016311236	
3000	0.916739546	0.017067936	
3300	0.924890936	0.017863603	
3600	0.935414161	0.018688715	
3900	0.948005215	0.019534276	
4200	0.962381049	0.020392266	
4500	0.978312798	0.021255839	

Fig. 34—Reservoir control file in NFFLOW:Fluid Properties part.

```
PRODUCE 1 AT 1000.00 PSI  
TIME 15.00  
PRODUCE 1 AT 1000.00 PSI  
TIME 30.00  
PRODUCE 1 AT 1000.00 PSI  
TIME 45.00  
PRODUCE 1 AT 1000.00 PSI  
TIME 60.00  
PRODUCE 1 AT 1000.00 PSI  
TIME 75.00
```

Fig. 35—Reservoir control file in NFFLOW:Production control part.

The compared results for gas production rate are summarized in **Fig. 36**. It was simulated for 1000 days, which shows that the initial high production diminishes rapidly within first 100 days and a stable production is prolonged for the rest of the simulation period. Both NFFLOW and the source function method show a similar production behavior. The simulation time for NFFLOW was 6 seconds and for source function was 37 minutes.

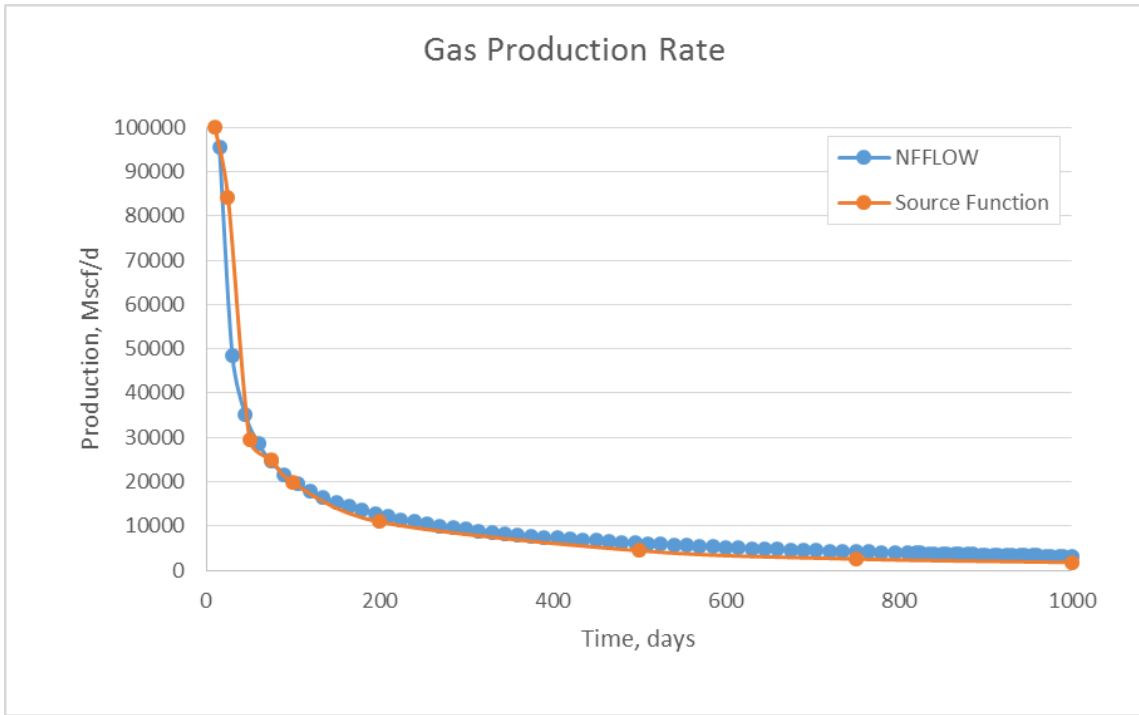


Fig. 36—Gas production rate comparison with NFFLOW and source function method.

CHAPTER IV

RESULTS AND PARAMETRIC STUDY

4.1 Introduction

It is commonly believed that fractured well performances in naturally fractured reservoirs are affected by several main factors. The properties of the reservoir such as reservoir permeability and complexity of natural fracture network play an important role. The properties of the hydraulic fractures are also considered as key factors which have a strong influence on well performance. This includes number of hydraulic fractures, fracture length, fracture height, fracture width and fracture conductivities.

In the subsequent part of this section, a number of simulations are performed to investigate the influence of number of hydraulic fractures, fracture length on well performance. Parametric study is conducted by using the base case input parameters for all the cases and changing only the particular parameter that is investigated. **Table 8** summarizes the input parameters used for the base case, which are mainly reservoir properties and hydraulic fracture properties. Reservoir is assumed to be 4000 ft by 2000 ft wide. Reservoir height is assumed to be 200 ft high. Reservoir porosity is 9% and permeability is 0.001 md. Reservoir initial pressure is 2335 psi and bottom hole pressure is maintained at 1885 psi. Gas viscosity is 0.0156 cp and gas specific gravity is 1.0. Total compressibility is $1.25e-5$. Horizontal well is 3000 ft long and ten hydraulic fractures are 1000 ft long each. A map which shows the complex fracture network used for the base case is provided in **Fig. 37**. There exist 55 natural fractures in the system.

Table 8—Input parameters for base case.

Reservoir Size, ft	4000 x 2000 x 200
Reservoir Permeability, md	0.001
Reservoir Porosity, fraction	0.09
Reservoir Initial Pressure, psi	2335
Bottom Hole Pressure, psi	1885
Gas Viscosity, cp	1.56e-2
Gas Specific Gravity, -	1.00
Total Compressibility	1.25e-5
Horizontal Well Length, ft	3000
Number of Hydraulic Fractures	10
Lengths of Hydraulic Fractures, ft	1000

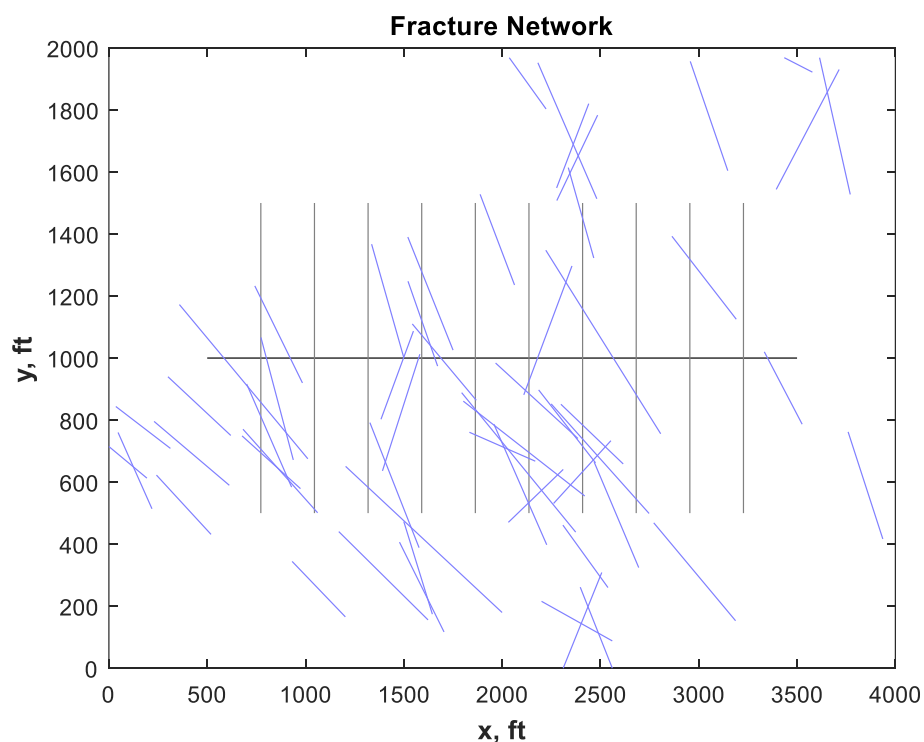


Fig. 37—Complex fracture network for base case with 10 hydraulic fractures and 1000 ft hydraulic fracture length.

4.2 Parametric Study of Number of Hydraulic Fractures

For this study, 10 fractures and 20 fractures were used to examine the effect of fracture spacing on well performance. **Fig. 38** is the complex fracture network map which gives 20 fractures case. All the hydraulic fractures are assumed to be equally spaced and it is assumed that there exist only 1 perforation cluster within each hydraulic fracture. **Fig. 39** shows gas production rate and **Fig. 40** presents cumulative production with different number of hydraulic fractures. As we can see in **Fig. 39**, 20 fractures case gives higher initial production than 10 fractures case but the gas production rate looks almost the same for the rest of the well life. Also we noticed that 20 fractures case actually gives higher (about 9% more) cumulative production from **Fig. 40**. The reason that we cannot observe distinguishable higher production with 20 fractures could be due to the similar connectivity with intersecting natural fractures for both 10 and 20 fractures. But if we place the hydraulic fractures unevenly according to the density of natural fractures, for example, more hydraulic fractures for dense natural fractures and less hydraulic fractures for sparse natural fractures, the effect of number of hydraulic fractures could be easily perceived.

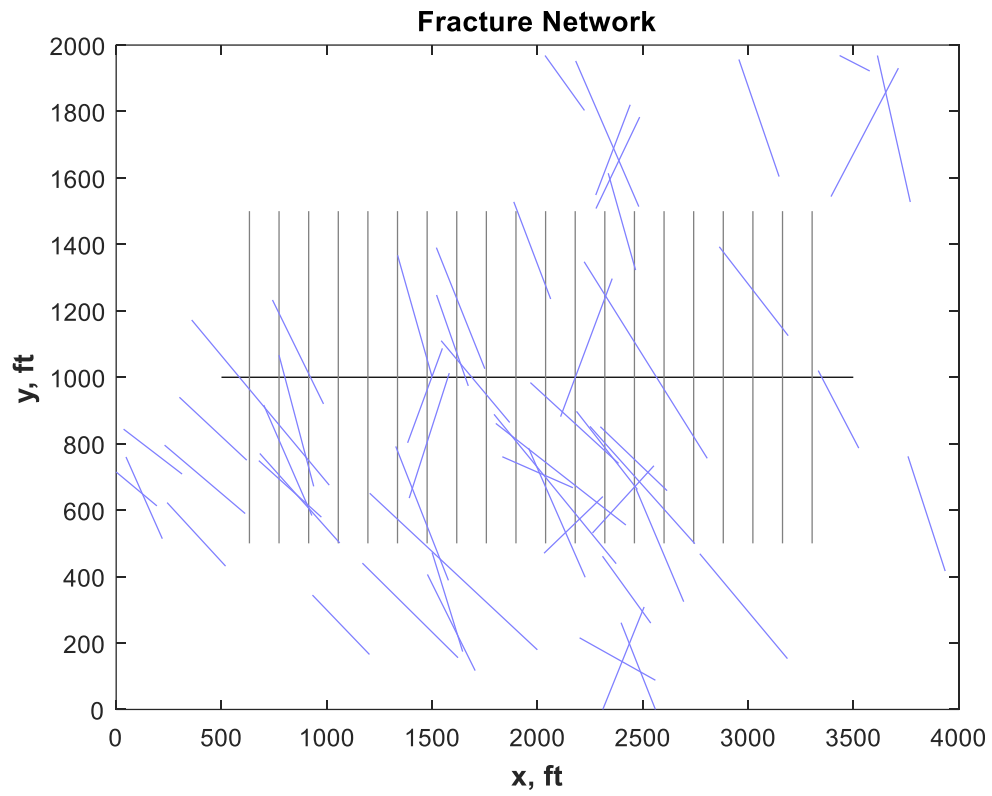


Fig. 38—Complex fracture network for 20 hydraulic fractures.

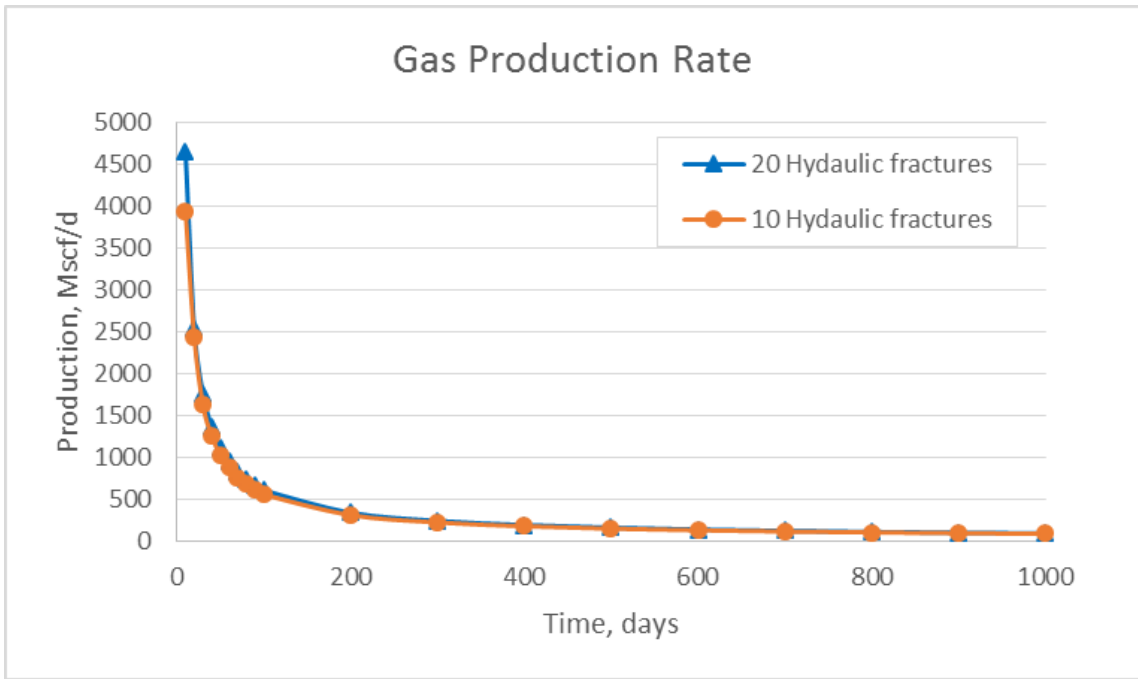


Fig. 39—Gas production rate with different number of hydraulic fractures.

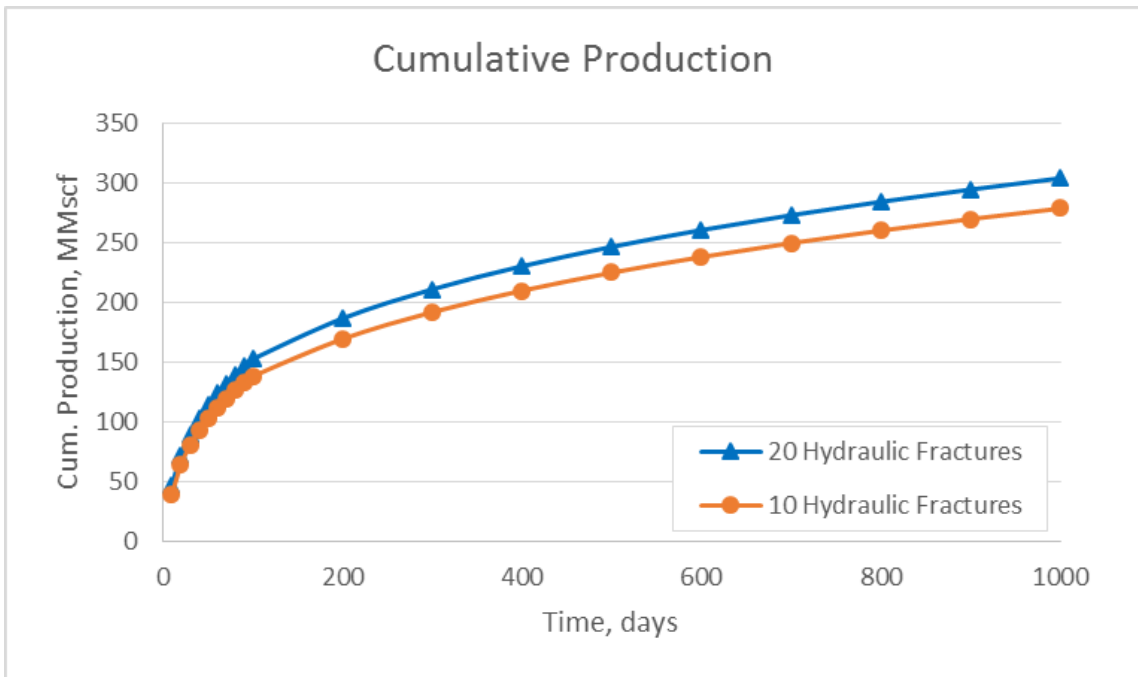


Fig. 40—Cumulative gas production with different number of hydraulic fractures.

To study the production contribution from the natural fractures, same hydraulically fractured horizontal well was simulated without considering the natural fractures in the system. **Fig. 41** shows the cumulative production for all four cases: 10 hydraulic fractures with 55 natural fractures in the system, 20 hydraulic fractures with 55 natural fractures in the system, 10 hydraulic fractures only and 20 hydraulic fractures only. From this, it was identified that the cumulative production from natural fractures increases the total production by 33% for 10 hydraulic fractures case. On the other hand, the cumulative production for 20 hydraulic fractures case gives similar results when natural fractures were considered or not considered. For 20 hydraulic fractures case, the natural fractures increase the total production by 9%. The natural fractures act as extending the reservoir contact and being a conduit, so the contribution to total production becomes more intense when proper number of hydraulic fractures exist in the system. On the other hand, when more than enough number of hydraulic fractures to exploit the reservoir are placed in the system, the contribution from natural fractures is reduced.

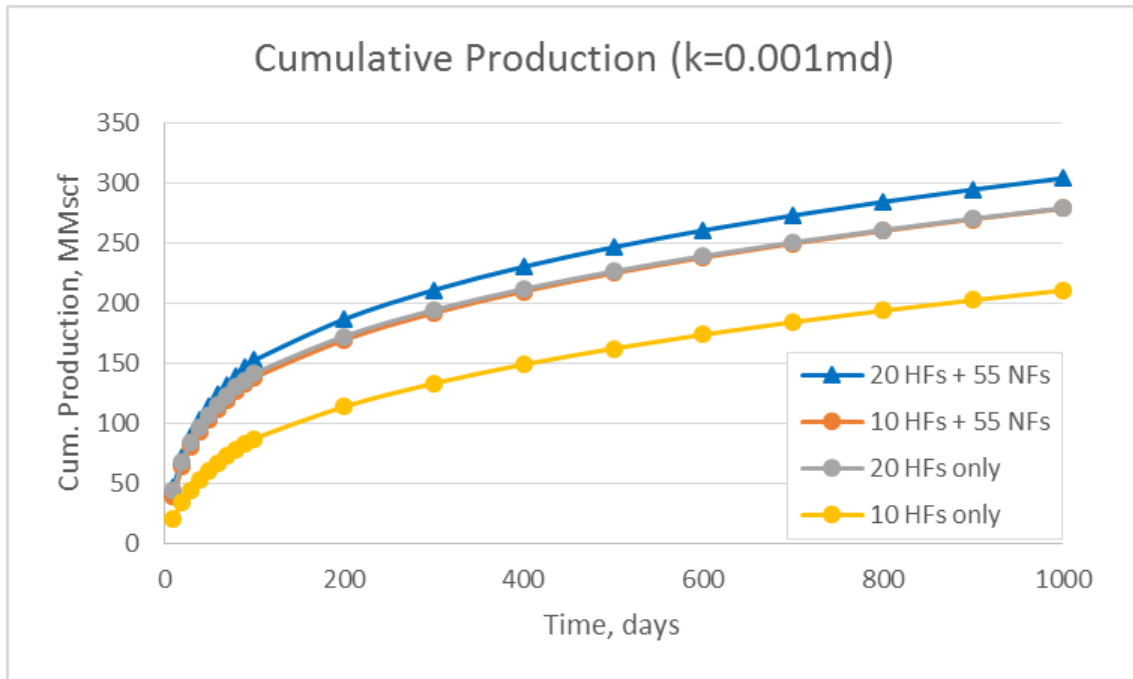


Fig. 41—Cumulative gas production with different number of hydraulic fractures with and without natural fractures in the system ($k=0.001\text{md}$).

To further study the effect of natural fractures on the well performance of different fracture spacing, reservoir permeability was varied. For this study, reservoir permeability of 0.0001md was used for comparison. **Fig. 42** summarizes the results for this simulation. It was identified that the cumulative production from natural fractures increases the total production by 26% for 10 hydraulic fractures case. For 20 hydraulic fractures case, the natural fractures increase the total production by 8%. The main difference from the case of $k=0.001\text{md}$ is that more hydraulic fractures give higher production whether natural fractures are considered or not. Since the reservoir permeability is extremely low, the production contribution from natural fracture network is not as high as the higher reservoir permeability. Therefore, the importance of hydraulic fracturing becomes crucial when the reservoir permeability is particularly low, which agrees with the common practice.

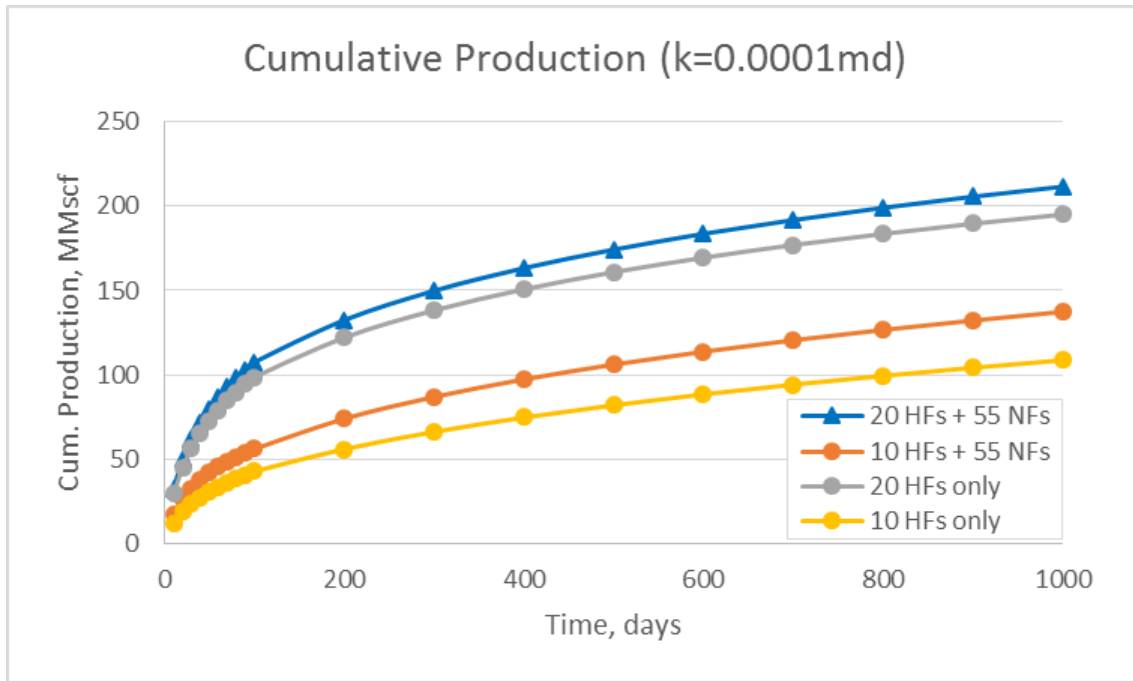


Fig. 42—Cumulative gas production with different number of hydraulic fractures with and without natural fractures in the system (k=0.0001md).

4.3 Parametric Study of Hydraulic Fracture Length

There are two classical models which predicts fracture geometry of length, height and width based on the injected fluid volume, fluid viscosity and rock mechanical properties of Poisson's ratio, Shear modulus. PKN (Perkins-Kern-Nordgren) and KGD (Kristianovitch-Geertsma-de Klerk) are the simple analytical fracture models and the fracture width becomes smaller as we approach to the tip of the fracture in both models. However, we are assuming the geometry of hydraulic fracture as a rectangular parallelepiped, and the all the length, height and width are assumed to be constant.

To study the effect of hydraulic fracture geometry on well performance, fracture length is changed. **Fig. 43** shows hydraulic fracture length of 500 ft case (half length of 250 ft) and **Fig. 44** gives hydraulic fracture length of 750 ft case (half length of 375 ft).

The results for changing hydraulic fracture lengths is shown in **Fig. 45** which displays gas production rate and in **Fig. 46** which presents cumulative production both with different hydraulic fracturing lengths. The figures show the production profile of high initial production and stable long term production. Longer hydraulic fracture length gives higher production rate and higher cumulative production. But when we doubled the hydraulic fracture length from 300 ft to 750 ft, the production did not exactly doubled. This could be due to the relatively long hydraulic fracture length compared to the reservoir size and the connectivity of natural fracture network. Longer hydraulic fracture is preferred in field since it usually increases production, but it also brings in operational challenges. Even we may be able to create a long half-length, propped length and effective length are usually much shorter. Therefore, by doing an economic analysis which considers additional revenue due to the production increase and additional treatment cost, the optimal fracture length can be identified.

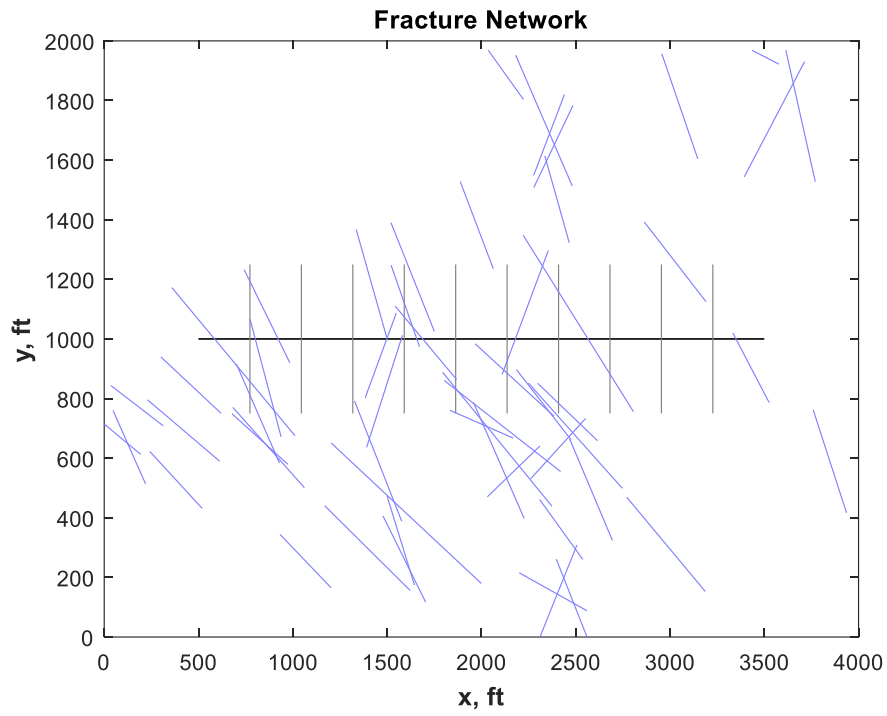


Fig. 43—Complex fracture network with hydraulic fracture length of 500 ft.

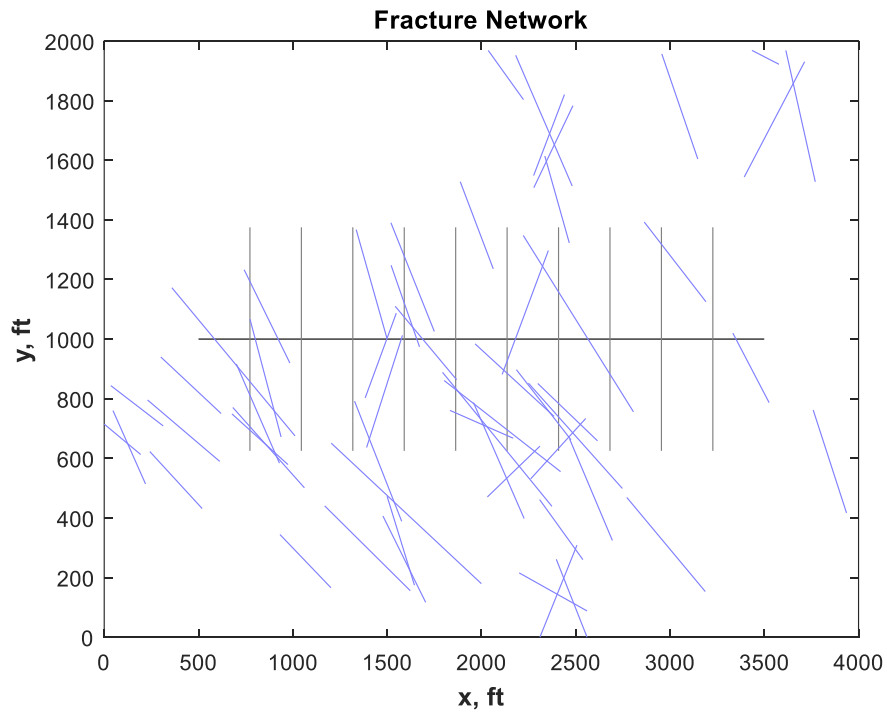


Fig. 44—Complex fracture network with hydraulic fracture length of 750 ft.

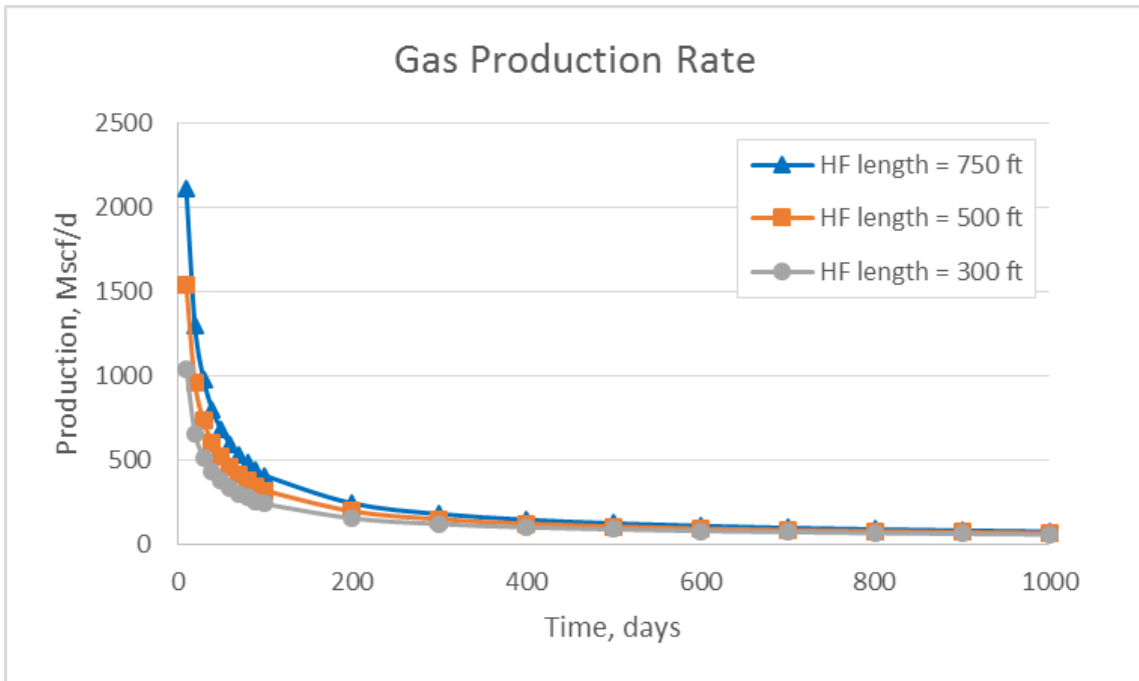


Fig. 45—Gas production rate for different hydraulic fracture lengths.

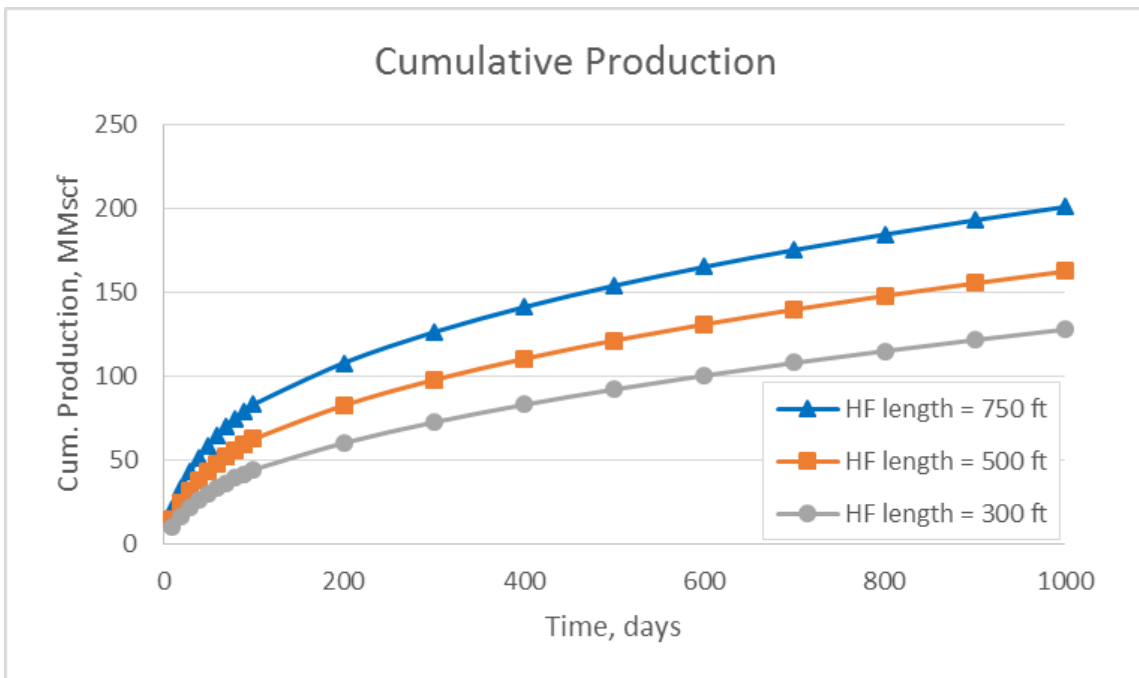


Fig. 46—Cumulative gas production with different hydraulic fracture lengths.

4.4 Parametric Study of Number of Fracture Segments

The foregoing parametric studies consider the effect of input parameters concerning reservoir properties and hydraulic fracture geometries. There are several intrinsic parameters which could affect the well performance in the source function itself and this section discusses two of them.

We divided fractures into several segments to accommodate the mutual effects which each segment has on the other segments. The number of segments is an important parameter which decides the size of the calculation matrix we need to solve, therefore it might have impact on overall solution. To examine this, the number of segments for each fracture was varied. 4 and 9 segments were used for natural fractures and 4, 9 and 16 segments were used for hydraulic fractures in infinite conductivity case. **Fig. 47** shows the result. As we can observe from **Fig. 47**, the cumulative production curves lay almost on top of each other. Large number of segments gives more production, but the difference is not meaningful because it is less than 1% of total production. Since the values are not distinguishable between each other, gas production rate plot was not displayed here. Therefore, segments of 4 were mostly used in the simulation for infinite conductivity case to save the calculation time.

Infinite conductive fracture is a reasonable assumption for unconventional reservoirs because the matrix permeability is extremely low. This assumption may not be valid for conventional reservoirs.

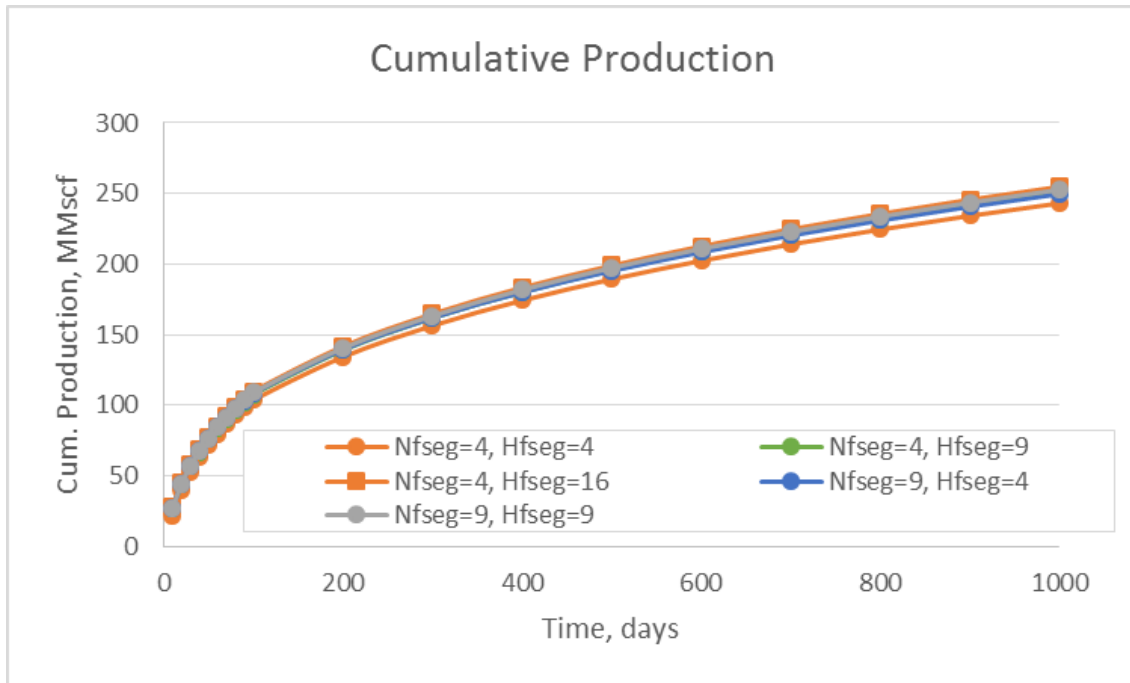


Fig. 47—Cumulative gas production with different number of segments.

4.5 Parametric Study of the Source Type

As an approach to handle natural fractures which can be positioned in any direction, pattern even non-orthogonal with the boundaries of the reservoir. To reduce the time takes for the calculation of the slab source approach, a plane source method was derived.

Fig. 48 shows the comparison of produced gas rate when each of slab source and plane source was used. The production trend is similar for both cases with high initial production and steady decline after that. The production from the slab source is slightly higher since the width of the fracture is additionally considered compared with the plane source. The result shown in **Fig. 48** proves that the plane source method can be safely used for natural fractures.

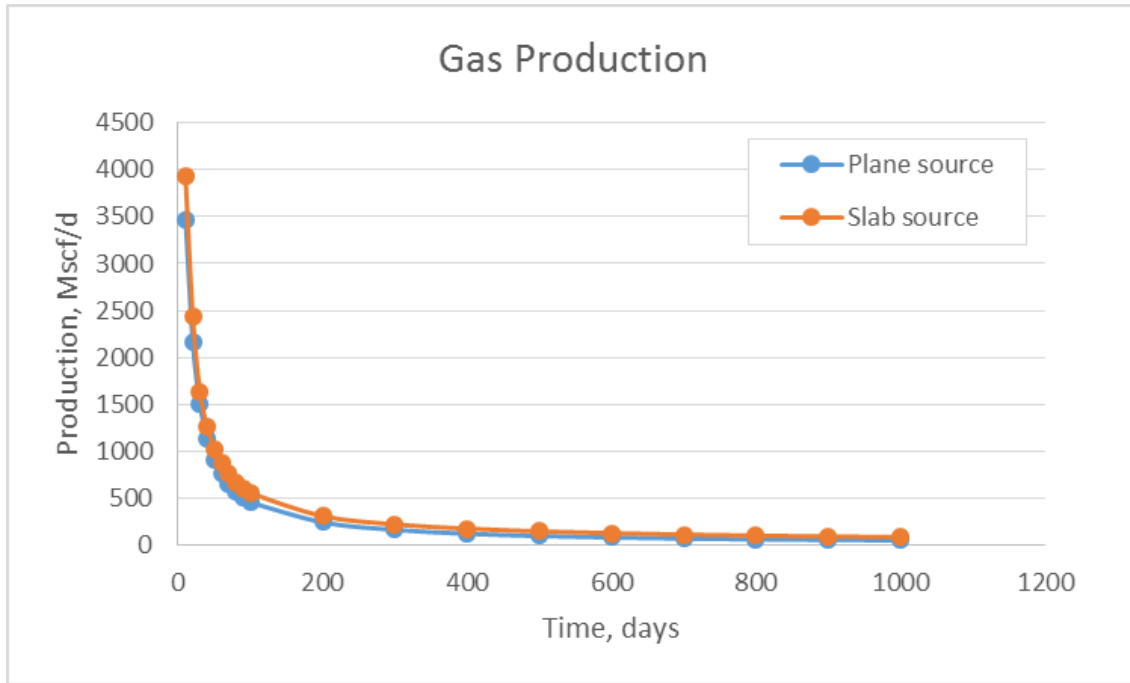


Fig. 48—Gas production rate comparison using slab source and plane source

4.6 Chapter Summary

In this chapter, the effects of different parameters on the well performance are discussed. The parameters that are studied include reservoir permeability, number of hydraulic fractures, hydraulic fracture geometries and number of fracture segments. The base case input parameters are used for all cases, unless otherwise stated.

The parametric study results show that more and longer hydraulic fractures overall increase gas production. But the increment of production is not proportional to the increment of the studied parameters. The connectivity with natural fracture network and relative reservoir size play a role. Besides, reservoir permeability has more significant effects on recovery as well when compared with fracture geometry.

CHAPTER V

APPLICATION EXAMPLE

In this section, field examples are used to present how the source function method is used. The input data is obtained from the literatures. Two examples are used to show the procedure of the model application with one for sparse natural fracture reservoir and the other for dense natural fracture reservoir. For sparse natural fracture case, we discuss the impact of absorbed gas and for dense natural fracture case, we show the contribution of natural fracture to the total production.

5.1 Sparse Natural Fractures

In this section, an example of horizontal well with multiple hydraulic fractures in a slightly naturally fractured reservoir is introduced. Input parameters are summarized in **Table 9**. Reservoir is assumed to be 4000 ft by 2000 ft wide. Reservoir height is assumed to be 200 ft high. Reservoir porosity is 9% and permeability is 0.001 md. Reservoir initial pressure is 2335 psi and bottom hole pressure is maintained at 1885 psi. Gas viscosity is 0.0156 cp and gas specific gravity is 1.0. Total compressibility is $1.25e-5$. Horizontal well is 3000 ft long. Following the current industry practice of large number of hydraulic fractures, it was assumed that there exist 50 hydraulic fractures and 55 natural fractures in the system (**Fig. 49**). Hydraulic fractures are equally spaced in the center of the reservoir. The lengths of hydraulic fractures are assumed to be the same as 1000 ft. Among 55 natural fractures, 33 are intersecting with any kind of hydraulic fractures and there exists 152 total intersection

points. Three important input values for the calculation of absorbed gas were obtained from the Barnett shale case, Langmuir pressure of 650 psi, matrix density of 2.58 gm/cc and adsorbed gas content of 96 scf/ton. Slab source approach was used to obtain the results. All the fractures were divided into 4 segments for the calculation efficiency. Therefore there exist 332 sources and the size of the source function matrix becomes 332 by 332.

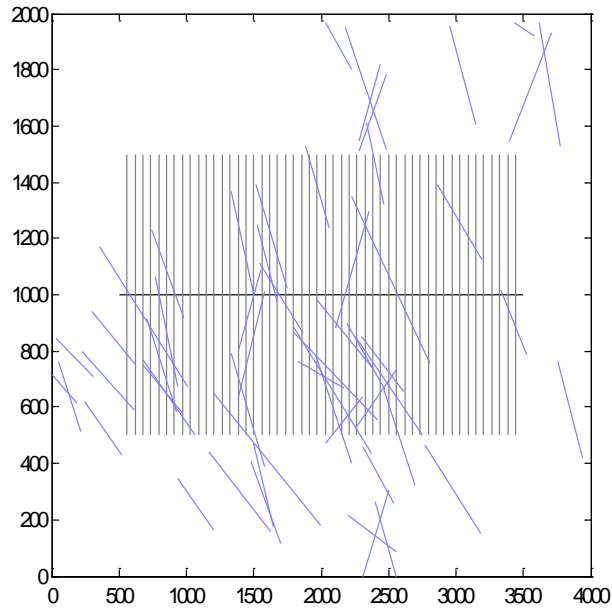


Fig. 49—Complex fracture network used for sparse natural fracture network.

Table 9—Input parameters for sparse natural fracture network.

Reservoir Size	4000 x 2000 x 200 ft
Reservoir Permeability	0.001 md
Reservoir Porosity	9%
p_i	2335 psi
p_{wf}	1885 psi
Gas viscosity	0.0156 cp

Table 9 Continued

Gas specific gravity	1
Number of Hydraulic Fractures	50
Lengths of Hydraulic Fractures	1000 ft
Number of Natural Fractures	55 (33 are intersecting with HFs)
p_L	650 psi (Barnett Shale)
ρ_B	2.58 gm/cc (Barnett Shale)
V_m	96 scf/ton (Barnett Shale)

Fig. 50 is the plot which shows free gas production, desorbed gas production and total gas production. Production sharply decreases to about 16% of initial production after 100 days, and to about 5% of initial production after 365 days. By comparing with the cumulative production which is shown in **Fig. 51**, we can observe that about two thirds of the production, 70%, occurs during the first 300 days. The cumulative desorbed gas production increases with time, but not as fast as free gas production. Since the reservoir pressure was not lowered enough to desorb more gas from the rock surface, the desorbed gas production rate occupies about 8% of total production for the simulation period.

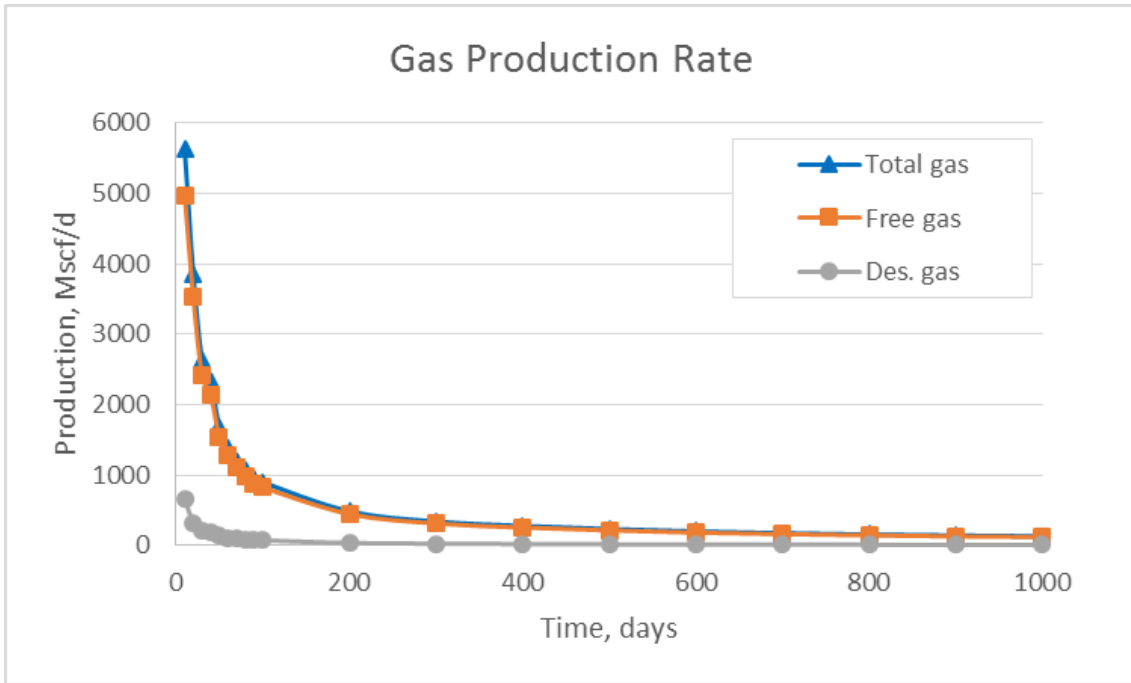


Fig. 50—Free gas, desorbed gas and total gas production rate.

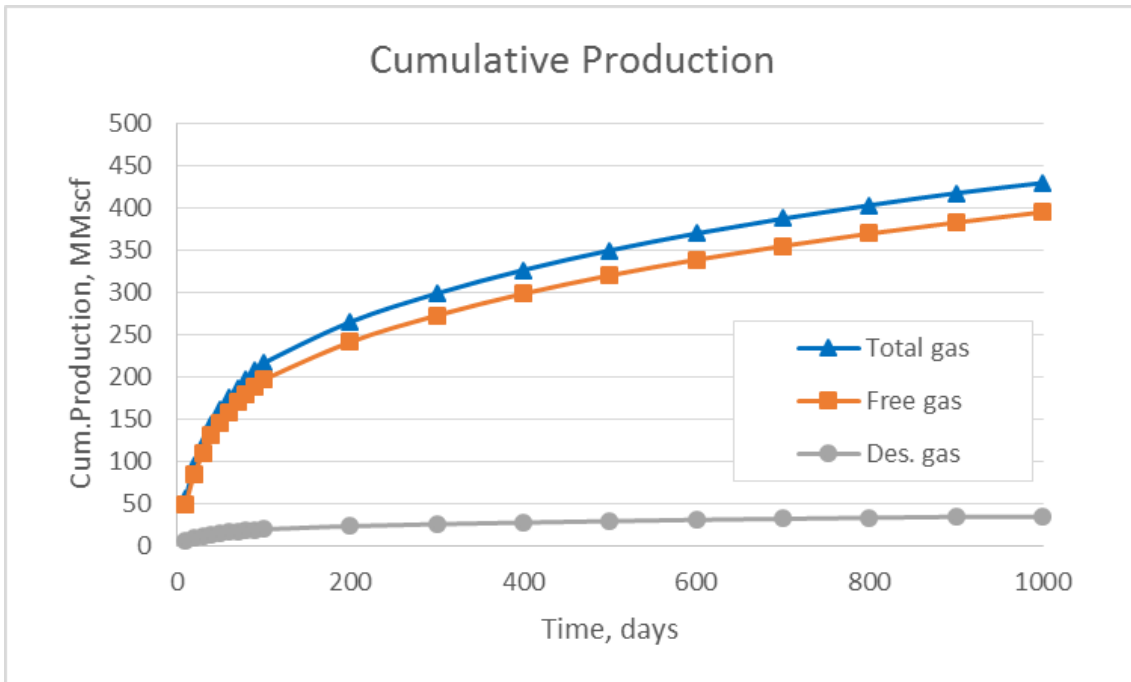


Fig. 51—Cumulative free gas, desorbed gas and total gas production.

5.2 Dense Natural Fractures

To compare the results from section 5.1, a more densely located natural fracture map was used such as **Fig. 52**. There are 50 hydraulic fractures and 145 natural fractures in the system. Hydraulic fractures are evenly spaced in the center of the reservoir with the same lengths of 1000 ft. These exist 352 total intersections and 71 natural fractures are intersecting with any kind of hydraulic fractures. Input parameters are summarized in **Table 10**. Reservoir is assumed to be 4000 ft by 2000 ft wide. Reservoir height is assumed to be 200 ft high. Reservoir porosity is 9% and permeability is 0.001 md. Reservoir initial pressure is 2335 psi and bottom hole pressure is maintained at 1885 psi. Gas viscosity is 0.0156 cp and gas specific gravity is 1.0. Total compressibility is 1.25e-5. Horizontal well is 3000 ft long. Slab source approach was used for simulation.

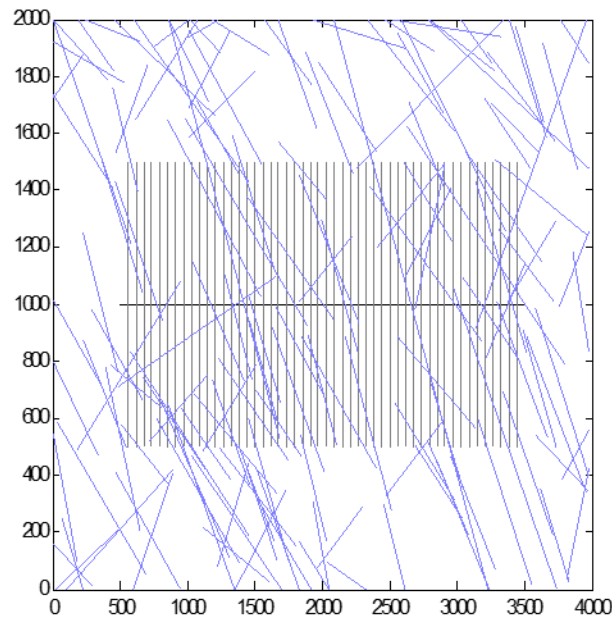


Fig. 52—Complex fracture network used for dense natural fracture network.

Table 10—Input parameters for dense natural fractures network.

Reservoir Size	4000 x 2000 x 200 ft
Reservoir Permeability	0.001 md
Reservoir Porosity	9%
p_i	2335 psi
p_{wf}	1885 psi
Gas viscosity	0.0156 cp
Gas specific gravity	1
Number of Hydraulic Fractures	50
Lengths of Hydraulic Fractures	1000 ft
Number of Natural Fractures	145 (71 are intersecting with HFs)

For the comparison of sparse and dense network, the natural fracture map in **Fig. 49** was used for sparse network case. Sparse network is composed of 55 natural fractures and dense network includes 145 natural fractures. As we observe from **Fig. 53**, the gas production rate is higher in dense natural fracture network. To easily differentiate the gas production rate between sparse and dense network, the gas production rate is visualized with semi-log plot. The rapid reservoir pressure drop due to increased production for dense natural fracture network was also recognized. **Fig. 54** shows the cumulative production comparison between sparse and dense natural fracture network cases. In this case, the dense natural fracture network produces about 44% more gas than the sparse natural fracture network.

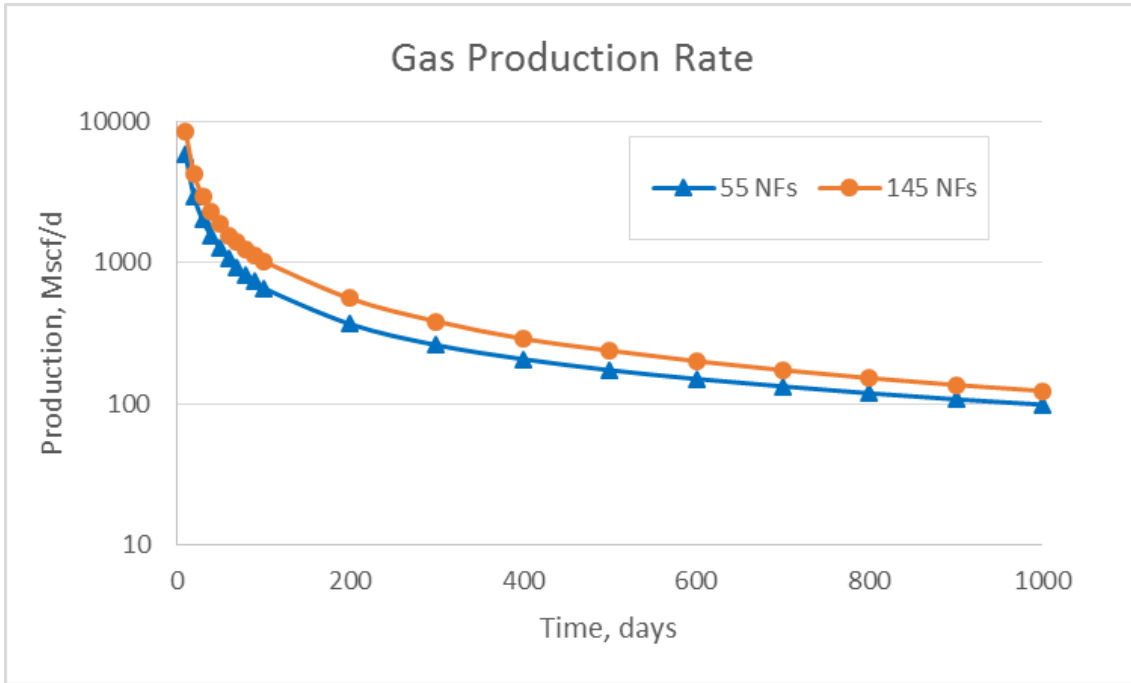


Fig. 53—Gas production rate for sparse and dense natural fracture network.

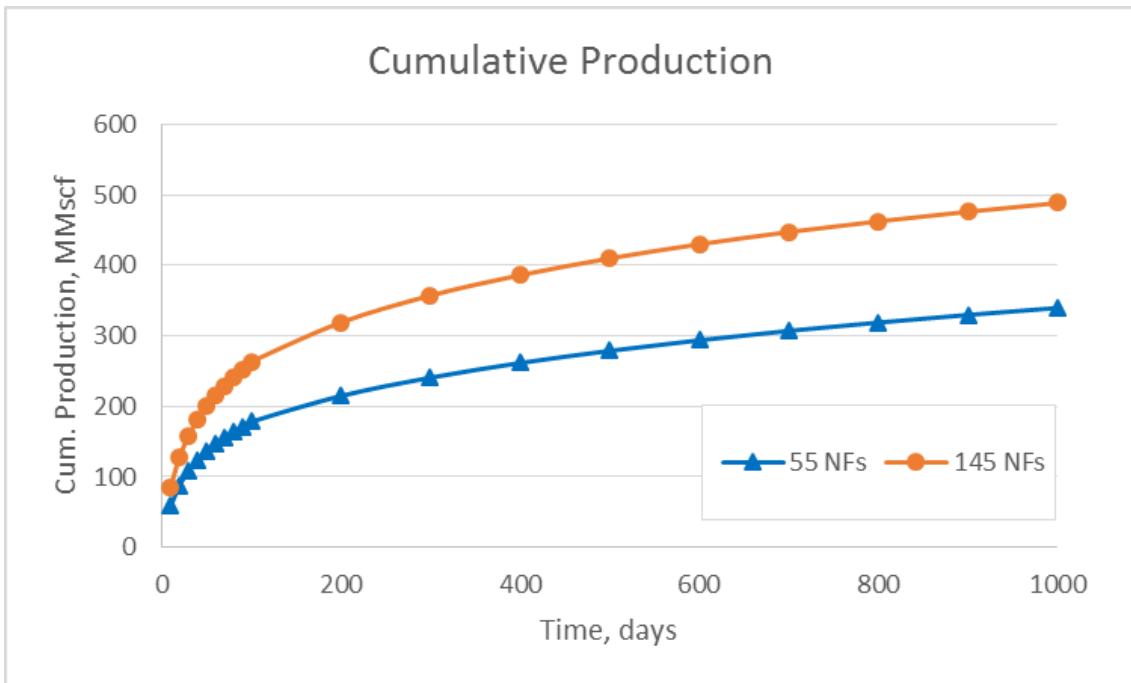


Fig. 54—Cumulative gas production for sparse and dense natural fracture network.

5.3 Large Number of Hydraulic Fractures

To accommodate industry technology development, the number of hydraulic fractures was increased. In this case study, the horizontal well performance with 100 equally spaced hydraulic fractures was examined. Dense network of 156 natural fractures was used. **Fig. 55** shows the complex fracture network used. 73 natural fractures are intersecting with any kind of hydraulic fractures and there exists 730 total intersection points. Input parameters are summarized in **Table 11**. Reservoir is assumed to be 4000 ft by 2000 ft wide. Reservoir height is assumed to be 200 ft high. Reservoir porosity is 9% and permeability is 0.001 md. Reservoir initial pressure is 2335 psi and bottom hole pressure is maintained at 1885 psi. Gas viscosity is 0.0156 cp and gas specific gravity is 1.0. Total compressibility is $1.25e-5$. Horizontal well is 3000 ft long. Slab source approach was used for simulation.

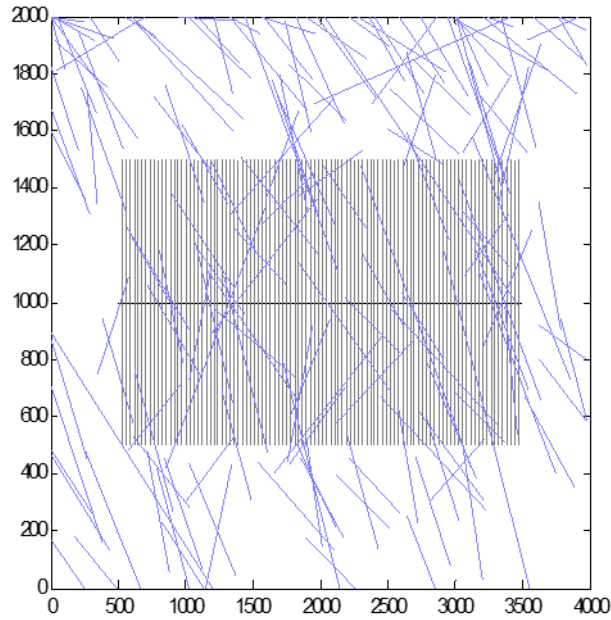


Fig. 55—Complex fracture network used for large number of hydraulic fractures.

Table 11—Input parameters for large number of hydraulic fractures.

Reservoir Size	4000 x 2000 x 200 ft
Reservoir Permeability	0.001 md
Reservoir Porosity	9%
p_i	2335 psi
p_{wf}	1885 psi
Gas viscosity	0.0156 cp
Gas specific gravity	1
Number of Hydraulic Fractures	100
Lengths of Hydraulic Fractures	1000 ft
Number of Natural Fractures	156 (73 are intersecting with HFs)

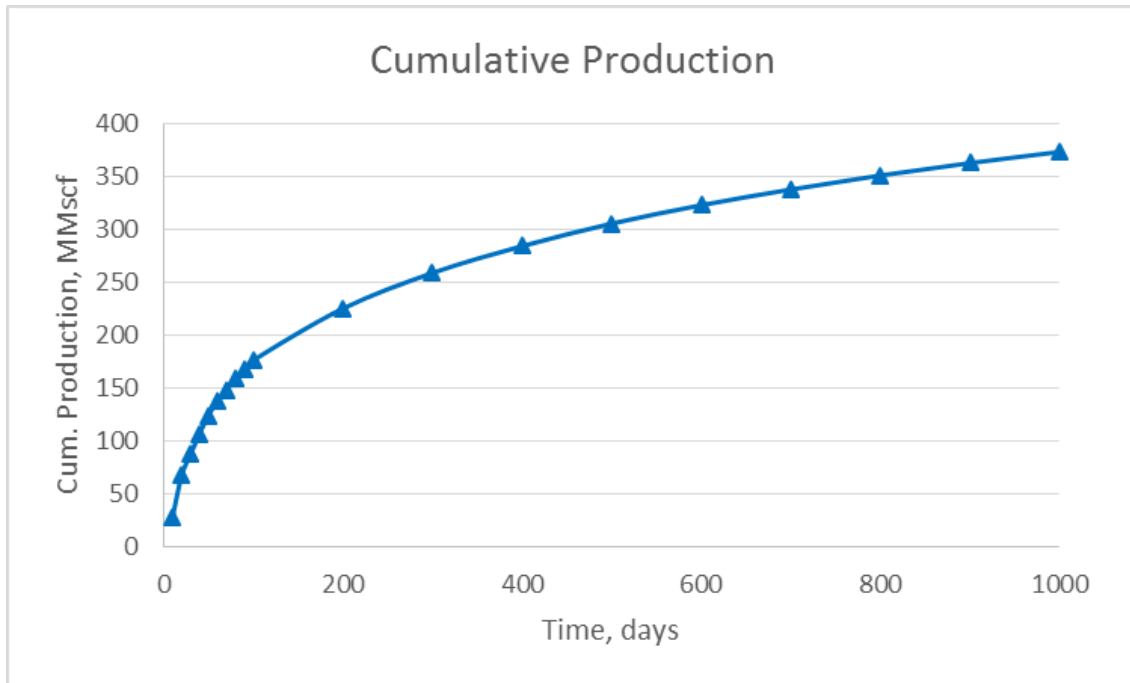


Fig. 56—Cumulative gas production for large number of hydraulic fractures.

Fig. 56 is the plot which shows the cumulative production for 1000 days. We can observe that when the natural fracture network is developed as **Fig. 55**, which shows lots of long natural fractures which are intersecting with many hydraulic fractures, 100 hydraulic fractures are more than needed to properly produce the hydrocarbon. For example, when one natural fracture is intersecting with about 20 hydraulic fractures, all 20 hydraulic fractures are not necessary since smaller number of hydraulic fracture can produce the hydrocarbon from the intersecting natural fracture. Therefore, the approach developed in this study can be used as a quick and simple estimate for hydraulic fracture treatment design.

5.4 Field-scale Case Study

In this section, the well performance in a reservoir with real field properties is predicted. Input parameters were taken based on the SPE papers regarding the hydraulic fracturing test well conducted in China. The reservoir properties of Longmaxi formation in Sichuan basin were mainly used for input. The Longmaxi Silurian age formation is one of three main target marine shales in China, the others being the Cambrian age Qiongzhusi and Niutitang. The Longmaxi serves as the more likely completion target for attempting to reach the production goals set forth by the government and state owned enterprises. The Longmaxi is an interbedded mudstone/siltstone formation with an organic-rich carbonaceous interval at its base. It experienced widespread deposition and is predominantly found in what is currently known as the Sichuan basin in Sichuan province and the Chongqing municipality, with some evidence of its occurrence farther south and east into Guizhou and Hunan provinces. The lower organic-rich interval is the target for completion as it serves to store more hydrocarbon, which also lends itself to effective hydraulic fracture stimulation and flow capacity enhancement. (Wang et al. 2013). The summarized values and their sources are presented in **Table 12**. The properties originally presented in SI unit were converted to field unit for simulation. Reservoir size was estimated to be 4000 ft by 2000 ft with the height of 120 ft. Permeability of 0.00025 md was taken from the work of Zou (2011). Reservoir pressure was calculated based on the pressure gradient given in the paper of Lv et al. (2013), and porosity of average 4% was taken from the same paper. Horizontal lateral length of 1000 ft was obtained from the work of Wang et al. (2013). Fluid properties were calculated using gas property

calculation program based on the reservoir pressure by assuming gas specific gravity of 0.746. Data about adsorbed gas were mainly taken from geochemistry papers of Zhang et al. (2012) and bulk density of 2.58 gm/cc was assumed to be consistent with the Barnett shale (Cluff 2006).

Table 12—Input parameters for field case study and their sources.

Reservoir Data	SI unit		Field unit		Source
Reservoir width, a,(x)	1200	m		ft	
Reservoir length, b,(y)	600	m		ft	
Reservoir Thickness, h,(z)	120	m		ft	Lv et al. 2013
Permeability, k		m ²	0.00025	md	Zou 2011
Reservoir pressure, p _i	28.28	MPa		psi	Lv et al. 2013
porosity	0.04				Lv et al. 2013
Horizontal well					
Length		m	1000	ft	Wang et al. 2013
Fluid Properties					
Viscosity, μ		Pa·s	0.0282	cp	Viscosity @ Reservoir pressure
Gas specific gravity, SG.		-	0.746	-	
Compressibility		1/Mpa	0.0001561	1/psi	Gas compressibility @ Reservoir pressure
Data for Adsorbed Gas					
Adsorbed gas content, V _m		m ³ /Kg	149	scf/ton	Zhang et al. 2012
Bulk density, ρ _b		Kg/m ³	2.58	gm/cc	Cluff 2006
Langmuir's pressure, p _L		Mpa	1036	psia	Zhang et al. 2012

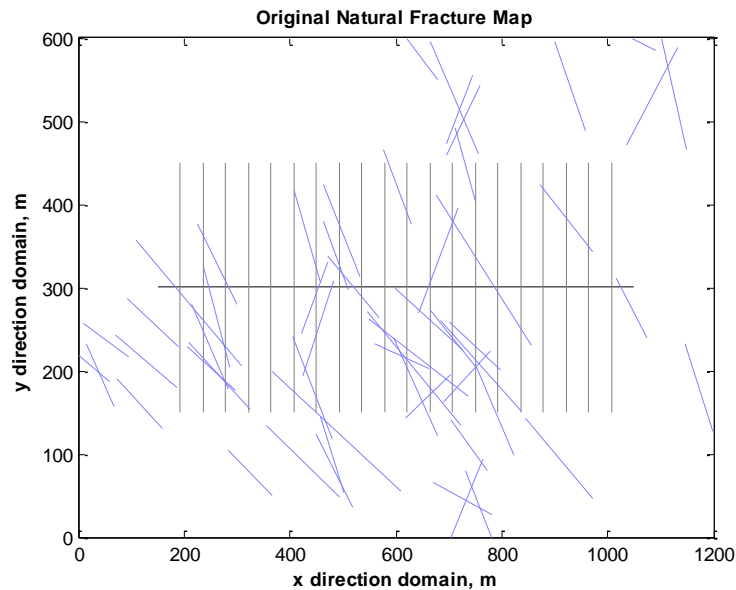


Fig. 57—Natural fracture map used and the multiple hydraulic fractures.

Fig. 57 presents the natural fracture map used and the multiple hydraulic fractures. 20 hydraulic fractures which have equal geometries and properties are assumed to be uniformly distributed within the reservoir. 55 natural fractures reside in the reservoir and it was identified that 29 of them are intersecting with hydraulic fractures. Fractures are assumed to be infinite conductive and gas adsorption was not considered.

Fig. 58 show the average reservoir pressure profile for the life of the well. The pressure declines steadily toward the bottom hole pressure. The production rate is presented in **Fig. 59**. The high initial production cannot be maintained, which reduces to about 10% of initial value within 500 days. The low production compared to the initial value is maintained for the whole well life by slightly declining with time. The recovery factor is assumed to be about 25% after 30 year well life (**Fig. 60**).

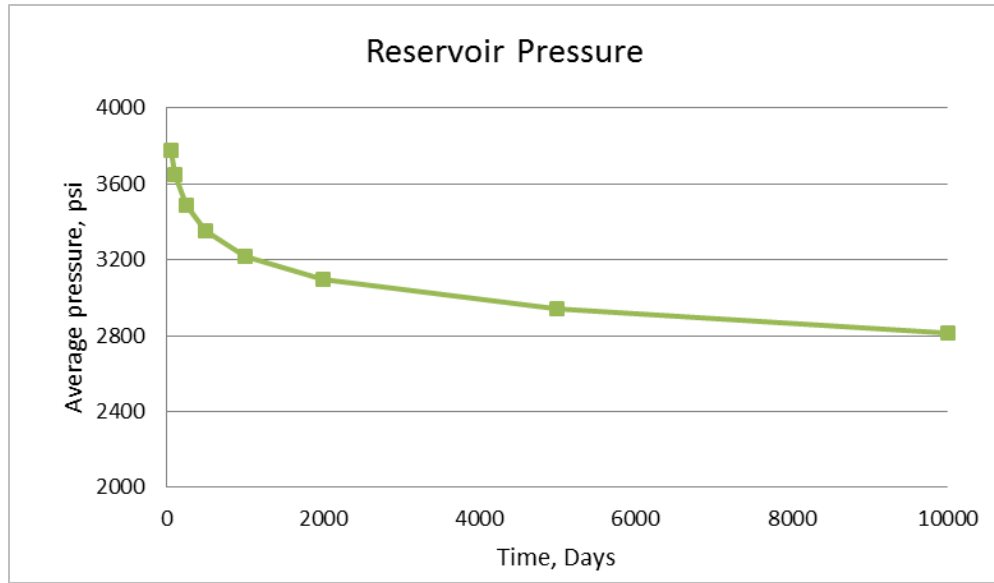


Fig. 58—Average reservoir pressure.

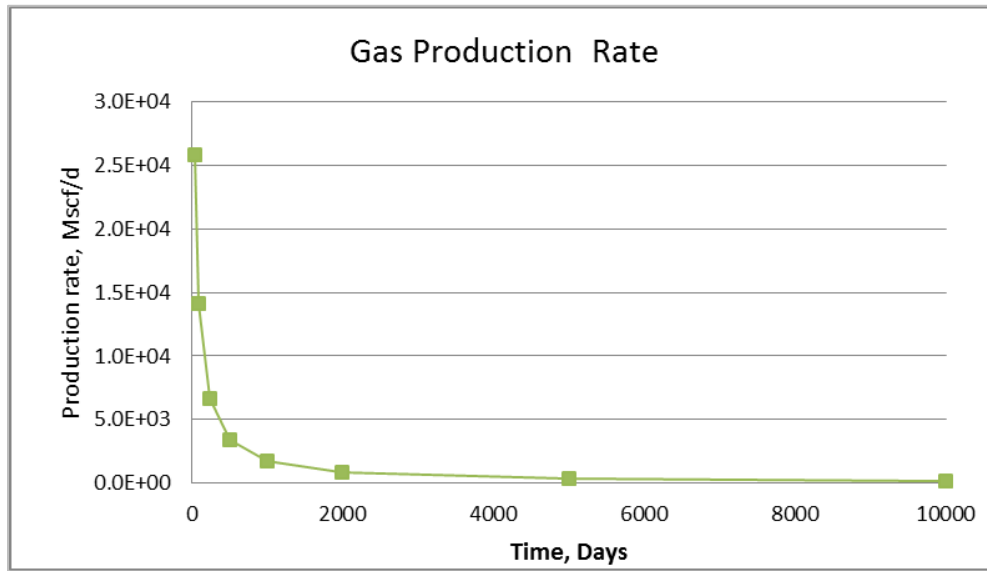


Fig. 59—Gas production rate.

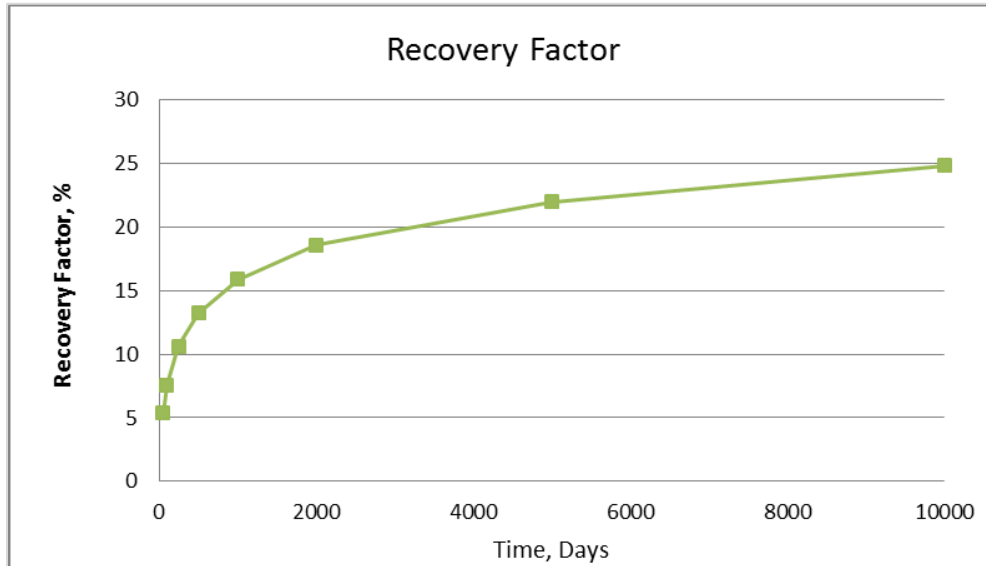


Fig. 60—Recovery factor.

CHAPTER VI

CONCLUSIONS

Natural fractures are commonly observed in unconventional reservoirs. Multi-stage hydraulic fracturing in horizontal wells has been applied to develop these shale/tight sands reservoirs to increase the production by creating a complex network with the existing natural fractures. It still remains a challenge to reasonably predict well performance in such a complex system, especially by honoring the distribution of natural fractures explicitly.

This study presents a combined methodology based on Green's source function and Fractal discrete fracture network (FDFN) model. FDFN model is used to generate realistic natural fracture network. Source function approach is used as a semi-analytical calculation tool to accommodate the influences of hydraulic fractures and natural fractures and obtaining the reservoir response as a final solution. It also presents the production from adsorbed gas, common in shale reservoirs, using modified material balance equation. The effects of important parameters, such as permeability, hydraulic fracture geometries and number of hydraulic fractures are discussed. Important developments and conclusions can be summarized as:

1. Source model and superposition principal was applied to calculate flow problems in complex fracture network. The hydraulic and natural fractures together are considered as independent sources, and their influence on each other is considered, which is more realistic than summing the flow from each fracture as total flow.

2. Fractal Discrete Fracture Network model was used to generate the complex fracture system. This model is a stochastic approach, which follows the identified distribution of natural fractures.
3. To estimate adsorbed gas production, Langmuir's isotherm and modified material balance were applied. It was also found that the inclusion of adsorbed gas could result in the total gas production increase up to 25%.
4. Calculation time was greatly reduced by introducing parallelization and using highly optimized calculation library.
5. Combined source function approach was compared and verified with commercial and open-source softwares.
6. Well performance in naturally fractured reservoir is dependent on natural fracture location, dimension and connectivity with hydraulic fractures.
7. This approach can be used as a quick and easy approach in predicting the optimum number of hydraulic fractures, hydraulic fracture lengths and the location when a natural fracture network is previously identified.
8. The geometry of each hydraulic fracture such as length, width and height and the spacing of hydraulic fractures can be varied to simulate more realistic case for the future work.

REFERENCES

- Babu, D. K. and Odeh, A. S. 1988. Productivity of a Horizontal Well. *SPE Res Eng* **4** (4):417-421. SPE-18298-PA. <http://dx.doi.org/10.2118/18298-PA>.
- Cardott, B. J. 2006. Frontier gas-shale plays of Oklahoma. *Ogs*, 23 October 2006, http://ogs.ou.edu/docs/presentations/OGS-presentation-cardott-oklahoma_gas_shales_2006.pdf (accessed 1 Jan 2017).
- Carslaw, H. S. and Jaeger, J. C. 1959. *Conduction of Heat in Solids*, second edition. Oxford: Clarendon Press.
- Cinco-Ley, H., Samaniego-V., F. and Dominguez-A., N. 1978. Transient Pressure Behavior for a Well with a Finite Conductivity Vertical Fracture. *SPE J* **18** (4):253-164. SPE-6014-PA. <http://dx.doi.org/10.2118/6014-PA>.
- Cinco-Ley, H. and Samaniego-V., F. 1981. Transient Pressure Analysis for Fractured Wells. *SPE J* **33** (9):1749-1766. SPE-7490-PA. <http://dx.doi.org/10.2118/7490-PA>.
- Cluff, B. 2006. Barnett Shale Barnett Shale-Woodford Woodford Shale play of the Delaware Shale play of the Delaware basin– is it another giant is it another giant shale gas field in Texas?. *Discovery-group*, 1 January 2006, <http://www.discovery-group.com/pdfs/2006%20W%20TX%20Barnett-Woodford%20shale.pdf> (accessed 1 Jan 2017).
- Darcel, C., Bour, O., Davy, P. et al. 2003. Connectivity Properties of Two-Dimensional Fracture Networks with Stochastic Fractal Correlation. *Water Resour. Res.* **39** (10): 1272. DOI: 10.1029/2002wr001628.
- Davy, P., Sornette, A. and Sornette, D. 1990. Some Consequences of a Proposed Fractal Nature of Continental Faulting. *Nature* **348** (6296): 56-58. <http://dx.doi.org/10.1038/348056a0>.
- Gale, J. F., Reed, R. M., Becker, S. P. et al. 2010. Natural Fractures in the Barnett Shale in the Delaware Basin, Pecos Co. West Texas: Comparison with the Barnett Shale in the Fort Worth Basin. *Searchanddiscovery*, 3 February 2010, http://www.searchanddiscovery.com/documents/2010/10226gale/ndx_gale.pdf (accessed 1 January 2017).
- Gringarten, A. C. and Ramey, H. J. 1973. The Use of Source and Green's Functions in Solving Unsteady-Flow Problems in Reservoirs. *SPE J* **13** (5):285-296. SPE-3818-PA.

<http://dx.doi.org/10.2118/3818-PA>.

Gringarten, A. C. and Ramey, H. J. 1974. Unsteady-State Pressure Distributions Created by a Well With a Single Horizontal Fracture, Partial Penetration or Restricted Entry. *SPE J* **14** (4):413-426. SPE-3819-PA. <http://dx.doi.org/10.2118/3819-PA>.

Gringarten, A. C., Ramey, H. J. and Raghavan, R. 1974. Unsteady-State Pressure Distributions Created by a Well With a Single Infinite-Conductivity Vertical Fracture. *SPE J* **14** (4):347-360. SPE-4051-PA. <http://dx.doi.org/10.2118/4051-PA>.

Guo, G., Evans, R. D. and Chang, M. M. 1994. Pressure-Transient Behavior for a Horizontal Well Intersecting Multiple Random Discrete Fractures. Presented at the SPE Annual Technical Conference and Exhibition, New Orleans, Louisiana, 25-28 September. SPE-28390-MS. <http://dx.doi.org/10.2118/28390-MS>.

Kim, T. H. and Schechter, D. S. 2009. Estimation of Fracture Porosity of Naturally Fractured Reservoirs with No Matrix Porosity Using Fractal Discrete Fracture Networks. *SPE Res Eval & Eng* **12** (2):232-242. SPE-110720-PA. <http://dx.doi.org/10.2118/110720-PA>.

King, G. R. 1990. Material Balance Techniques for Coal Seam and Devonian Shale Gas Reservoirs. Presented at the SPE Annual Technical Conference and Exhibition, New Orleans, Louisiana, 23-26 September. SPE-20730-MS. <http://dx.doi.org/10.2118/20730-MS>.

Lin, J. and Zhu, D. 2010. Modeling Well Performance for Fractured Horizontal Gas Wells. Presented at the International Oil and Gas Conference and Exhibition, Beijing, China, 8-10 June. SPE-130794-MS. <http://dx.doi.org/10.2118/130794-MS>.

Mengal, S. A. and Wattenbarger, R. A. 2011. Accounting for Adsorbed Gas in Shale Gas Reservoirs. Presented at the SPE Middle East Oil and Gas Show and Conference, Manama, Bahrain. 25-28 September. SPE-141085-MS. <http://dx.doi.org/10.2118/141085-MS>.

Nelson, R. A. 2001. *Geologic Analysis of Naturally Fractured Reservoirs*, second edition. Houston: Gulf Professional Publishing.

Newman, A. B. 1936. Heating and Cooling Rectangular and Cylindrical Solids. *Ind. Eng. Chem.* **28** (5):545-548. <http://dx.doi.org/10.1021/ie50317a010>.

Ozkan, E., Sarica, C., Hacıislamoglu, M. et al. 1995. Effect of Conductivity on Horizontal Well Pressure Behavior. *SPE Advanced Technology Series* **3** (1):85-94. SPE-24683-PA. <http://dx.doi.org/10.2118/24683-PA>.

Priest, S. D. 1993. *Discontinuity Analysis for Rock Engineering*, first edition. London: Chapman and Hall.

Raghavan, R. and Hadinoto, N. 1978. Analysis of Pressure Data for Fractured Wells: The Constant-Pressure Outer Boundary. *SPE J* **18** (2):139-150. SPE-6015-PA. <http://dx.doi.org/10.2118/6015-PA>.

Song, B. 2010. *Pressure Transient Analysis and Production Analysis for New Albany Shale Gas Wells*. MS thesis, Texas A&M University, College Station, TX (August 2010).

Voss, R. F. 1988. Fractals in Nature: From Characterization to Simulation. In *The Science of Fractal Images*, first edition. R.F. Voss, Chap. 1, 21-70. New York city: Springer-Verlag New York.

Wang, W., Olson, J. E. and Prodanovic, M. 2013. Natural and Hydraulic Fracture Interaction Study Based on Semi-circular Bending Experiments. Presented at the Unconventional Resources Technology Conference, Denver, Colorado. 12–14 August. SPE-1576910-MS. <http://dx.doi.org/10.2118/1576910-MS>.

Lv, Z., Wang, L., Deng, S. et al. 2013. China's Marine Qiongzhusi Shale Play: First Deep Asia Pacific Region Horizontal Multiple Stage Frac: Case History, Operation & Execution. Presented at International Petroleum Technology Conference, Beijing, China, 26-28 March. IPTC-16391-MS. <https://doi.org/10.2523/IPTC-16391-MS>.

Wang, L., Dumesnil, J., Deng, S. et al. 2013. Sichuan Basin Longmaxi Shale Gas Stimulation and Completion Case Study. Presented at the SPE Unconventional Resources Conference and Exhibition-Asia Pacific, Brisbane, Australia. 11-13 November. SPE-167006-MS. <http://dx.doi.org/10.2118/167006-MS>.

Warren, J. E. and Root, P. J. 1963. The Behavior of Naturally Fractured Reservoirs. *SPE J* **3** (3):245-255. SPE-426-PA. <http://dx.doi.org/10.2118/426-PA>.

Zeng, F. and Zhao, G. 2009. A New Model for Reservoirs with Discrete Fracture System. Presented at Canadian International Petroleum Conference, Calgary, Alberta, 16-18 June. PETSOC-2009-064. <http://dx.doi.org/10.2118/2009-064>.

Zhang, T., Ellis, G. S., Ruppel, S. C. et al. 2012. Effect of organic-matter type and thermal maturity on methane adsorption in shale-gas systems. *Org. Geochem.* **47**:120–131. <http://dx.doi.org/10.1016/j.orggeochem.2012.03.012>.

Zou, C., Dong, D., Wang, Y. et al. 2011. Shape Types and Reservoir Characteristics of China. *Searchanddiscovery*, 9 May 2011,

http://www.searchanddiscovery.com/pdfz/abstracts/pdf/2011/hedberg-beijing/abstracts/ndx_zou.pdf.html (accessed 1 January 2017).

APPENDIX I

SOURCE FUNCTIONS FOR VARIOUS BOUNDARY CONDITION

The pressure distribution in a reservoir having dimensions of a, b, and h due to the small source in the middle of the domain is calculated by

$$\Delta p = p_i - p(x, y, z, t) = \frac{q}{\phi \mu c_t} \int_0^t (S_x \cdot S_y \cdot S_z) d\tau$$

If we assume the outer boundaries of the reservoir are no-flow boundaries, the source function S has the form as follows according to Gringarten and Ramey (1973).

$$S_x = \frac{x_f}{a} \left[1 + \frac{4a}{\pi x_f} \sum_{n=1}^{\infty} \frac{1}{n} \sin \frac{n\pi x_f}{2a} \cos \frac{n\pi x_0}{a} \cos \frac{n\pi x}{a} \exp\left(-\frac{n^2 \pi^2 k_x \tau}{\alpha a^2}\right) \right]$$

$$S_y = \frac{y_f}{b} \left[1 + \frac{4b}{\pi y_f} \sum_{n=1}^{\infty} \frac{1}{n} \sin \frac{n\pi y_f}{2b} \cos \frac{n\pi y_0}{b} \cos \frac{n\pi y}{b} \exp\left(-\frac{n^2 \pi^2 k_y \tau}{\alpha b^2}\right) \right]$$

$$S_z = \frac{z_f}{h} \left[1 + \frac{4h}{\pi z_f} \sum_{n=1}^{\infty} \frac{1}{n} \sin \frac{n\pi z_f}{2h} \cos \frac{n\pi z_0}{h} \cos \frac{n\pi z}{h} \exp\left(-\frac{n^2 \pi^2 k_z \tau}{\alpha h^2}\right) \right]$$

If all the outer boundaries of the reservoir are assumed to be in constant pressure state, the source function S is written as follows.

$$S_x = \frac{4}{\pi} \sum_{n=1}^{\infty} \frac{1}{n} \sin \frac{n\pi x_f}{2a} \sin \frac{n\pi x_0}{a} \sin \frac{n\pi x}{a} \exp\left[-\frac{n^2 \pi^2 k_x \tau}{\alpha a^2}\right]$$

$$S_y = \frac{4}{\pi} \sum_{n=1}^{\infty} \frac{1}{n} \sin \frac{n\pi y_f}{2b} \sin \frac{n\pi y_0}{b} \sin \frac{n\pi y}{b} \exp\left[-\frac{n^2 \pi^2 k_y \tau}{\alpha b^2}\right]$$

$$S_z = \frac{4}{\pi} \sum_{n=1}^{\infty} \frac{1}{n} \sin \frac{n\pi z_f}{2h} \sin \frac{n\pi z_0}{h} \sin \frac{n\pi z}{h} \exp \left[-\frac{n^2 \pi^2 k_z \tau}{\alpha h^2} \right]$$

Various boundary conditions can be handled by properly using **Table 2**. When one boundary is assumed to be in no-flow state (at x=0) and the other is in constant pressure state (at x=a) in x direction and all the y and z direction boundaries are no-flow boundaries, the source function can be written as follows.

$$S_x = \frac{8}{\pi} \sum_{n=1}^{\infty} \left(\frac{1}{2n+1} \sin \frac{(2n+1)\pi x_f}{4a} \cos \frac{(2n+1)\pi x_0}{a} \cdot \cos \frac{(2n+1)\pi x}{a} \cdot \exp \left[-\frac{(2n+1)^2 \pi^2 k_x \tau}{4\alpha a^2} \right] \right)$$

$$S_y = \frac{y_f}{b} \left[1 + \frac{4b}{\pi y_f} \sum_{n=1}^{\infty} \frac{1}{n} \sin \frac{n\pi y_f}{2b} \cos \frac{n\pi y_0}{b} \cos \frac{n\pi y}{b} \exp \left(-\frac{n^2 \pi^2 k_y \tau}{\alpha b^2} \right) \right]$$

$$S_z = \frac{z_f}{h} \left[1 + \frac{4h}{\pi z_f} \sum_{n=1}^{\infty} \frac{1}{n} \sin \frac{n\pi z_f}{2h} \cos \frac{n\pi z_0}{h} \cos \frac{n\pi z}{h} \exp \left(-\frac{n^2 \pi^2 k_z \tau}{\alpha h^2} \right) \right]$$